The Meningeal Response to Traumatic Brain Injury

A Dissertation

Presented to
the faculty of the School of Medicine in partial fulfillment of the requirements for the degree of

Doctor of Philosophy

by

Ashley Bolte

January 2021

Abstract

Traumatic brain injury (TBI) is a devastating event that results in a heightened risk for long-term disease sequelae including anxiety, depression, Alzheimer's disease (AD) and chronic traumatic encephalopathy. TBI affects 12% of the adult population; yet, our mechanistic understanding of the factors that render the TBI brain more susceptible to neurological disease remains poorly understood. Recent findings point to dysregulated and sustained immune responses as contributing to negative outcomes. However, why inflammatory responses persist in the brain long after injury is still largely unknown.

In this dissertation, we examine the meningeal tissue and its response to brain injury. The meninges serve as the interface between the brain and the immune system, and facilitate many important brain-immune interactions both in health and disease. We couple a bioinformatic approach to determine gene expression alterations in meningeal tissue following TBI with experimental methods for interrogating how the meningeal lymphatic system specifically influences TBI pathogenesis.

To determine how the meningeal lymphatic system affects TBI pathogenesis, we utilized an experimental mouse model of TBI to demonstrate that mild forms of brain trauma cause severe deficits in meningeal lymphatic drainage that begin within hours and last at least one month post-injury. To investigate a mechanism underlying impaired lymphatic function in TBI, we examined how increased intracranial pressure (ICP) influences the meningeal lymphatics. We demonstrate that increased ICP can contribute to meningeal lymphatic dysfunction. Moreover, we show that pre-existing lymphatic dysfunction before TBI leads to increased neuroinflammation and negative cognitive outcomes. Finally, we report that rejuvenation of meningeal lymphatic drainage function in aged mice can ameliorate TBI-induced gliosis. These findings provide insights into both the causes and consequences of meningeal lymphatic dysfunction in TBI and suggest that therapeutics targeting the meningeal lymphatic system may offer strategies to treat TBI.

To further elucidate the meningeal response to TBI, we utilized single cell and bulk RNA sequencing one week post injury to determine how different cell populations within the meninges are affected by injury. We found that the meninges are a heterogeneous tissue that includes many types of immune cells, fibroblasts and endothelial cells. We find that following a mild TBI, there are increases in frequencies of meningeal macrophages and fibroblasts. These cells undergo upregulation of inflammatory related genes. Moreover, we find that the meningeal response to TBI is substantially altered in aging, even 1.5 months post injury.

In this dissertation, we examined the meningeal responses to TBI. The findings here present novel insights into the role of the meningeal lymphatic system and the meninges as a whole in shaping the immune response following brain injury. These findings will allow for a deeper understanding of the immune responses following brain injury with the goal of eventually developing therapies to mitigate negative long-term outcomes following brain injury.

Acknowledgments

I feel incredibly grateful to obtain my doctoral training in the Biomedical Sciences Graduate Program within the School of Medicine. Moreover, I have had the fortune to be a part of several different training environments which have offered many different opportunities throughout my time as a graduate student. Specifically, I would like to thank the Brain Immunology and Glia (BIG) Center for their valuable and candid discussions, the access to the most advanced technology and experts in the field, and for a truly collaborative and vibrant atmosphere. Additionally, I would like to thank the Immunology Training Program (ITP) for providing the funding and environment for me to improve my skills in immunology to become a truly interdisciplinary scientist. Likewise, my home department, Microbiology, Immunology and Cancer Biology (MIC), has connected me with fantastic scientists and my dissertation committee: Dr. Young Hahn (co-mentor), Dr. Loren Erickson (chairperson), Dr. Sarah Kucenas, and Dr. Melanie Rutkowski. I would like to thank them for their evaluation of my work and for their unique perspectives and thoughts. I appreciate the time and thought they put into our meetings.

Most of all, I would like to thank my mentor, Dr. John Lukens. Thank you for always believing in me and supporting me through successes and failures. You have always championed my successes and I feel lucky to have had the opportunity to work in your lab for these past years. You have taught me the importance of resilience, dedication, and critical thinking in performing research. Thank you for all the time you have invested in my development as a scientist and my wellbeing as a person. You certainly serve as a role model for me.

I am also very grateful for the fantastic environment in the Lukens Lab. Cat- I knew the Lukens lab was special when I first rotated with you. That first rotation made me incredibly excited for my lab years and helped me realize that I had a home in the BIG Center. Thank you for all you taught me! Mariah- I never could have done the TBI project without you. Working together to figure out how to do all the surgeries and experiments was one of my favorite parts of graduate school. I am so glad that I had a buddy to work with while discussing our favorite podcasts. Hannah, Elizabeth and Kristine- you all have been such as fantastic team to work with. I look forward to coming into lab and seeing your faces every day. You all are truly inspirational and I feel lucky to work alongside such brilliant and fantastic people. I have learned a lot from each of you and am very grateful for that.

I would be remiss if I didn't mention my other friends and colleagues who greatly contributed to this project. Mike- thank you for all you taught me. I am very grateful to have learned a lot of the lymphatic techniques and procedures from someone as meticulous and smart as you. I always appreciated your sage input and advice along the way. Arun-I almost included you up in the Lukens lab section as an honorary lab member. I am so lucky to have such a fantastic friend who is also a rad bioinformatician. You were instrumental for not only performing some of the analyses for my first paper, but in spending hundreds of hours working with me while I tried to learn these techniques. This was the epitome of a fantastic collaboration and I am incredibly thankful for your patience and kindness throughout my PhD.

Lastly, I would like to thank my friends and family who have supported me along the way. To my amazing family- I never would have been here or made it through without you all. My favorite times are spending time with you. You have taught me the importance of hard work, grit and determination and have always been there to support me in whatever way I need. To my husband Fabian- we've had such a journey to get here but you have always been an inspiration both with science, medicine, and just life in general. I am so lucky to have you all in my life!

Table of Contents

Table of Figures and Tables

Chapter 1

Introduction

Central nervous system (CNS) injury affects millions of people worldwide each year [1]. Stroke, subarachnoid hemorrhage (SAH) and traumatic brain injury (TBI), while of different etiologies, all involve an acute injury to the brain followed by an immune response. Brain injuries can cause debilitating impairments in motor function, cognition, sensory function, and mental health. Stroke is the second leading cause of death in the developed world [2] and accounts for the largest amount of long-term disability [3]. In addition, mounting evidence indicates that having a history of TBI markedly increases the risk of developing numerous other neurological disorders later in life including chronic traumatic encephalopathy (CTE), Alzheimer's disease, anxiety, depression, and amyotrophic lateral sclerosis [4-9]. Despite being prominent global medical issues, the pathoetiology of both stroke and TBI remains incompletely understood and improved treatment options are desperately needed.

Tissue damage and cellular stress resulting from brain injuries incite activation of the immune system, which aids in the disposal of neurotoxic material and coordinate tissue repair [10, 11]. While immune responses can play beneficial roles in TBI and stroke, unchecked and/or chronic immune activation following brain trauma can lead to secondary tissue damage, brain atrophy, and neurological dysfunction [10-15]. Balancing the beneficial and the detrimental arms of the immune response will be critical for developing new strategies to effectively manage recovery after brain injuries.

In this dissertation, we will examine the role of the immune system in the events following brain injury. Resident cells in the CNS are the first line of response to brain injury, and their roles in dampening or enhancing inflammation have been shown to be critical for neuronal survival, brain

health, and long-term cognitive outcomes. As the “immune cells of the brain”, microglia have a multifaceted role following brain injury. Moreover, the recent discovery of the meningeal lymphatic system has led to increased understanding of how the brain resident cells can interact with immune cells from the periphery. This CNS lymphatic system has been shown to modulate neuroinflammatory responses following brain injury. Finally, the manner in which immune cells and brain resident cells respond to injury differs with age. Herein, we will examine the developing understanding of the nuanced interactions between the immune system and the brain in the context of brain injury.

1.1 Microglia Response to Injury

Microglia are responsible for various tasks in development and adulthood including synaptic pruning [16, 17], engulfment of apoptotic cells [18, 19], and sculpting of neural circuits [20]. Microglia tile the brain and are often the first responders to brain injury or disease. Early work by Davalos et al. demonstrated the dynamic nature of microglia following injury [21]. Within minutes of injury, microglia extend their processes to surround the site of injury in an ATP-dependent manner [21] (Figure 1.1). More recently, the initial dynamics of microglial responses to injury have been further defined. In response to a compression injury, microglia first retract their ramified processes. A few microglia surrounding the injury site extend their processes to form a continuous network around surviving cells, termed a ‘honeycomb’ structure [15] (Figure 1.1). This structure is apparent within an hour after injury and can last for up to 12 hours. Upon astrocyte death, microglia have been shown to extend one phagocytic process to the area of cell death, resembling a ‘jellyfish’ [15] (Figure 1.1). These honeycomb and jellyfish responses to injury are dependent on purinergic signaling and are important for walling off the initial injury before other infiltrating immune cells arrive [15]. In cases of more diffuse TBI using a murine fluid percussion model of

injury, microglia have been shown to adopt a “rod” shape and align closely with apical dendrites in areas containing axotomized neurons [22] (Figure 1.1).

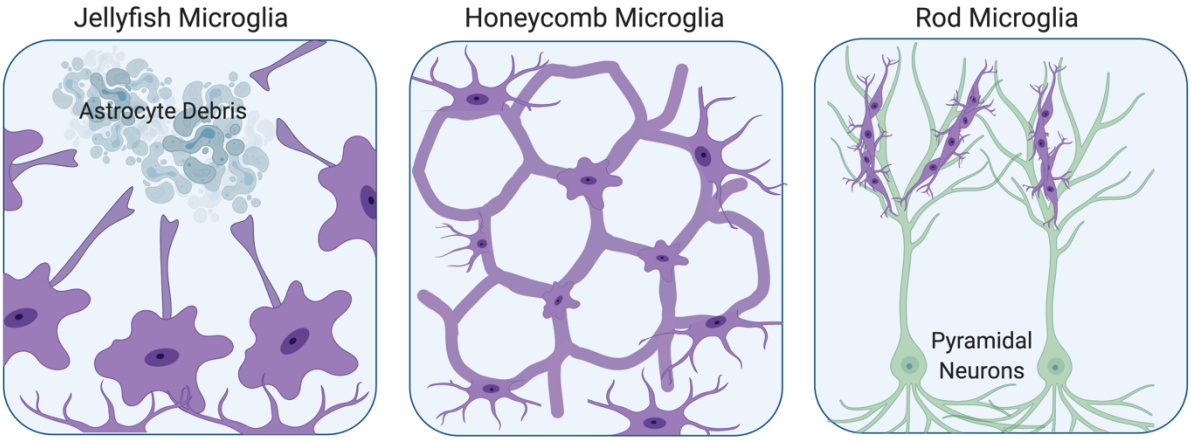

Figure 1.1. Morphological alterations in microglia following injury. Microglia adopt several unique morphological characteristics following brain injury, including the phagocytic jellyfish microglia, the network of honeycomb microglia, and the rod microglia that align with the apical dendrites of injured pyramidal neurons. Microglia begin altering their morphology from a ramified state within minutes of injury.

While the initial response of microglia to injury is generally thought to be beneficial, their long-term response has been more widely debated. Microglia lose their ramified, highly branched nature when they become activated, and adopt a more compact morphology [23]. Microglia have been shown to remain activated for years following brain injury, with some studies showing heightened activation even decades later [22, 24, 25]. Chronic inflammation after brain injury can lead to dendritic spine loss and other neuronal alterations that are spread throughout the brain and are evident greater than a year after injury [26]. Consequentially, chronic immune activation has been thought to contribute to the elevated risk for neurodegenerative diseases, dementia and psychiatric diseases that follows brain injury [7, 27-37].

More recently, microglial signatures that appear to be common among several neurodegenerative diseases have been identified and characterized. Microglia that proceed through two stages of "disease-associated" genetic signatures are termed "Disease-Associated Microglia" (DAM) [38-40]. The first stage results in the downregulation of homeostatic markers characteristic of microglia including *P2ry12*, and *Tmem119*, and the upregulation of inflammatory markers including *Tyrobp, Ctsb, Ctsd*, and *Apoe* [38]. The second stage, which is *Trem2* dependent, results in the upregulation of other genes important for activation and phagocytosis including *Trem2, Csf1, Itgax* and *Clec7a* [38]. This response is shared amongst Alzheimer's disease, aging and amyotrophic lateral sclerosis disease models, and appears to be at least partially conserved following injury [38]. One group examined microglia by single cell and bulk RNA sequencing in 141 neurosurgery patients, 54 of which experienced hemorrhage or trauma [41]. Two populations of microglia were identified to be largely unique to individuals with acute brain injury, and featured microglia that had an upregulation of inflammation associated genes (including *IL-1β, CCL3, NFkB, STAT3, RUNX1*), stress induced senescence, DNA damage (*HIST1H2BG*), proliferation, and chemotaxis (*FLT1, CCL4*) [41]. They found that the microglia examined in these patients had a partial overlap with the previously described DAM phenotype [41]. Whether this common microglial signature is beneficial or harmful in these different disease contexts has been widely debated, and this same question must be assessed in the context of brain injuries.

In order to investigate the role of microglia after brain injury, multiple groups have utilized different pharmacologic and genetic approaches to delete microglia. Intriguingly, depletion of microglia following various types of CNS injury has shown mixed results, with some indicating depletion has little to no effect, others indicating depletion is actually detrimental to recovery and a few indicating that depletion can attenuate inflammation. These differences in results likely stem from the type, timing and duration of the depletion as well as the type and severity of CNS injury. In a controlled cortical impact mouse model of TBI, selective depletion of microglia using PLX6522, a

CSF-1R antagonist that induces death of microglia with little effect on circulating monocytes [42], did not have any effects on spatial learning and memory as assessed by the Active Place Avoidance (APA), Morris Water Maze (MWM) and Y-maze behavioral tests [43]. Furthermore, studies in the optic nerve have shown that depletion of microglia has no impact on survival of retinal ganglion cells after an optic crush injury, or in the regenerative potential of these cells after lens injury [44]. Alternatively, one study using a fluid percussion model of TBI in mice demonstrated a reduction of neuroinflammatory genes when microglial depletion occurred 14 days before injury and lasted 7 days post injury [22].

Multiple studies have reported that depletion of microglia may actually result in detrimental long term outcomes. A study examining closed-head injury in neonatal rats found that depletion of microglia using clodronate resulted in increased Fluoro-JadeB staining, indicating a larger area of disrupted neurons [45]. Microglia depletion after ischemic stroke in mice has also been shown to lead to a 60% increase in infarct size and increased neuronal death which can be attributed to dysregulated calcium responses [46]. Likewise, findings establish a protective role for microglia after adult spinal cord injury (SCI) as well; depletion of microglia following injury results in reduced neuronal survival and impaired locomotor recovery, while increased microglia proliferation reduced lesion size [47]. Interestingly, microglia are critical for spinal cord healing after a crush injury in neonatal mice; they create a conducive environment for axons to successfully regenerate through the injury site by secretion of fibronectin and a quick return to a homeostatic state [48]. Transplantation of neonatal microglia into adult mice with SCI was able to improve axonal regeneration and reduce scar formation [48]. The factors that differentiate neonatal microglia from adult microglia in injury repair processes are not fully understood, but determining the components of the microglial response promote successful healing after CNS injury will be important for developing targeted therapies.

Collectively, these findings indicate that total depletion of microglia following CNS injury is likely not beneficial. However, other studies highlight that long-term activation of microglia can be harmful. Therefore, creative approaches to modulate the microglial response to injury are required. Recent advances have shown that repopulation of microglia following depletion leads to a restoration of more homeostatic state and that this beneficial for behavioral and neuronal outcomes after brain injury [43, 49, 50] (Figure 1.2). Using both a genetic [51], and pharmacologic mechanism to transiently deplete microglia before TBI, Willis et al. found that repopulation of microglia after injury attenuated learning and memory deficits seen in the APA, MWM and Y-maze behavioral tests, and these benefits lasted out to 9 months post injury [43] (Figure 1.2). Interestingly, depletion and replenishment of microglia appears to increase hippocampal neurogenesis, which is generally decreased after TBI. Repopulation of microglia led to an increase in both hippocampal doublecortin-positive immature neurons and Tbr2-positive neural precursor cells [43] (Figure 1.2). These differences in neurogenesis were seen both when targeting microglia genetically through intra-peritoneal administration of diphtheria toxin (DT) and through local administration of DT to the hippocampus in CX3CR1cre^{ERT2} x iDTR mice. Moreover, the increased neurogenesis seen with repopulation of microglia after injury appears to be necessary for the improved behavioral outcomes seen in this paradigm [43]. Surprisingly, IL-6 was shown to drive both the improved neurogenesis and behavioral outcomes seen after injury with repopulating microglia [43]. Often thought to be part of the detrimental inflammatory response after brain injury [52, 53], IL-6 production by hippocampal granule cells stimulated by repopulating microglia may actually be critical for improved hippocampal neurogenesis after TBI [43].

Other similar studies also found that repopulation of microglia after injury resulted in beneficial neuronal effects [49, 50]. Henry et al. found that microglial depletion and repopulation a month after controlled cortical impact had beneficial effects on motor performance and memory on the balance walk, Y-maze and MWM behavioral tests, and resulted in reduced neuronal loss three

months post injury [49] (Figure 1.2). Additionally, in a murine model where withdrawal of doxycycline results in the expression of diphtheria toxin A chain in forebrain neurons and causes neuronal death, it was shown that repopulating microglia facilitated increased neuronal spine formation following injury [50] (Figure 1.2). These beneficial changes, demonstrated upon microglial repopulation, may stem from a disruption in the typical inflammation program after injury.

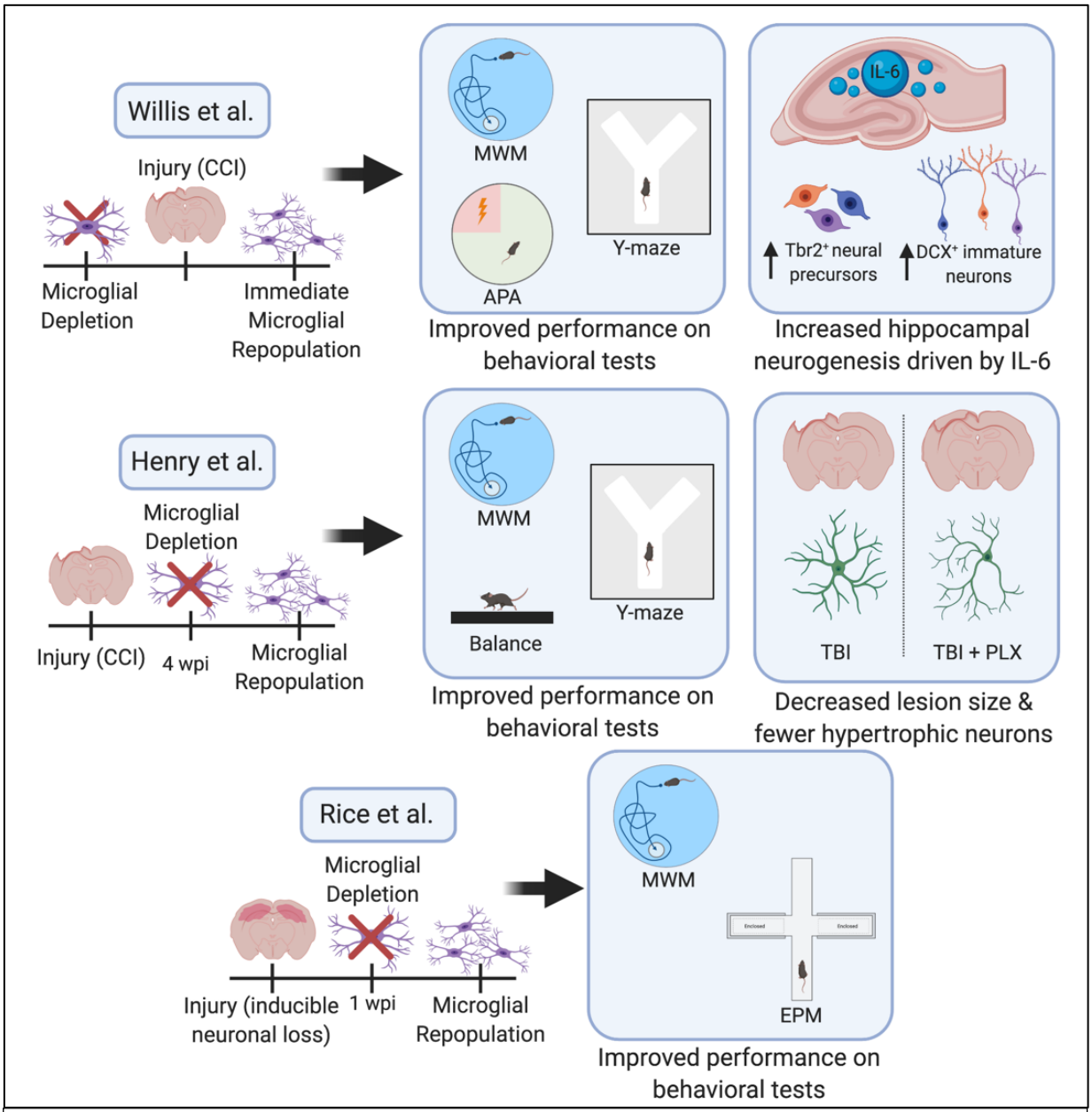

Figure 1.2. Microglial repopulation following brain injury. Several studies indicate that depletion and repopulation of microglia, rather than depletion alone, may lead to beneficial outcomes following brain injury. Following injury, animals that have experienced depletion and repopulation perform better on memory tasks (MWM, APA, Y-maze), anxiety-related tasks (EPM) and motor-coordination assessments (Balance beam), Additionally, in different contexts, they experience increased hippocampal neurogenesis and decreased lesion size. APA; active place avoidance, CCI; controlled cortical impact, DCX; doublecortin, EPM; elevated plus maze, MWM; Morris Water Maze, PLX; Plexicon, TBI; traumatic brain injury, wpi; weeks post injury.

While microglia may adopt an activated DAM-like signature following brain injury [38], the repopulating microglia have a substantially different gene signature including a downregulation in type I IFN pathways and an upregulation in genes important for wound repair [43]. Moreover, the gene signatures in the brain after microglial repopulation one month after injury show a reduction in genes important for oxidative stress, reduced inflammatory receptors and inflammation-associated genes, and decreased expression of caspases involved in apoptosis [49]. Together, these findings indicate that repopulating microglia may serve to "reset" the environment in the brain following injury by reducing inflammatory and stress responses.

While microglial repopulation does affect neurons and mouse behavior, it has not been shown to influence astrocyte reactivity [49, 50]. Microglia are capable of promoting astrocyte reactivity through the secretion of cytokines including IL-1α, TNF, and C1q [54]. These reactive astrocytes are present in multiple neurodegenerative diseases and may contribute to neuronal death [54]. However, both the number of $GFAP^+$ astrocytes and GFAP mRNA were substantially elevated after injury, regardless of microglia depletion treatments [49, 50]. Likely, infiltration of other immune cells and the intense inflammation following injury is sufficient to promote astrocyte activation without the requirement of additional microglia cytokines. In this context, it is clear that microglia repopulation following brain injury does not resolve all inflammation.

Interestingly, Willis et al. found that the beneficial timing of microglial repopulation appears to be limited to the days immediately following injury; repopulation before injury or later in the injury course did not have a beneficial effect [43]. Conversely, other groups found that microglial depletion and repopulation both a week and a month following injury resulted in beneficial behavioral outcomes [49, 50]. The timing of when microglial repopulation results in beneficial effects likely depends on various factors including TBI location, severity, and length of depletion. Additionally, it is known that many approaches that target microglia also affect other immune cells,

including macrophages [55]. Whether the benefits seen upon depletion and repopulation of microglia can be tied exclusively to microglia cannot yet be determined.

Overall, the emerging picture of microglia following CNS injury is complex. It is clear the microglia change their morphology and activation state to respond to brain injury. However, long-term activation and inflammation propagated by microglia may facilitate ongoing neuronal death and lead to increased risk for other neurodegenerative diseases. On the other hand, a complete lack of microglia does not appear to be beneficial, and can be harmful in some contexts. Depletion and repopulation of less-activated microglia following brain injury may serve as a middle-ground in terms of resetting the inflammatory response, while still allowing for microglia to perform the functions that render them necessary for healing. Further research is required to determine the most ideal timepoint for this repopulation and in which contexts it may be helpful.

1.2 Meningeal Involvement in Brain Injury

1.2.1 Meningeal Immunity

The meninges have emerged as an important interface between the brain and the immune system. They play critical roles in facilitating proper CNS development, modulating behavior, and regulating disease processes. The meninges consist of three layers: the pia, the arachnoid, and the dura mater, which contain different cell populations including fibroblasts, immune cells, blood vasculature, and endothelial cells [56]. The meninges develop alongside the CNS, and are critical for shaping brain development [57, 58]. Important signals released from the meninges in development, including all-trans retinoic acid, have been shown to be critical for corticogenesis [58]. Moreover, meningeal release of Cxcl12 is instrumental for proliferation of cerebellar

progenitor cells and proper spatial arrangements of granule cells in the cerebellum and hippocampus [59-62].

In adulthood, the meninges serve as an important source of cytokine signaling, often from immune cells that are not present in the brain in appreciable amounts under homeostatic conditions [63, 64]. Some cytokine signaling, including production of IFN-γ, IL-4, and IL-17a by resident T cells in the meninges, has been shown to be important for normal behaviors. IFN-γ is important in maintaining social behavior networks, whereas IL-4 has been implicated in positive performance in learning and memory cognitive tests [63, 64]. Meningeal γδ T cell production of IL-17a is important for modulating anxiety-like behaviors and memory [65, 66]. Alternatively, other cytokines, including TNF, IL-1β, and IL-6 have been linked to poor cognitive performance in certain instances [67, 68]. Interestingly, these cytokines are often found upregulated after brain injury [11, 12].

One of the first indications implicating the meninges in the response to brain injury is that meningeal enhancement with post-contrast fluid attenuated inversion MRI can be seen in 50% of patients with mild TBIs and no apparent parenchymal damage; one of the few signs of mild TBI that can be detected by modern imaging techniques in human patients [15]. This enhancement seen on contrast-enhanced MRI has been shown to occur within minutes of injury [69]. Moreover, many individuals who experienced mild TBIs still experienced extravasation of contrast into the sub-arachnoid space, indicating that the blood-brain-barrier is compromised [69]. While 83% of patients experienced resolution in meningeal enhancement, on average, 19 days after injury, 17% had persistent enhancement 3 months post-injury, indicating that some patients experienced prolonged periods without complete meningeal repair in mild TBI [70]. The factors that influence this differential response to mild head injury are just beginning to be understood.

Experimental animal models of TBI have clearly demonstrated that the meninges are exquisitely sensitive to injury; even mild compression injuries result in death of meningeal macrophages and disruption of the glial limitans [10, 15]. Different layers of the meninges appear to respond in unique ways to injury. For instance, the blood vasculature within the dura regenerates within 7 days of injury, whereas regeneration in the pia and the brain seems to proceed much more slowly [71]. It is unclear whether revascularization within the pia and brain returns to completely normal levels [71, 72], and which factors influence in this differential revascularization ability. One study points to VEGFR2 signaling in endothelial cells as the critical mediator for revascularization after injury in all meningeal layers [71], whereas other findings point to the meningeal macrophages in promoting angiogenesis [70]. While meningeal macrophages have been shown to be important for beneficial revascularization after TBI [70], they are also some of the first sources of alarmins and ROS generated after injury [10, 15]. Recent studies show a heterogeneous population of meningeal macrophages likely accounts for these differing responses; $CD206^+$ non-classical monocytes seem to promote angiogenesis, whereas a $CD206^-$ population of inflammatory macrophages cluster at the injury site. Overall, the layer of the meninges, the heterogeneity of each meningeal cell population, and the temporal progression of the immune response drive a very complex response to brain injury. More studies are needed to investigate this heterogeneous tissue both in homeostasis and in response to TBI and stroke.

1.2.2 Meningeal Lymphatics

Until recently, how the brain parenchyma and meningeal compartment communicated with the peripheral immune system was poorly understood. While the lymphatic vasculature in the meninges was first described in the 1780s by Paolo Mascagni [73], and other evidence of CSF drainage to cervical lymph nodes was established in the early 1990s [74, 75], it was not until recently that landmark studies began to unveil their function and anatomy [76, 77]. These

lymphatic vessels drain cerebrospinal fluid (CSF), interstitial fluid (ISF), CNS-derived molecules, and immune cells from the brain and meninges to the deep cervical lymph nodes (dCLN) [76-85], which reside in the periphery. The meningeal lymphatic network development in mice begins postnatally, and does not reach completion until 28 days post birth [78], however, more murine and human studies are needed to determine when the vessels are actually functional in draining CSF and other CNS elements to the periphery. Importantly, studies using *in vivo* magnetic resonance imaging (MRI) techniques have also identified the existence of meningeal lymphatic vessels in both humans and nonhuman primates [86, 87]. The recent findings surrounding the meningeal lymphatic system have opened new doors for understanding how brain injury influences the immune system, and vice versa. The ability of these meningeal lymphatic vessels to facilitate traffic of immune cells from the CNS to the periphery leads to the intriguing question of how these vessels play a role in injury states.

Recently, new research has implicated the meningeal lymphatic system in the pathogenesis after brain injury [88, 89]. One recent study found that the lymphatic system was critical for clearing extravasated blood after sub-arachnoid hemorrhage (SAH) [88], and that pharmacologic ablation of the meningeal lymphatic system before SAH resulted in a lack of drainage of erythrocytes [88] (Figure 1.3). This study implicates that backup of potentially harmful cells and inflammatory products from injury-induced dysfunction of the lymphatic system can contribute to injury-related pathology. Indeed, other studies demonstrated that after TBI, drainage of microbeads to the dCLN was significantly reduced and this reduction in drainage lasted months after even a mild injury [89]. Moreover, in the case of TBI, the reduction in lymphatic drainage could be attributed to, at least in part, increased intracranial pressure [89]. However, the reductions seen in lymphatic flow and drainage of products within the CSF to the dCLN can likely be attributed to more than one aspect of injury. A combination of increased intracranial pressure, buildup of inflammatory cells, erythrocytes, and debris that must be cleared from the CNS, and damage to the lymphatic

vasculature from the injury may all converge to cause lymphatic dysfunction in the context of brain injury. Further research is needed to delineate the contributions of these factors after injury and in different injury contexts.

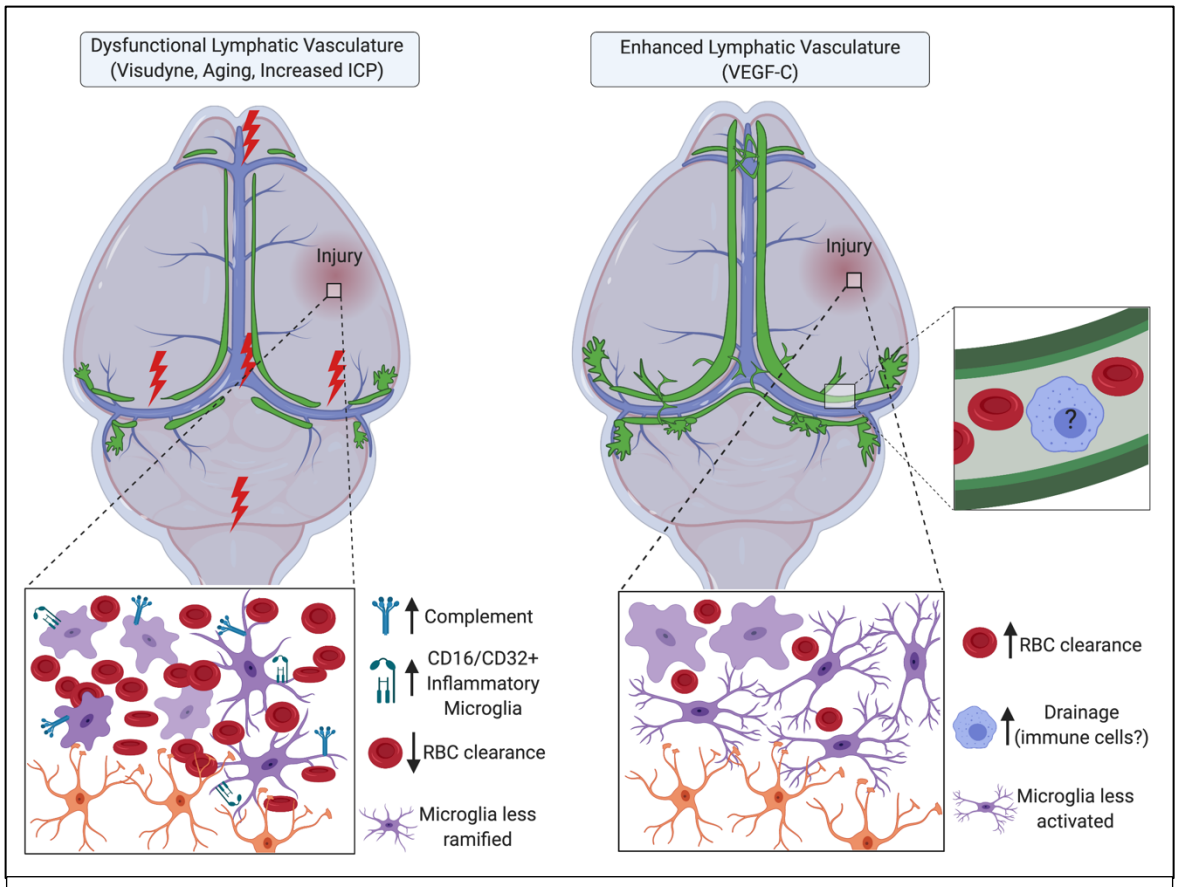

Figure 1.3. Meningeal lymphatic involvement in traumatic brain injury. Disruption or dysfunction of the meningeal lymphatic system has been shown to lead to increased inflammation following brain injury, including increased complement, activated microglia and decreased red blood cell clearance. Enhancement of the meningeal lymphatic system has demonstrated opposite effects. ICP; intracranial pressure, RBC; red blood cell, VEGF-C; vascular endothelial growth factor-C.

Dysfunction of the lymphatic system before brain injury, as can be seen in individuals with a recent history of a previous brain injury or in aged individuals, can lead to more severe outcomes after brain injury. Both in the context of SAH and TBI, more severe inflammation unfolds [88, 89]. With pharmacologic ablation of the dorsal meningeal lymphatics before SAH, there was an increase in the proportion of $CD16/32^{+}$ proinflammatory microglia as compared to anti-inflammatory $CD206^{+}$

microglia [88] (Figure 1.3). In the context of TBI, lymphatic ablation before injury lead to heightened activation of the adaptive and innate immune systems, especially the complement system, and increased gliosis when compared to mice that suffered from TBI without lymphatic dysfunction [89] (Figure 1.3). Furthermore, after brain injury, findings have consistently demonstrated that impairment of the lymphatic system can lead to cognitive deficits and other detrimental behavioral outcomes. It appears that disruption of the lymphatic drainage also leads to behavioral deficits, including increased anxiety after SAH [88], and impairments in memory and learning after TBI [89].

The role that the meningeal lymphatic system plays in development of adaptive immunity after brain injury and potentially autoimmunity has not yet been fully elucidated. Recent studies have established the meningeal lymphatic system as critical for immune responses to brain antigens, which in certain cases can be beneficial or detrimental to overall health. For instance, delivery of VEGF-C to the lymphatic vasculature to cause growth results in a stronger immune response to glioblastoma as compared to a sham intervention [90]. This leads to an overall increase in survival in the mice with glioblastoma, whereas mice without VEGF-C all succumbed to the disease within 40 days. Interestingly, when used in combination with anti-PD-1, VEGF-C seemed to have synergistic effects in increasing overall survival and decreasing tumor burden [90]. This study links improved lymphatic drainage with the recruitment of more antigen-specific T cells, which are important for combating glioblastoma cancer cells [90]. Conversely, in instances of autoimmunity, like multiple sclerosis (MS), increased antigen presentation to immune cells in the periphery is not desired. Indeed, studies have shown that ablation of the dorsal meningeal lymphatic system was sufficient to reduce $CD4^+$ T cell infiltration to the spinal cord in the context of experimental autoimmune encephalomyelitis (EAE) [91]. Moreover, other findings demonstrate that lymphangiogenesis near the cribriform plate in EAE is a hallmark of disease progression, and suggest that this may augment the peripheral adaptive immune response to myelin peptides [92].

These recent findings implicating the meningeal lymphatic system in peripheral immune cell activation to brain antigens highlight the need for further information of the meningeal lymphatic system's role in adaptive immunity after brain injury. Brain antigens were present in peripheral lymph nodes in both human and mice after stroke and other conditions such as MS [93-96], and studies have found a systemic response to brain injury highlighting various levels of connection between the CNS and the PNS [97]. The presence of brain-specific antigens in the peripheral lymph nodes suggests the meningeal lymphatic system may be playing a role in priming an immune response to brain-derived antigens, and thus promoting autoimmunity. Indeed, there is a higher risk of developing MS after a TBI than compared to the rate in the general population [98, 99]. While the findings are still preliminary, one pre-print study shows that in mice lacking lymphatic vasculature in several organ systems, including the meninges, there is a significant reduction in $CD4^+$ T cells infiltrating into the brain [100]. In general, T cell infiltration into the brain after injury is detrimental for long-term outcomes. Depletion of $CD8^+$ T cells in a mouse model of TBI was shown to improve neurologic outcomes and promote a more neuroprotective immune response [101]. In the context of stroke, $CD4^+$ T cells also play detrimental roles in recovery, and $CD4^+$ T cell deficiency attenuates negative outcomes after stroke [102, 103]. Therefore, while the disruption in meningeal lymphatic flow seen after brain injury may be detrimental in the initial immune response to injury [89], it may also serve to prevent too strong of an adaptive immune response to brain-derived antigens. Along these lines, a recent study showed that lymphadenectomy of the superficial cervical lymph nodes reduced stroke infarct volume, suggesting that elimination of the brain-to-periphery signaling axis was capable of preventing worsened long-term outcomes [79]. Further research is needed to explore the role of the meningeal lymphatic system in development of adaptive immunity to brain-derived antigens after brain injury, and whether this contributes to autoimmunity.

Interestingly, several studies have now indicated that brain injury may result in lymphangiogenesis in both the cervical lymph nodes and the dorsal meningeal vasculature [79, 89]. Just three hours after middle cerebral artery occlusion in a mouse model of stroke, the lymphatic vasculature in the cervical lymph nodes had increased, and this lymphangiogenesis was maintained 24 hours post stroke. Moreover, inihibition of signaling through VEGFR3 not only blocked the lymphangiogenesis, but also decreased the number of proinflammatory macrophages present in the brain following focal cerebral ischemia [79]. This suggests that the lymphangiogenesis seen in the cervical lymph nodes may be necessary for mounting a full immune response. Furthermore, lymphangiogenesis of the dorsal meningeal lymphatic vasculature was seen one and two weeks after injury, but returned to the levels of uninjured mice by one- and two-months post injury [89]. How the dorsal meningeal lymphatic lympangiogenesis is contributing to immune responses remains to be elucidated.

Overall, it is apparent that the lymphatic system is both affected by brain injury and also influences outcomes after brain injury. More research is needed to determine which specific cells, molecules and debris the lymphatic system drains post-brain injury, how this system is affected after injury in different individuals, and more broadly, how this system is affected in humans.

1.3 The Pathogenesis of Brain Injury in Aging

Stroke and TBI commonly affect elderly populations [2, 104-106], and evidence clearly indicates that the elderly experience worse outcomes, including higher mortality rates, when compared to younger counterparts affected by similar strokes or TBIs [2, 104, 106-108]. In murine experiments, aged mice have larger lesion sizes, fail to stabilize weight loss as quickly as their younger counterparts, and perform more poorly on several behavior tests assessing locomotion and anxiety [109-111]. Advances into understanding the pathogenesis of brain injury in the elderly

have broadened our understanding of how the aged brain is unique in its response and have provided valuable insight into potential treatment options.

The aged brain, outside of injury or disease, already exhibits widespread changes when compared to the young brain. It is well known that the aged brain exhibits decreased neuronal activity and fewer synapses than a younger brain [112]. Additionally, the glial cells of the aged brain, astrocytes, microglia and oligodendrocytes, all display altered gene expression and upregulation of genes important for orchestrating the common inflammatory pathways [39, 113-116]. For instance, astrocytes upregulate genes important for inflammation and reactivity, and in turn, these same processes can be damaging to neuronal synapse maintenance [114]. Microglia accumulate lipid droplets in aging, and these lipid-laden cells have poor phagocytosis capabilities and are prone to production of reactive oxygen species (ROS) and proinflammatory cytokines

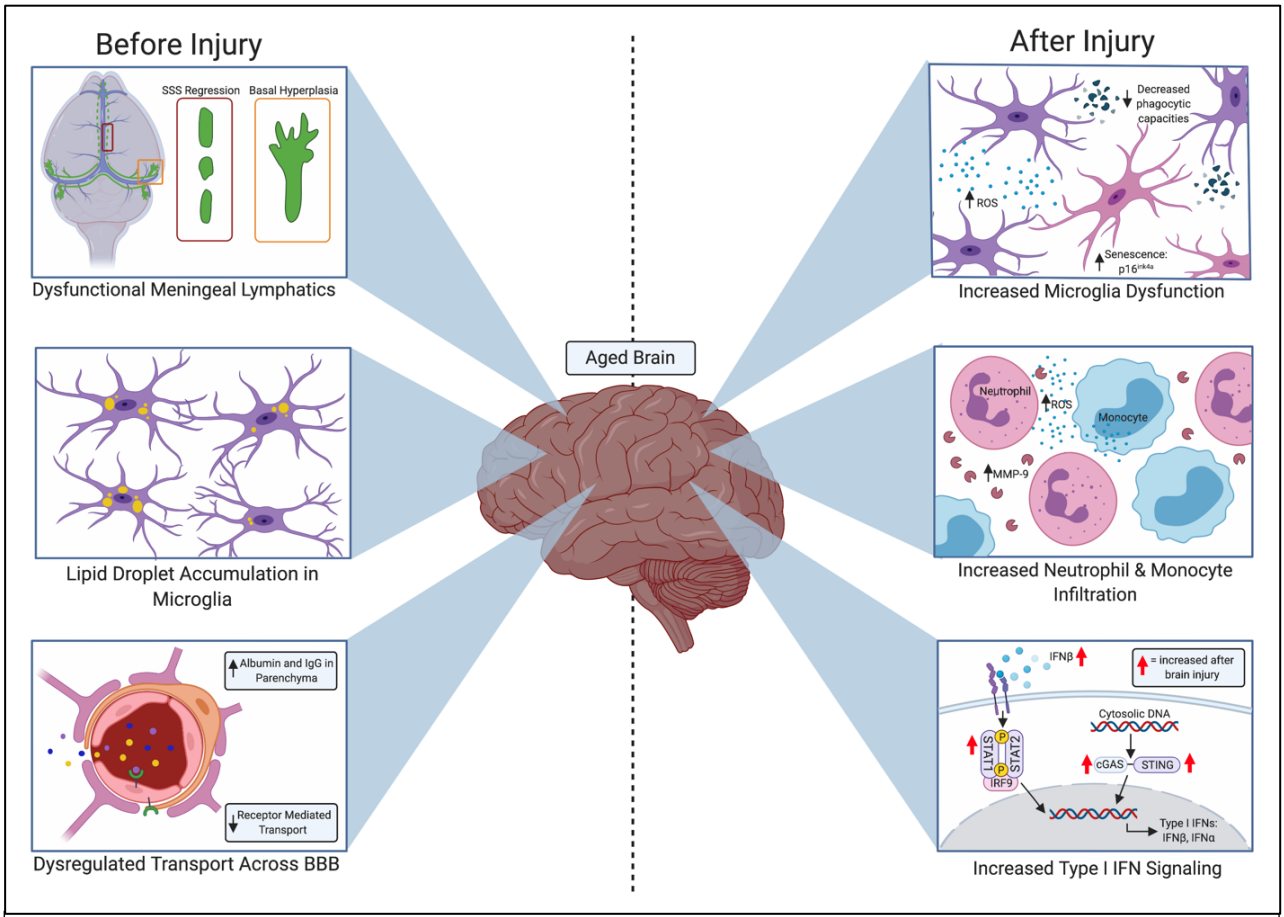

Figure 1.4. The aged brain before and after brain injury. The aged brain exhibits alterations both before and after injury. At baseline, aged mice experience a dysfunctional meningeal lymphatic system, lipid droplet accumulation in microglia, and altered blood brain barrier transport. Following injury, aged mice experience dysfunctional microglial phagocytosis and senescence, increased peripheral immune cell recruitment and production of reactive oxygen species and an upregulation of type I IFN signaling. All of these changes likely contribute to the increased negative outcomes aged individuals experience as compared to young individuals.

[117] (Figure 1.4). In addition to glial cell upregulation of inflammatory signatures, the aged choroid plexus also is the source of heightened production of type I interferons; contributing to cognitive decline and memory deficits [118]. Moreover, recent findings indicate that there are substantial changes in the blood brain barrier (BBB) dynamics in aging; young mice have substantial amounts of receptor-mediated transcytosis across the BBB, while aged mice have less receptor mediated transport, but more indiscriminate permeability to large and neurotoxic proteins [119] (Figure 1.4). All of these changes prime the aged brain to a more inflammatory state, which likely influence how the response to injury unfolds after stroke or TBI.

1.3.1 Type I Interferons

When examining how the aged brain responds to injury, one study showed that the transcriptional response to stroke in aged mice is of a greater magnitude than in young mice, including a substantial upregulation of genes involved with type I interferon (IFN) signaling and the cell cycle [113]. This age dependent increase in interferon stimulated genes (ISGs) was STAT-dependent and also detectable at the protein level by mass spectrometry [113] (Figure 1.4). Type I IFN induction occurred at earlier timepoints after stroke in aged mice as compared to young mice, and while endothelial cells express type I IFN related genes under homeostasis, microglia and oligodendrocytes seem to be the main brain-resident drivers of the increased ISGs after stroke [113]. More research is required to determine whether non-brain-resident populations contribute to this type I IFN response, including infiltrating leukocytes and cells residing in the meninges.

Consistent findings in young mice point to type I IFN signaling as detrimental to outcomes after both stroke and TBI [120-124], indicating that this heightened type I IFN signature seen in aging may explain some of the particularly devastating outcomes seen in the elderly after brain injury. Genetic abrogation of IFNAR1 in young mice decreased infarct size after stroke and improved neuronal survival [122], suggesting that an upregulation of type I IFN signaling after injury is detrimental to outcomes. Indeed, Irf9, an interferon regulatory factor (IRF), was shown to directly cause neuronal death after ischemic stroke in young mice through upregulation of death signaling pathways [120]. In the context of TBI, type I IFN signaling components, including cyclic GMP-AMP synthase (c-GAS), stimulator of interferon genes (STING), STAT1 and IFN-β were all found to be upregulated following injury in young mice [121]. This upregulation of IFN-β was also seen in post-mortem tissue from human patients six hours after TBI, in the brain hemisphere affected

by TBI [124]. In young mouse experiments, blocking IFN-β signaling resulted in a dampened neuroinflammatory response, improvement in motor coordination as assessed by the beam walk, and improved memory at 18 days post injury as assessed by the novel object recognition test [121]. Overall, mice lacking IFN-β signaling or STING signaling had a smaller lesion volume after TBI [121, 123], and had less hippocampal neuronal loss [121]. Unfortunately, these type I IFN signatures persist for months after injury; several ISGs and STING remained elevated 60 days post-TBI [121], and other immune responses associated with type I IFN signaling are still upregulated in microglia at 90 days post injury [125]. While some of these findings regarding the detrimental nature of type I IFN signaling are in young mice, it can be extrapolated that the heightened type I IFN response in aged mice may be equally, if not more, dangerous. Future research is required to determine this more definitively. Put together, these findings indicate that increased type I IFN signaling may contribute to the more severe pathologies and negative outcomes seen in aged mice as compared to young mice after brain injury.

1.3.2 Cellular changes after brain injury

Several studies highlight changes in microglia as a driver of the differences in the aged-brain response post injury. Microglia in aged mice proliferate to a greater extent after TBI and secrete more ROS when compared to microglia in young mice [109]. While ROS have generally been found to be detrimental after TBI regardless of age [10, 15], studies show that the neurons within the aged brain are particularly sensitive to ROS and die more frequently upon exposure to ROS [126-128]. Aged mice after stroke also had significant upregulation of genes related to lipid metabolism after stroke as compared to young mice. Moreover, microglia in aged mice have impaired phagocytic capabilities [109] (Figure 1.4). Whether this upregulation in lipid processing after stroke and the decreased phagocytic capabilities after TBI in aged mice relates to the

dysfunctional lipid-laden microglia described by Marschallinger et. al remains to be seen [117]. Moreover, while microglia in aged mice exhibit up-regulation of senescence markers in homeostasis, their expression of these senescence markers, including $p16^{ink4a}$, greatly increases after injury [109] (Figure 1.4) Overall, senescent cells tend to impair normal functioning of a tissue or organ and are resistant to apoptosis, which may enable these cells to respond to injury in an inflammatory manner for a prolonged period of time and to contribute to the chronic immune dysregulation seen in aged mice [129].

In addition to the changes seen in the aged microglial response, genes related to neuronal synaptic plasticity and synaptic signaling were more highly downregulated in aged mice after stroke as compared to younger mice [113], indicating neuronal changes as well. Using a transcriptional deconvolution program to gain insight into cell type alterations, this study showed a downregulation in parvalbumin-positive (PV^+) GABAergic interneuron markers after stroke that was greater in aged animals as compared to their younger counterparts [113]. PV^+ neurons are important for maintaining cortical plasticity, and this reduction in PV^+ neuron marker expression may correlate with worsened outcomes in aging. Additional evidence points to ongoing neuronal degeneration in aged mice even after a TBI at a younger age. In a closed-skull murine model of TBI, dendritic spine density continued to decrease with age in the hippocampus [26]. While a loss of dendritic spines in the ipsilateral hemisphere was observed both one week and 1.5 years after injury, a reduction of dendritic spines in the contralateral hippocampus that was not present initially was apparent 1.5 years after injury [26]. This indicates that the aged brain continues to undergo processes after a TBI that are detrimental to neuronal health, which may provide insights into the link between TBI as a risk factor for Alzheimer's disease and dementia [4, 29-31, 35, 36, 130].

Several studies have indicated a higher frequency of peripheral cell infiltration into the aged brain after injury. After stroke, a transcriptional analysis of the mouse brain indicates an increased presence of peripheral immune cells in the aged mice as compared to the young mice [113]. These findings are consistent with murine TBI models that find that the total number of infiltrating leukocytes is drastically increased in the aged mice as compared to the young mice, and that the aged mice tend to exhibit a bias towards neutrophil recruitment [109]. Higher amounts of neutrophils are found in the systemic circulation after stroke in aged mice, and more severe neutrophilia is associated with more severe neurological deficit scores [131] (Figure 1.3). Neutrophils make up a higher proportion of the infiltrating cells in aged mice as compared to young mice, whilst young mice experience a monocyte predominance in the infiltrating leukocyte population after stroke [131]. The neutrophils recruited to the injury site in aged mice also possess a higher preponderance for ROS and matrix-metalloproteinase (MMP) production than in younger mice [131], again contributing to a more highly inflammatory environment (Figure 1.3). Moreover, the findings of increased neutrophils in murine mouse models of stroke were also confirmed in human patients [131]. Older individuals had more neutrophils, higher expression of matrix metalloproteinase-9 (MMP-9), and this higher expression of MMP-9 was associated with increased instances of hemorrhage and hyperemia [131]. Overall, this greater peripheral infiltration likely stems from a combination of the baseline changes seen in BBB transport and selectivity [119], and an increase in chemotactic signals that occur with aging [131-133], amongst other factors.

Increases in both CCL5 and CCL2, ligands for CCR2 and CCR5, and important chemokines involved in leukocyte migration, were seen at higher levels in aged mice after stroke and TBI, and likely contribute to the increased leukocyte infiltration [111, 131, 132]. Indeed, CCR5 inhibition results in less $Ly6C^{lo}$ macrophage recruitment after stroke [133], and lower monocyte/macrophage infiltration has been associated with improved motor recovery [134, 135].

Findings in aged mice after TBI show an increased number of $CCR2^{+}$ monocytes in aged mice as compared to young mice [132], supporting the previous findings of increased chemokine signaling.

In addition to its role in leukocyte chemotaxis, CCR5 has been shown to play an important role in memory and synaptic plasticity [136]. Inhibition of CCR5 enhances learning and memory potentially through increasing hippocampal plasticity [136]. Conversely, overexpression of CCR5 resulted in memory deficits [136]. Interestingly, while homeostatic neurons do not express CCR5, cortical neurons greatly upregulate CCR5 after stroke and maintain this upregulation up to 28 days post injury [133]. Moreover, when CCR5 was antagonized using the FDA-approved drug, maraviroc, mice exhibited significantly improved motor control after stroke compared with control groups with intact CCR5 signaling [133]. The same study showed maraviroc treatment after TBI resulted in better performance on memory tasks, highlighting the conserved nature of CCR5 across brain injuries [133]. CCR5 inhibition results in an increase in both the survival of dendritic spines and formation of new spines after stroke and an increase in axonal sprouting to the contralateral hemisphere, which has shown to be important for long-term recovery after brain injury [133, 137, 138]. Interestingly, axonal sprouting and regeneration appears to be less effective in aged mice [137], suggesting that CCR5 inhibition may be of particular relevance for treatment in an aged population. To determine whether inhibition of CCR5 signaling might have clinical relevance, Joy et al. examined patients with the CCR5-Δ32 mutation, which results in a loss of function in CCR5 signaling [133]. While all patients had similar scores at baseline in Neurotrax cognitive assessments, the patients with the CCR5-Δ32 mutation showed better performance in memory, verbal function, attention and total cognitive scores one year after stroke [133]. In summation, signaling through the CCR5/CCL5 axis may result in detrimental outcomes, particularly for aged mice, both through the increased recruitment of peripheral immune cells to

the cite of injury and also through the decreased plasticity of neurons. Furthermore, findings suggest that targeting CCR5 may serve as a viable therapeutic opportunity to improve long-term outcomes in patients after stroke or TBI. Targeting this axis in aged individuals may be even more important, as these signaling molecules are more highly upregulated with increased age.

1.3.3 Aging in the meningeal lymphatic system

In addition to the inherent differences in the manner in which the aged brain responds to injury, there have also been several studies that have shown a decline in meningeal lymphatic function in aged mice [139-141] (Figure 1.4). While the dorsal meningeal lymphatic network becomes discontinuous as portions of the lymphatic tracts regress, the basal lymphatic network becomes hyperplastic and has fewer lymphatic valves [140]. Multiples studies have shown a decreased flow of various tracers out to the peripheral lymph nodes in aged mice, indicating that these morphological changes likely contribute to decreased function [139, 140]. Therefore, the question of how pre-existing lymphatic dysfunction before a brain injury affects subsequent outcomes is important for understanding how brain injury may differentially affect aged individuals.

Multiple findings have provided support for the idea that pre-existing impairment in lymphatic drainage could result in worse neuroinflammatory outcomes than in injury alone. Two studies have reported more activated and less ramified microglial populations in the context of pre-existing lymphatic dysfunction before brain injury [88, 89]. Additionally, RNA sequencing of the brain with pre-existing lymphatic dysfunction followed by TBI showed increased involvement of the complement system and other neuroinflammatory pathways when compared to TBI alone at both 24 hours and 1 week after injury [89]. These findings indicate that impaired lymphatic function before injury may contribute to the worsened outcomes commonly experienced by the elderly. Interestingly, one study showed that administering VEGF-C, a lymphangiogenic factor, to the

meningeal lymphatic vasculature in aged mice lessened gliosis after TBI [89]. This suggests that boosting lymphatic function in the elderly may actually serve as a protective measure against severe consequences of brain injury, as VEGF-C administration to the meningeal lymphatic vasculature in elderly mice resulted in improved cognitive performance [139]. Even outside of an injury context, this treatment could have potential benefits.

1.4 Concluding Remarks

The complex interactions between the brain and the immune system that occur after brain injury are not fully understood. However, recent findings have shed light on some of the cellular mechanisms that ensue after brain injury or stroke. Activation and involvement of both peripheral immune cells and brain-resident glial cells is both necessary for the response to the injury but can also result in secondary damage and long-lasting negative effects. Deeper understanding into the programmatic response of microglia to injury and neurodegeneration has led to new ideas to disrupt this chronic inflammation and activation. Depletion and repopulation of microglia is a promising strategy to reset a portion of the immune response following TBI. In multiple contexts, it has been shown to improve behavioral outcomes and neurogenesis. Furthermore, the repopulation strategy completely alters the transcriptional environment of the microglia and also of the surrounding brain.

In addition to the cellular responses in the brain, the immune response in the meninges has also been shown to be important in TBI pathogenesis. Meningeal macrophages are necessary for revascularization but are also key sources of ROS that are damaging. Further research is required to understand how the various cell populations in the meninges are responding to injury and stroke. Recent advances have shown that the meningeal lymphatic system that resides in the dura is important in shaping immune responses after brain injury. Impairments in this system

worsen initial inflammation both after TBI and SAH. How the meningeal lymphatic system affects adaptive immune responses following brain injury is still not understood and is an area that requires further investigation.

Finally, the aged brain presents a vastly different environment than the young brain. Aged individuals fair far worse than younger counterparts both in the contexts of brain trauma or stroke. Recent findings have highlighted important differences in the aged brain, both before and after injury, that likely contribute to the worsened outcomes following CNS injury. Differences in microglia phagocytosis, impaired meningeal lymphatic function, increased type I IFN signaling and increased peripheral immune cell infiltration following injury are just a few of these factors. A combinatorial approach to target multiple of these aspects may offer the best chance to improve outcomes following CNS injury in the elderly.

Overall, exciting new advances in the field of neuroimmunology have led to a better understanding of how the immune system and the brain are interacting following injury. It is clear that the immune response after injury is nuanced and that large scale manipulations of this response will likely not be beneficial across all injury contexts. However, targeted approaches to dampen portions of the immune response that may contribute to additional injury and neuronal death may serve as promising therapeutic targets for the future.

1.5 Overview of this dissertation

In this dissertation, we utilize innovative approaches to manipulate the meningeal lymphatic system in order to study this system in the context of traumatic brain injury. Moreover, we use high-throughput sequencing techniques in order to understand more about the response of the meningeal tissue following TBI.

In this chapter, we provided an introduction highlighting the most recent advances in the field of neuroimmunology and how these advances are shaping our understanding of the CNS response to brain injury. In Chapter 2, we discuss how the meningeal lymphatic system can be disrupted by traumatic brain injury, and how this can contribute to differences in the immune response following injury. We also study how manipulations of the meningeal lymphatic system can modulate inflammation in the brain.

In Chapter 3, we bring together the findings from our work and work from others to begin to discuss the implications of the lymphatic system in modulating disease and what future directions arise from these findings. Additionally, we highlight areas that require further research and begin to address some of these outstanding questions in the field including the following:

- What mechanistically underlies the ability of brain injury to increase one's risk of developing neurodegenerative and psychiatric disease later in life?
- How does the meningeal tissue respond to brain injury both in young and aged mice?
- Does the meningeal lymphatic system play an important role in brain development?
- How does meningeal lymphatic dysfunction after brain injury affect neuronal health? Can some of the negative impacts on neurons after TBI be mitigated through boosting the lymphatic system?

These questions, amongst many others, are just some of the interesting directions which the research can continue in the future.

The work presented in this dissertation expands upon our understanding of how the immune system and the brain interact with each other in a disease context. We discovered an important role for the meningeal lymphatic system in modulating inflammation following TBI, which we believe could have important implications for developing new therapies for TBI patients in the

future. More broadly, this dissertation expands our understanding of the unique meningeal compartment, and how the rich immune environment within this tissue can influence the brain.

Chapter 2

Meningeal lymphatic dysfunction exacerbates traumatic brain injury pathogenesis

2.1 Forward

Traumatic brain injury (TBI) is a leading global cause of death and disability. In this chapter, we demonstrate in an experimental mouse model of TBI that mild forms of brain trauma cause severe deficits in meningeal lymphatic drainage that begin within hours and last out to at least one month post-injury. To investigate a mechanism underlying impaired lymphatic function in TBI, we examined how increased intracranial pressure (ICP) influences the meningeal lymphatics. We demonstrate that increased ICP can contribute to meningeal lymphatic dysfunction. Moreover, we show that pre-existing lymphatic dysfunction before TBI leads to increased neuroinflammation and negative cognitive outcomes. Finally, we report that rejuvenation of meningeal lymphatic drainage function in aged mice can ameliorate TBI-induced gliosis. These findings provide insights into both the causes and consequences of meningeal lymphatic dysfunction in TBI and suggest that therapeutics targeting the meningeal lymphatic system may offer strategies to treat TBI.

This work was published in *Nature Communications* in August 2020, with me as the first author [89]. I have adapted the text and figures from the publication for this Chapter. Below is the full citation and the contributions of the co-authors.

Ashley C. Bolte[1,2,3,4], Arun B. Dutta[3,5], Mariah E. Hurt[1], Igor Smirnov[1], Michael A. Kovacs[1,2,3,4], Celia A. McKee[1], Hannah E. Ennerfelt[1,6], Daniel Shapiro[1], Bao H. Nguyen[5], Elizabeth L. Frost[1], Catherine R. Lammert[1,6], Jonathan Kipnis[1,6], and John R. Lukens[1,3,4,6*]

[1]Center for Brain Immunology and Glia (BIG), Department of Neuroscience, [2]Department of Microbiology, Immunology and Cancer Biology, [3]Medical Scientist Training Program, [4]Immunology Training Program School of Medicine, [5]Department of Biochemistry and Molecular

Genetics, [6]Neuroscience Graduate Program, University of Virginia, Charlottesville, VA 22908, USA.

Author Contributions

A.C.B, J.K. and J.R.L. designed the study; A.C.B., M.E.H., I.S., E.L.F., C.R.L., C.A.M., M.A.K., D.S. and J.R.L. performed experiments. B.H.N. contributed to data analysis. A.C.B., A.B.D and J.R.L. analyzed data and wrote the manuscript; J.R.L. oversaw the project.

2.2 Introduction

Traumatic brain injury (TBI) affects millions of people worldwide each year [1]. TBI can cause debilitating impairments in motor function, cognition, sensory function, and mental health. In addition, mounting evidence indicates that having a history of TBI markedly increases the risk of developing numerous other neurological disorders later in life including *chronic traumatic encephalopathy* (CTE), Alzheimer's disease, anxiety, depression, and amyotrophic lateral sclerosis [4-7, 9]. Despite being a prevalent and pressing global medical issue, the pathoetiology of TBI remains incompletely understood and improved treatment options are desperately needed.

Tissue damage and cellular stress resulting from TBI incites activation of the immune system, which is intended to aid in the disposal of neurotoxic material and coordinate tissue repair [10, 11]. While immune responses can play beneficial roles in TBI, unchecked and/or chronic immune activation following brain trauma can lead to secondary tissue damage, brain atrophy, and eventual neurological dysfunction [10-15]. Notably, the inability to properly dispose of danger/damage-associated molecular patterns (DAMPs) such as protein aggregates, necrotic cells, and cellular debris is widely thought to be a pivotal driver of both persistent and maladaptive immune activation in numerous neurological disorders [142, 143]. In the case of central nervous system (CNS) injury, inefficient removal of DAMPs has been proposed to perpetuate neuroinflammation and incite secondary CNS pathology and neurological complications [11, 142]. However, we currently lack complete knowledge of the drainage pathways that the brain relies on to dispose of DAMPs and resolve tissue damage following TBI.

Emerging studies over the last few years have shown that the meningeal lymphatics are centrally involved in the drainage of macromolecules, cellular debris, and immune cells from the brain to the periphery during homeostasis [76, 77]. The anatomy and function of this CNS drainage

pathway are just now being defined [76-78, 90, 91, 139, 140], and its role in many neurological diseases, including TBI, has not been elucidated. In recently published work, it was shown that these lymphatic vessels drain cerebrospinal fluid (CSF), interstitial fluid (ISF), CNS-derived molecules, and immune cells from the brain and meninges to the deep cervical lymph nodes (dCLN) [76-79]. Importantly, studies using *in vivo* magnetic resonance imaging (MRI) techniques have also identified the existence of meningeal lymphatic vessels in both humans and nonhuman primates [86, 87]. More recent studies have also shown that the meningeal lymphatic system is critical for clearing amyloid beta, extracellular tau, and alpha synuclein from the brain, and that disruption of this drainage system can promote the accumulation of these neurotoxic DAMPs in the brain [139, 144, 145]. Whether meningeal lymphatic dysfunction plays a role in TBI remains poorly understood.

Here, we explore how the meningeal lymphatics are impacted following TBI, and how possessing defects in this drainage system before brain trauma influences TBI pathogenesis. We find that TBI results in compromised meningeal lymphatic drainage that can last out to at least one month post-injury. Mechanistically, we report that increased intracranial pressure (ICP), which is commonly observed in TBI, can impair meningeal lymphatic drainage. We further show that pre-existing deficits in meningeal lymphatic function predispose the brain to exacerbated neuroinflammation and cognitive deficits following brain trauma. Lastly, we demonstrate that prophylactic recuperation of meningeal lymphatic drainage capabilities in aged mice with viral delivery of VEGF-C mitigates gliosis in TBI.

2.3 Results

2.3.1 TBI causes meningeal lymphatic dysfunction

To investigate whether meningeal lymphatic drainage function is impacted by TBI, we employed a mild closed-skull model of TBI that uses a stereotaxic electromagnetic impactor to deliver a single hit to the right inferior temporal lobe in the piriform region of the brain. This model is ideal for studying CNS lymphatic function because it does not rely on a craniotomy to perform the TBI and also does not result in a direct impact to the lymphatic vessels (Figure 2.1a). Following TBI, injured mice had an average righting time of 300 seconds post-injury, compared to the average of 30 seconds for the sham mice (Figure 2.1b), however TBI mice performed as well as sham mice in a series of behavioral tasks assessing injury-associated deficits in balance, motor coordination, reflex, and alertness (Figure 2.1c). In addition, brain injury in this model did not affect performance on an accelerating rotarod (Figure 2.1d) and brains from TBI mice only showed modest increases in measures of gliosis (Iba1 and GFAP staining) (Figure 2.2a,b). Together, these data indicate that this injury paradigm is relatively mild and does not result in noticeable behavioral deficits immediately after injury.

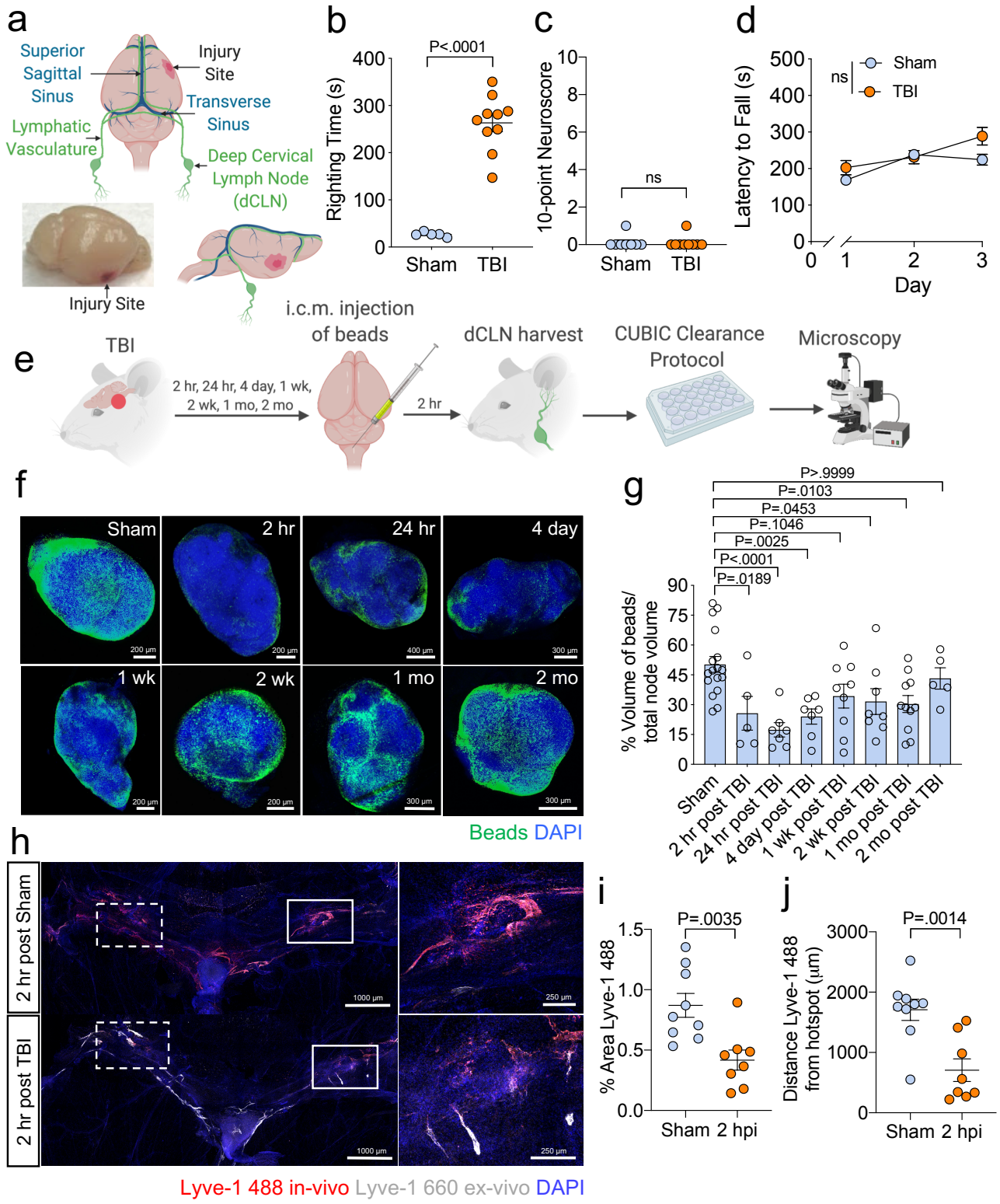
a
Superior Sagittal Sinus
Injury Site
Transverse Sinus
Lymphatic Vasculature
Deep Cervical Lymph Node (dCLN)
Injury Site
b
P<.0001
Righting Time (s)
Sham
TBI
c
10-point Neuroscore
ns
Sham
TBI
d
Latency to Fall (s)
ns
Sham
TBI
Day
e
TBI
2 hr, 24 hr, 4 day, 1 wk, 2 wk, 1 mo, 2 mo
i.c.m. injection of beads
2 hr
dCLN harvest
CUBIC Clearance Protocol
Microscopy
f
Sham
2 hr
24 hr
4 day
1 wk
2 wk
1 mo
2 mo
Beads DAPI
g
P>.9999
P=.0103
P=.0453
P=.1046
P=.0025
P<.0001
P=.0189
% Volume of beads/ total node volume
Sham
2 hr post TBI
24 hr post TBI
4 day post TBI
1 wk post TBI
2 wk post TBI
1 mo post TBI
2 mo post TBI
h
2 hr post Sham
2 hr post TBI
Lyve-1 488 in-vivo Lyve-1 660 ex-vivo DAPI
i
P=.0035
% Area Lyve-1 488
Sham
2 hpi
j
P=.0014
Distance Lyve-1 488 from hotspot (µm)
Sham
2 hpi

Figure 2.1. TBI leads to impairments in meningeal lymphatic drainage. a) Location of injury site in relation to the CNS lymphatic vasculature. b) Righting times of TBI and sham mice (Sham n=5, TBI n=10; representative data from 10 independent experiments). c) The 10-point gross neuroscore test 1 hour after TBI (Sham n=8, TBI n=9; representative data from 2 independent experiments). d) The accelerating rotarod behavioral test was used to assess motor function the first 3 days after TBI (n=10 mice per group; representative data from 2 independent experiments). e) Schematic of the experimental layout where mice received TBI and then were injected intra-cisterna magna (i.c.m.) with 0.5 μm fluorescent beads. f) Representative images and (g) quantification of bead accumulation in the cleared dCLN at 2 hours, 24 hours, 4 days, 1 week, 2 weeks, 1 month, and 2 months post TBI. Each data point represents an average of the 2 dCLNs from an individual mouse (Sham n=17, 2 hours n=5, 24 hours n=7, 4 day n=7, 1 week n=9, 2 weeks n=8, 1 month n=11, 2 months n=5; pooled data from 5 independent experiments). h) Representative images of meningeal whole mounts 2 hours after TBI stained for Lyve-1 488 (in vivo, red), Lyve-1 660 (ex vivo, grey), and DAPI (blue). Solid boxes show zoomed insets of the hotspots along the transverse sinus on the right. Dashed boxes indicate the other hotspots not featured in the inset. i) Percent area of Lyve-1 488 (in vivo, red) coverage at 2 hours post TBI or sham, and j) distance traveled of Lyve-1 488 staining along the transverse sinus 15 minutes after injection (Sham n=9, TBI n=8; pooled data from 2 independent experiments). All n values refer to the number of mice used and the error bars depict mean ± s.e.m. *P* values were calculated by two-tailed unpaired Student's t-test (b,c,i,j), repeated-measures two-way ANOVA with Bonferroni's post hoc test (d), and one-way ANOVA with Bonferroni's multiple comparison test (g). hpi, hour(s) post injury; hr, hour(s); mo, month(s); wk, week(s).

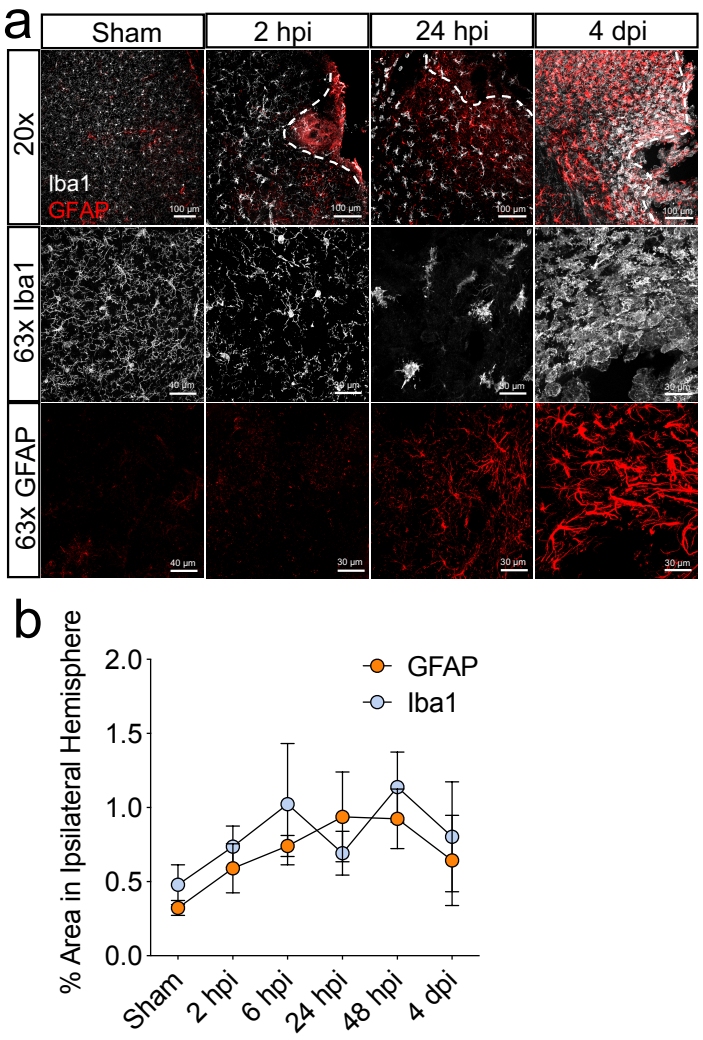

Figure 2.2. Mild closed-skull TBI results in modest increases in gliosis. Brains were harvested at various time points after TBI and stained for GFAP and Iba1. a) Representative images of immunofluorescence staining and b) percent area coverage of Iba1 and GFAP in the brain hemisphere containing the TBI lesion site (Sham n=4, 2 hours n=4, 6 hours n=2, 24 hours n=6, 48 hours n=2, 4 days n=2; pooled data from 2 independent experiments). Dashed lines indicate edge of lesion. All n values refer to the number of mice used and the error bars depict mean ± s.e.m. dpi, days post injury; hpi, hours post injury.

In order to assess whether meningeal lymphatic drainage is altered in this model of TBI, 0.5 μm fluorescent beads were injected intra-cisterna magna (i.c.m.) at various time points after injury and the dCLN, meninges, and brain were harvested 2 hours after injection to assess for the presence of beads (Figure 2.1e). Interestingly, when we examined cleared dCLN using confocal microscopy, we observed a substantial decrease in bead drainage to the dCLN in TBI mice as early as 2 hours post-injury (Figure 2.1f,g). Moreover, meningeal lymphatic drainage function remained significantly impaired out to one month post-injury (Figure 2.1f,g) and it was not until two months post-injury that bead drainage function returned to pre-injury levels (Figure 2.1f,g). Analysis of the brain and meningeal whole mounts revealed that the beads were taken up along the transverse sinuses as previously published [91], and were also detected around the fourth ventricle and in the cerebellum, both of which are areas close to the i.c.m. injection site (Figure 2.3a,b). However, we were unable to detect any appreciable number of beads in the systemic circulation even after TBI (Figure 2.3c,d). To evaluate whether severity of the TBI plays a role in the duration of meningeal lymphatic drainage deficits, we performed TBI in the same location but with a higher impact velocity (6.2 meters (m) per second (s)) than the TBI used for the rest of the studies (5.2 m per s). At one month post injury, we found that there was a noticeable trend towards decreased drainage in the mice that had received the higher velocity injury (Figure 2.4a-b), suggesting that meningeal lymphatic drainage capacity is also likely affected by injury severity.

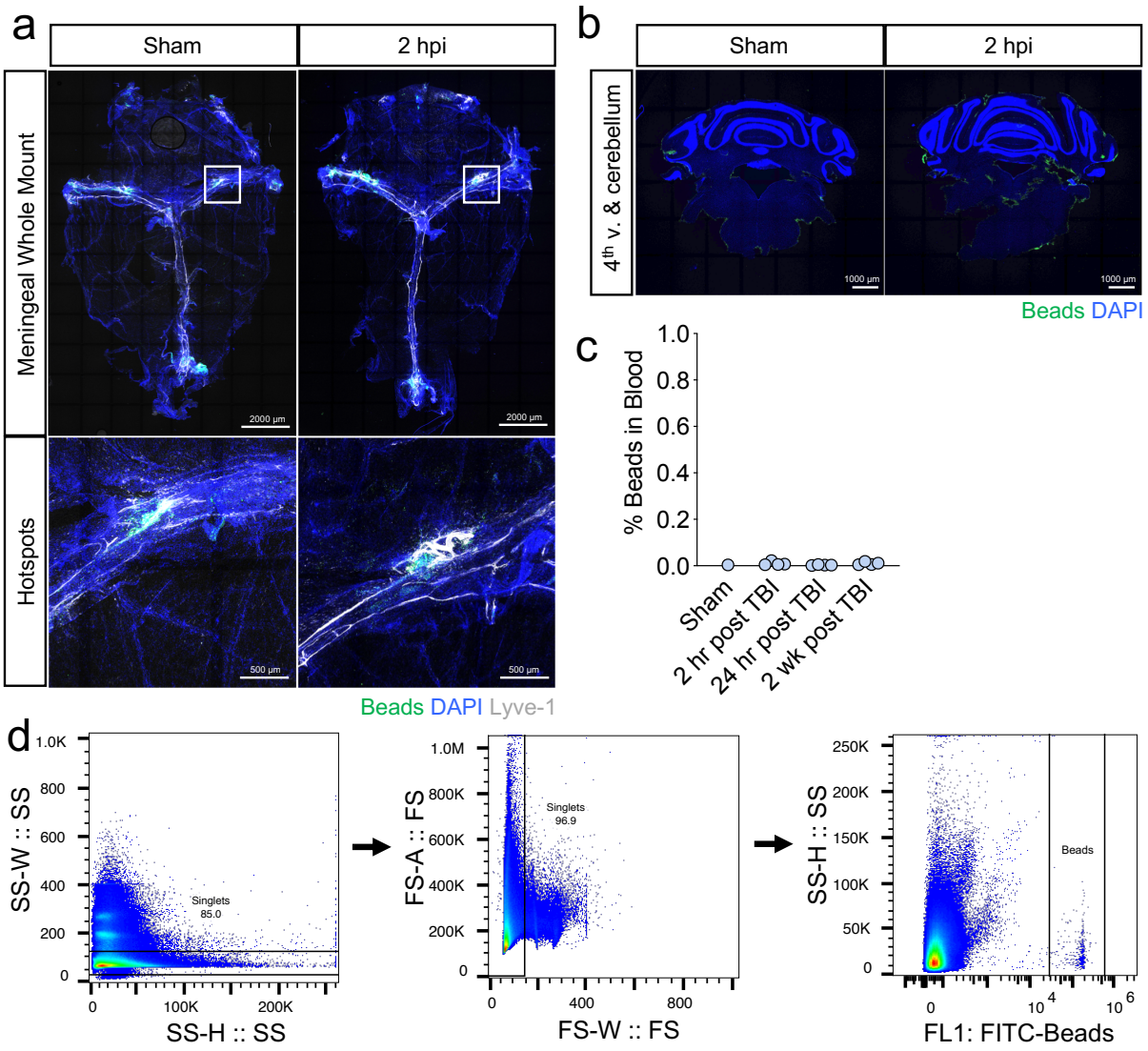

Figure 2.3. Bead localization following i.c.m. injection. Mice received TBI or sham treatment and then received 0.5 µm fluorescent beads (green) by i.c.m. injection 2 hours later. Meningeal whole mounts and brains were harvested 2 hours after injection. a) Representative images of meningeal whole mounts stained with DAPI (blue) and Lyve-1 660 (grey) after TBI or a sham procedure and fluorescent bead injection. Solid box shows inset of bead uptake at the hotspot along the transverse sinus. b) Representative images of fluorescent beads in the fourth ventricle (4^{th} v.) and cerebellum. Images (a,b) are representative of two independent experiments with similar results. c) Flow cytometry data depicting frequency of beads in the blood 2 hours, 24 hours, or 2 weeks post-TBI (Sham n=1, 2 hours n=4, 4 hours n=4, 2 weeks n=4; representative data from 2 independent experiments). d) Gating strategy for flow cytometry data to analyze the frequency of microbeads from total singlet events in blood. All n values refer to the number of mice used and the error bars depict mean ± s.e.m. hpi, hours post injury.

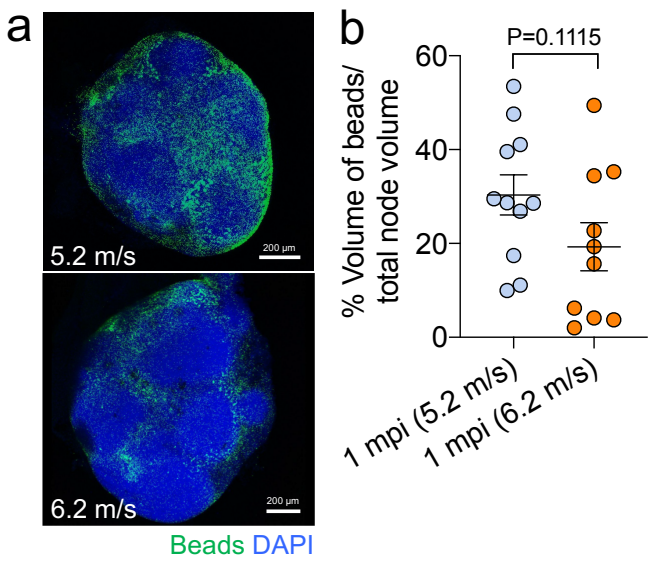

Figure 2.4. Higher velocity TBI negatively affects bead drainage. Mice received TBI with an impact velocity of either 5.2 m/s or 6.2 m/s, and then one month later were injected i.c.m. with 0.5 µm fluorescent beads. dCLN were harvested 2 hours after bead injection and cleared according to the CUBIC protocol. a) Representative images of cleared dCLN and b) quantification of the percent volume of beads in the total node volume one month after injury (5.2 m/s n=11, 6.2 m/s n=10; pooled data from 2 independent experiments). All n values refer to the number of mice used and the error bars depict mean ± s.e.m. *P* value was calculated by two-tailed unpaired Student's t-test. mpi, month(s) post injury.

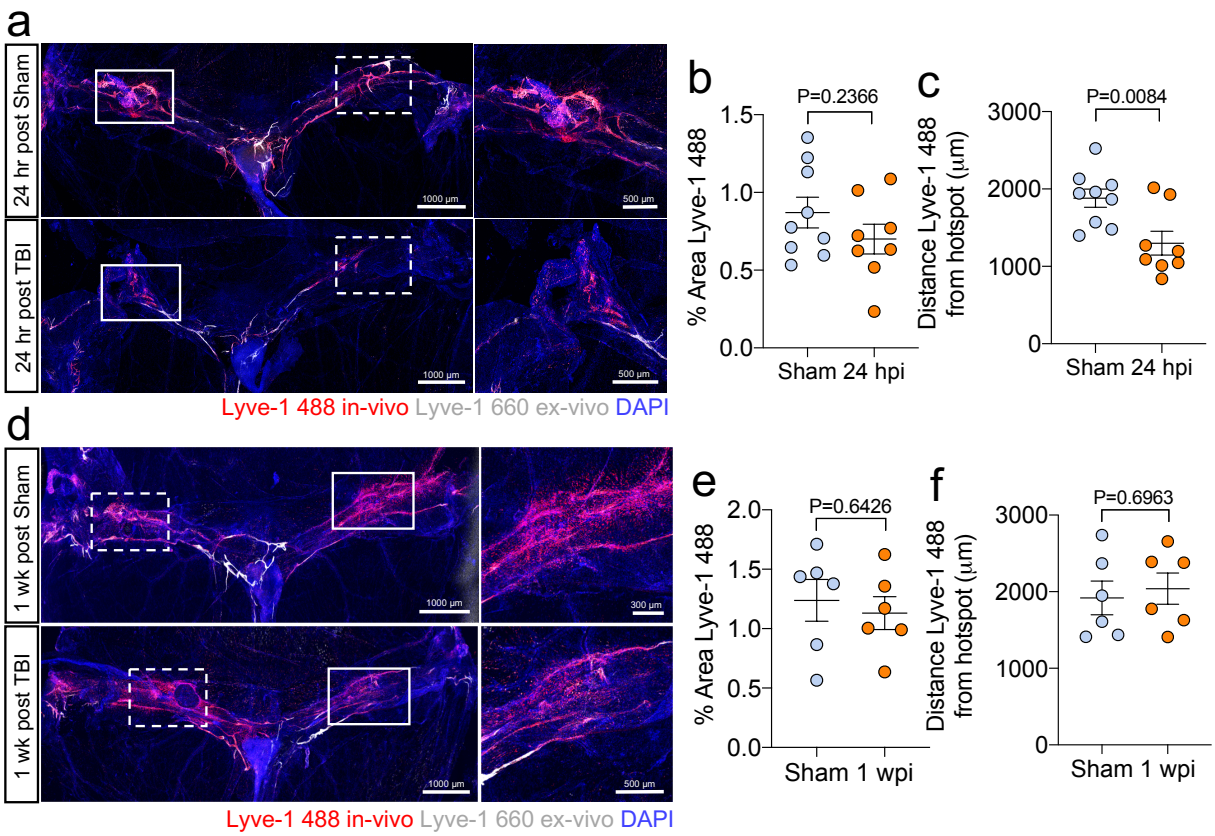

Figure 2.5. Meningeal lymphatic uptake of CSF at hotspots is impaired after TBI. Mice received TBI or sham treatment and then fluorescently labeled anti-Lyve-1 488 antibodies (red) were injected i.c.m. into the CSF 24 hours or 1 week later. 15 minutes after injection of Lyve-1 488 antibodies (red), meningeal whole mounts were harvested and ex vivo stained with anti-Lyve-1 660 (grey). a,d) Representative images of meningeal whole mounts (a) 24 hours and (d) 1 week after TBI, stained for Lyve-1 488 (in vivo, red), Lyve-1 660 (ex vivo, grey) and DAPI (blue). Solid boxes show zoomed insets of the hotspots along the transverse sinus on the right. Dashed boxes indicate the other hotspots not featured in the insets. b,e) Percent area of Lyve-1 488 coverage at (b) 24 hours and (e) 1 week post-TBI. c,f) Distance traveled of Lyve-1 488 (in vivo, red) staining along the transverse sinus 15 minutes after injection (c) 24 hours and (f) 1 week after injury. a-c) (Sham n=9, 24 hours n=8; pooled data from two independent experiments) (d-f) (Sham n=6, 1 week n=6; data from one experiment). All n values refer to the number of mice used and the error bars depict mean ± s.e.m. *P* values were calculated by two-tailed unpaired Student's t-test. hpi, hour(s) post injury; wpi, week(s) post injury.

To determine whether the uptake of CSF into the meningeal lymphatic vasculature was altered in TBI, we examined the hotspots of CSF uptake from the sub-arachnoid space along the transverse sinuses [76, 140]. Fluorescently labeled Lyve-1 antibody was injected into the CSF i.c.m. at either 2 or 24 hours after TBI, and then the meninges were harvested to examine uptake of CSF contents in the hotspots 15 minutes after injection (Figure 2.1h-j and Figure 2.5a-c). Analysis of the meningeal whole mounts revealed that mice that had received TBI 2 hours prior demonstrated significantly decreased uptake of fluorescently labeled Lyve-1 antibodies at the hotspots when compared to mice that underwent a sham procedure (Figure 2.1h-i). Moreover, Lyve-1 antibody did not travel as far along the lymphatics lining the transverse sinus in the TBI mice at both 2 and 24 hours post brain injury (Figure 2.1j and Figure 2.5c). Taken together, these findings indicate that even mild forms of TBI can result in meningeal lymphatic dysfunction and that these deficits persist out to one month post-injury. Moreover, we find that disruption in CNS drainage post-TBI is associated with impaired uptake of CSF at meningeal lymphatic hotspots.

2.3.2 TBI induces morphological changes to lymphatic vasculature

In order to determine whether the functional deficits in meningeal lymphatic drainage were also accompanied by morphological changes, we assessed the meningeal lymphatic vasculature at different time points post injury. At one week post TBI, there was an overall increase in Lyve-1 percent area coverage in the dorsal meningeal lymphatics (Figure 2.6a,c), which are known to be especially sensitive to growth factors in comparison to the larger and less labile collecting ducts at the base of the skull [78, 140]. To further assess changes in Lyve-1 coverage and structure, we quantified the number of loops and sprouts within the dorsal lymphatic vasculature, as these morphological changes are believed to represent an overall higher lymphatic vasculature complexity and may also indicate lymphangiogenesis [146]. Interestingly, we observed a significant increase in the number of capillary loops and sprouts in TBI mice one week following

head trauma (Figure 2.6a,b,d,e). We also quantified the lymphatic diameter, another measure for lymphatic growth [139], and saw an increase in TBI mice at one week post injury as compared to the sham group (Figure 2.6f). These same alterations continued out to two weeks after TBI, where we saw significantly increased Lyve-1 percent area coverage, loop formation, and sprout numbers, as well as a trend toward increased lymphatic vessel diameter (Figure 2.6a-f). By one and two months post injury, many of these measures of lymphangiogenesis had returned to baseline levels, although loop numbers remained significantly increased at one month post injury, taking longer to return to pre-injury levels (Figure 2.6a-f). Additionally, when we injected Lyve-1 antibody into the CSF i.c.m. one week post TBI or sham, we saw that there were no apparent differences in CSF uptake at the hotspots on the transverse sinuses between sham and TBI mice (Figure 2.5d-f), indicating that the lymphangiogenesis seen at one week post injury may have helped to restore proper CSF uptake into the meningeal lymphatic vasculature. Overall, these data indicate that traumatic brain injury induces morphological changes in the meningeal lymphatic vasculature and that these morphological changes occur maximally at one and two weeks post injury. Moreover, the results indicate that the lymphangiogenesis seen after a mild TBI is likely not permanent.

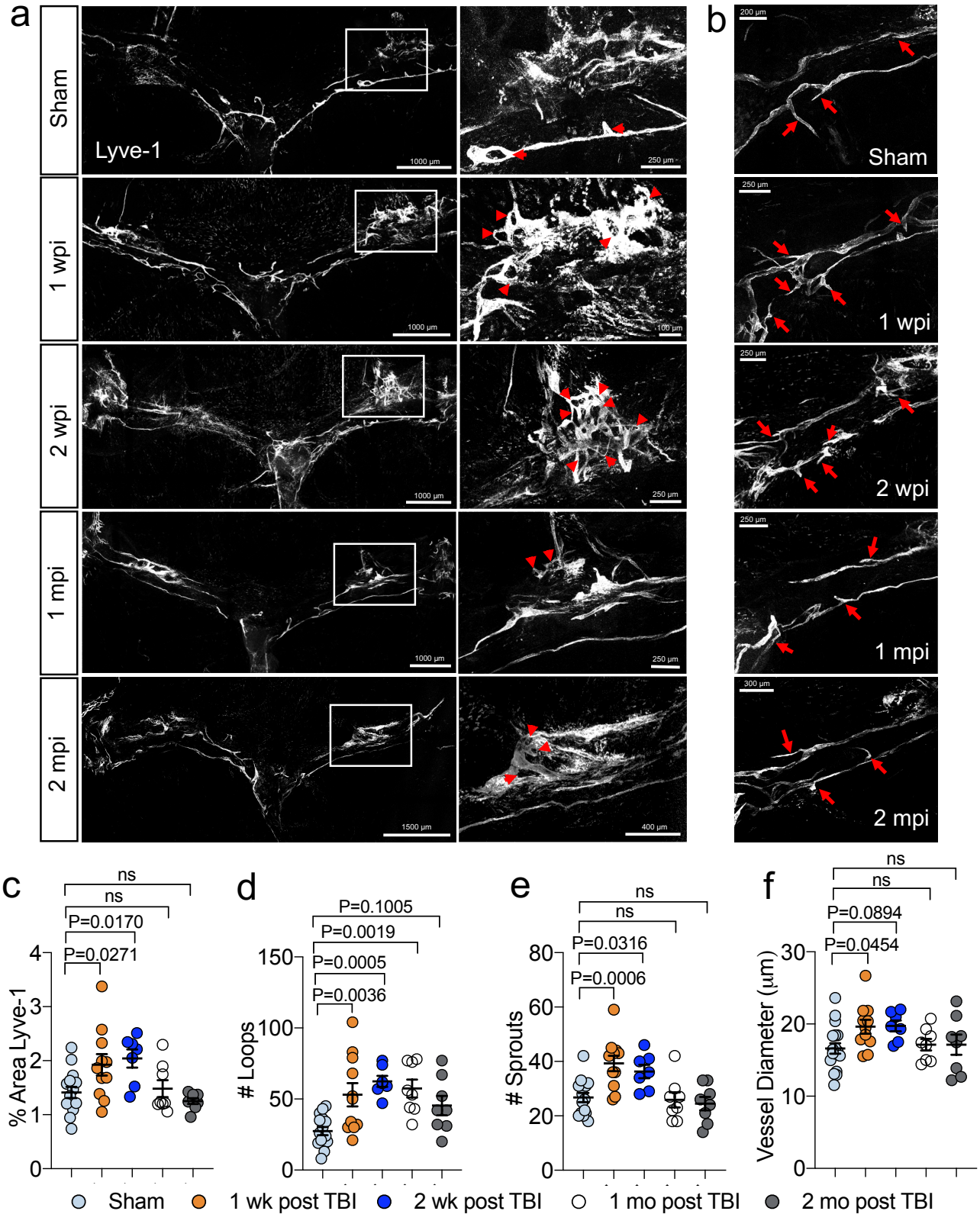
a
Sham
1 wpi
2 wpi
1 mpi
2 mpi
Lyve-1
1000 µm
250 µm
100 µm
1500 µm
400 µm
b
200 µm
Sham
250 µm
1 wpi
2 wpi
1 mpi
300 µm
2 mpi
c
% Area Lyve-1
ns
ns
P=0.0170
P=0.0271
d
# Loops
P=0.1005
P=0.0019
P=0.0005
P=0.0036
e
Sprouts
ns
ns
P=0.0316
P=0.0006
f
Vessel Diameter (µm)
ns
ns
P=0.0894
P=0.0454
Sham
1 wk post TBI
2 wk post TBI
1 mo post TBI
2 mo post TBI

Figure 2.6. TBI causes changes in meningeal lymphatic vasculature morphology. Mice received TBI or sham treatment and then meningeal whole mounts were harvested 1 week, 2 weeks, 1 month, and 2 months later. a) Representative images depicting transverse sinuses (left) and meningeal lymphatic vasculature loops near lymphatic hotspots (right) and (c) quantification of the percent area coverage of Lyve-1 antibody staining and (d) the number of loops in meningeal whole mounts. Solid boxes show zoomed insets of the hotspots along the transverse sinus on the right. Red arrow heads in the insets of panel (a) denote meningeal lymphatic vasculature loops. b) Representative images depicting meningeal lymphatic vasculature sprouts along the transverse sinuses and (e) quantification of the number of sprouts found in meningeal whole mounts. Red arrows in panel (b) denote meningeal lymphatic vasculature sprouts. f) Quantification of the diameters of the meningeal lymphatic vessels. Each data point represents an independent mouse and is an average of 70 measurements along the transverse and superior sagittal sinuses per mouse. Data in (c-f): Sham n=15, 1 week n=11, 2 weeks n=7, 1 month n=8, 2 months n=8; pooled data from 4 independent experiments. All n values refer to the number of mice used and the error bars depict mean ± s.e.m. *P* values were calculated by a one-way ANOVA with Dunnett's multiple corrections test (c-f). mo, month(s); mpi, month(s) post injury; wk, week(s); wpi, week(s) post injury.

2.3.3 Increased ICP contributes to CNS lymphatic dysfunction

Elevated intracranial pressure (ICP) is a major driver of mortality after TBI and is associated with negative clinical outcomes [147, 148]. Because the lymphatic drainage deficits were substantial even 2 hours after injury, we next examined whether there were associated changes in ICP after TBI. Two hours after injury, TBI mice exhibited markedly increased ICP as compared to sham mice (Figure 2.7a,b). At later time points post-TBI, ICP levels stabilized at slightly higher (~5-7.5 mmHg) levels than baseline; however, the differences in ICP at these later time points were not found to be statistically significant (Figure 2.7a,b).

Because the meningeal lymphatic vasculature is not associated with smooth muscle, it is especially vulnerable to changes in pressure and brain swelling inside the fixed skull [77, 78]. Therefore, we speculated that an acute rise in ICP might lead to disruptions in meningeal lymphatic drainage. To specifically test this hypothesis, we subjected mice to bilateral internal jugular vein ligation (JVL, Figure 2.7c), which is known to transiently increase ICP in both humans

and mice [91, 149, 150]. Consistent with previous findings, we observed that JVL substantially increased ICP to an average of 10 mmHg 3 hours after surgical ligation, and that the ICP normalized by 24 hours post ligation (Figure 2.7d) [91, 149, 150]. This reflected a similar acute spike in ICP that is seen at 2 hours after TBI (Figure 2.7a). To investigate what effect this rise in ICP has on meningeal lymphatic drainage function, we injected beads and assessed drainage to the dCLN at 3 and 24 hours after JVL. We found that there was significantly less drainage to the dCLN 3 hours after bilateral JVL (Figure 2.7e,f) and that there was reduced bead accumulation around the meningeal lymphatic vasculature of ligated mice (Figure 2.7h,i), indicating that there are deficits in the uptake of CSF contents in the CNS lymphatic vasculature. Moreover, we found that even after pressure normalized at 24 hours (Figure 2.7d), there was still a prolonged period of decreased lymphatic drainage as seen by the diminished uptake of beads into the meningeal lymphatics (Figure 2.7j) and a trend towards decreased beads in the dCLN at 24 hours post injury (Figure 2.7g). Collectively, these findings suggest that increased ICP is capable of provoking meningeal lymphatic dysfunction.

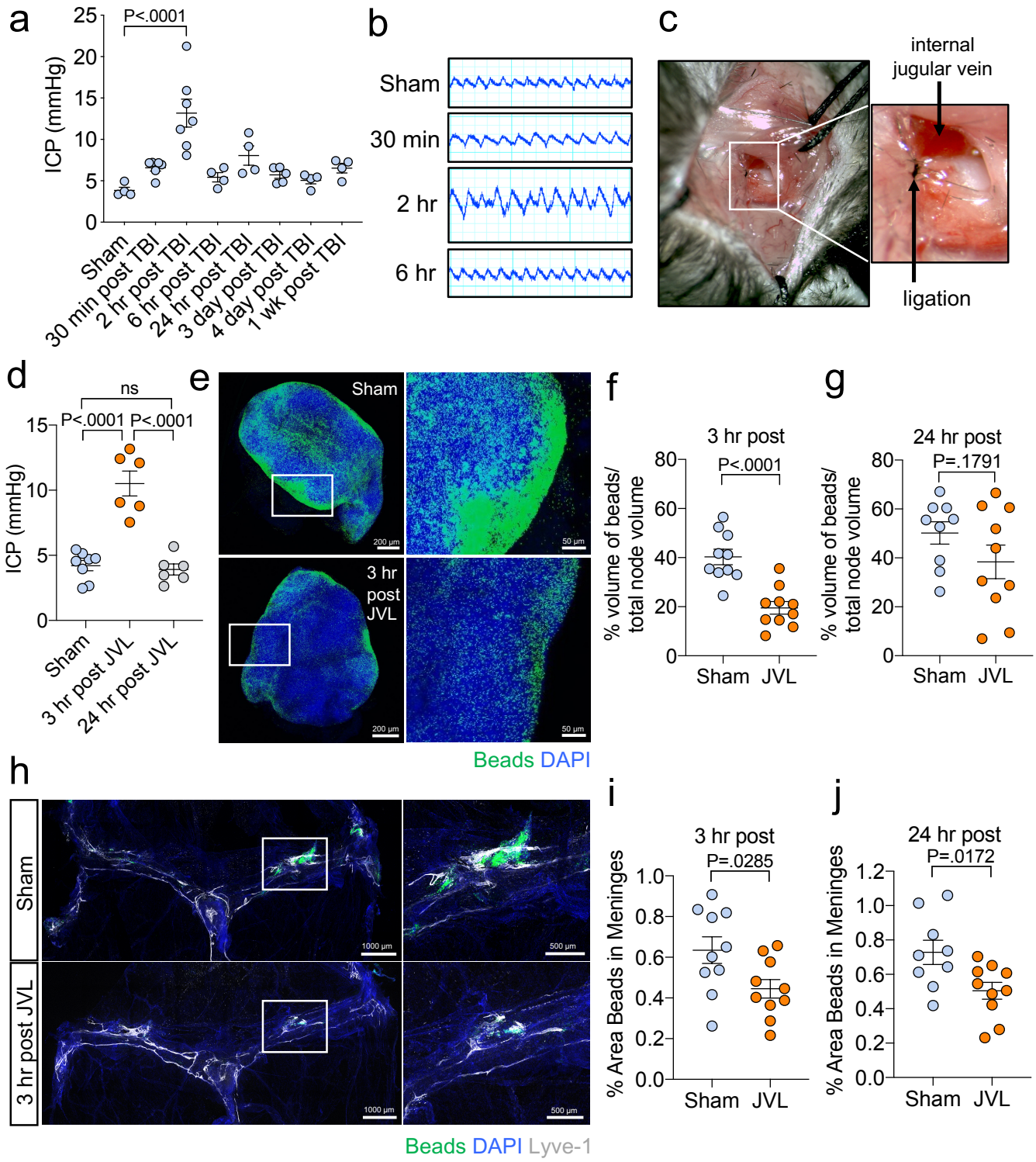
a
P<.0001
ICP (mmHg)
25
20
15
10
5
0
Sham
30 min post TBI
2 hr post TBI
6 hr post TBI
24 hr post TBI
3 day post TBI
4 day post TBI
1 wk post TBI
b
Sham
30 min
2 hr
6 hr
c
internal jugular vein
ligation
d
ns
P<.0001
P<.0001
ICP (mmHg)
15
10
5
0
Sham
3 hr post JVL
24 hr post JVL
e
Sham
3 hr post JVL
200 µm
50 µm
Beads DAPI
f
3 hr post
P<.0001
% volume of beads/ total node volume
80
60
40
20
0
Sham
JVL
g
24 hr post
P=.1791
% volume of beads/ total node volume
Sham
JVL
h
Sham
3 hr post JVL
1000 µm
500 µm
Beads DAPI Lyve-1
i
3 hr post
P=.0285
% Area Beads in Meninges
1.0
0.8
0.6
0.4
0.2
0.0
Sham
JVL
j
24 hr post
P=.0172
% Area Beads in Meninges
1.2
1.0
0.8
0.6
0.4
0.2
0.0
Sham
JVL

Figure 2.7. Increases in intracranial pressure disrupt CNS lymphatic drainage. a) Measurements of intracranial pressure (ICP) and (b) representative pressure readings were collected at various time points after TBI (Sham n=4, 30 minutes n=6, 2 hours n=7, 6 hours n=4, 24 hours n=4, 3 days n=5, 4 days n=4, 1 week n=4; pooled data from 3 independent experiments). c) Representative images of internal jugular vein ligation (JVL). d) ICP readings from mice that underwent bilateral JVL or a sham procedure 3 or 24 hours prior (Sham n=8, 3 hours n=6, 24 hours n=6; pooled data from 3 independent experiments). (e-j) The internal jugular vein was ligated bilaterally and then 0.5 μm fluorescent beads were injected i.c.m. 3 hours later. dCLN and meninges were then harvested from mice 2 hours after bead injection. e) Representative images of dCLN and graph showing drainage of beads (f) 3 hours and (g) 24 hours after jugular venous ligation. Each data point represents an average of the 2 dCLNs from an individual mouse (3 hours: Sham n=10, JVL n=10, 24 hours: Sham n=9, JVL n=10; pooled data from 2 independent experiments). Solid boxes of the node images on the left show zoomed insets of the images on the right. h) Representative images of meningeal whole-mounts with 0.5 μm beads (green) stained with DAPI (blue) and Lyve-1 660 (grey) and graph depicting percent area of bead coverage (i) 3 hours and (j) 24 hours post-JVL. Solid box shows a zoomed inset of the hotspot along the transverse sinus on the right (3 hours: Sham n=10, JVL n=10, 24 hours: Sham n=9, JVL n=10; pooled data from 2 independent experiments). All n values refer to the number of mice used and the error bars depict mean ± s.e.m. *P* values calculated by one-way ANOVA with Bonferroni's multiple comparison test (a) and Tukey's multiple comparison test (d) and two-tailed unpaired Student's t-test (f,g,i,j). ICP, intracranial pressure; JVL, jugular venous ligation; hr, hour(s); min, minute(s).

2.3.4 Prior lymphatic defects worsen TBI-induced inflammation

TBI is an especially serious condition in the elderly and in individuals sustaining repetitive brain injuries [28, 33, 104, 151-154]. For instance, similar injuries result in more severe pathology and neurological impairment in the elderly than in other age groups [132, 151, 153, 155]. Mounting evidence also suggests that repetitive TBI can have devastating consequences that includes increasing one's risk of developing CTE, psychiatric disorders, and other forms of neurological disease later in life [28, 156]. However, why TBI leads to worsened neurological disease in the elderly and following repetitive brain trauma remains poorly understood. Interestingly, it has recently been shown that CNS lymphatic drainage function significantly declines during aging [139-141]. Moreover, as we demonstrated in Figure 2.1, a single mild head injury can provoke pronounced disruptions in meningeal lymphatic function. This led us to question whether pre-

existing meningeal lymphatic dysfunction contributes to exacerbated disease following TBI, and if this might help to explain the increased severity of TBI-associated disease seen in repetitive TBI and the elderly.

Therefore, to formally investigate how antecedent meningeal lymphatic deficits affect outcomes after TBI, we utilized a pharmacological approach to selectively ablate the meningeal lymphatic vessels before head injury. Visudyne, a photoconvertible drug that has been shown to effectively ablate lymphatic vasculature [91, 139, 157], was injected i.c.m. into the CSF and allowed to travel into the CNS lymphatics. A nonthermal 689 nm laser was then aimed through the skull to selectively photoablate the meningeal lymphatics. Visudyne photoablation has been shown to selectively target lymphatic endothelial cells and results in the loss of lymphatic endothelial cell markers including Lyve-1, Prox1 and Podoplanin, while largely sparing the surrounding blood vasculature [91, 157]. Indeed, other studies show that this photoablation procedure has no impact on blood flow or blood oxygenation four days after treatment when measured by photoacoustic imaging [91]. After performing this procedure, mice were then rested for one week before receiving either sham treatment or brain injury (Figure 2.8a). Photoablation after Visudyne injection (Visudyne + laser) resulted in a significant decrease in area of the meninges covered by Lyve-1-expressing lymphatic vessels in comparison to mice that received vehicle and laser treatment (Vehicle + laser) or Visudyne without laser treatment (Visudyne) (Figure 2.8b,c). Consistent with previous reports [91, 139, 157], the area of $CD31^{+}Lyve\text{-}1^{-}$ blood vasculature was unchanged between all experimental groups, both when measured throughout the entire meninges and also in the region surrounding the sites of photoablation (Figure 2.8b,d,e). Overall, this indicates that the meningeal lymphatic vasculature was ablated without visible changes to the blood vasculature.

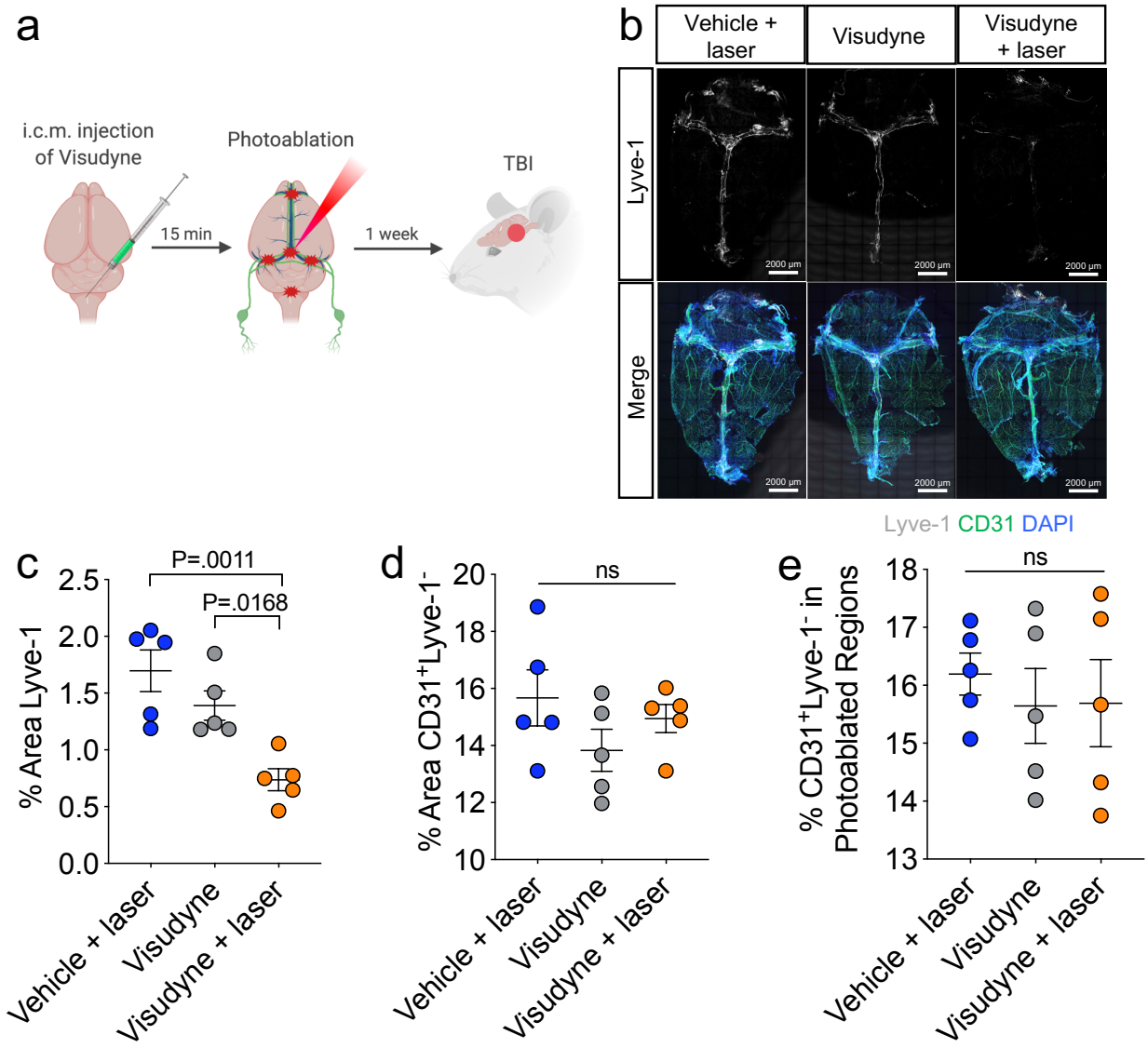

Figure 2.8. Visudyne photoablation of the meningeal lymphatic vasculature. a) Schematic of experimental layout. Mice were subjected to an injection of Visudyne or vehicle i.c.m., and 15 minutes later a red laser was directed at 5 spots along the sinuses through the skull. b-e) Meningeal whole mounts were harvested 1 week post-photoablation and then were stained with Lyve-1 660 (grey), CD31 (green), and DAPI (blue) to assess lymphatic (Lyve-1$^+$) and blood (CD31$^+$Lyve-1$^-$) vasculature. Percent area coverage of (c) Lyve-1 660 or (d) CD31$^+$Lyve-1$^-$ in meningeal whole mounts. e) Percent area coverage of CD31$^+$Lyve-1$^-$ in regions specifically targeted by photoablation (n=5 for all groups; representative data from 3 independent experiments). All n values refer to the number of mice used and the error bars depict mean ± s.e.m. *P* values calculated by one-way ANOVA with Tukey's post hoc test (c,d,e).

In order to determine how pre-existing meningeal lymphatic dysfunction affects subsequent TBI, we performed bulk RNA sequencing 24 hours and 1 week post injury in mice that had undergone either Visudyne ablation or a sham procedure one week prior. At 24 hours, while the sham groups clustered close together in the principal component analysis, the groups of mice that received TBI clustered separately (Figure 2.9a). Moreover, the group that received both TBI and ablation clustered separately from the group that received TBI alone (Figure 2.9a). Not surprisingly, at this early time point post brain injury, the injury itself caused the largest changes in differentially regulated gene expression (Figure 2.9b,c). We found 1573 upregulated and 1409 downregulated genes (FDR<0.1), when comparing TBI mice to the mice that underwent a sham procedure. We found similar numbers of upregulated (1511) and downregulated (1363) genes when comparing injured and uninjured mice that underwent meningeal lymphatic ablation (FDR<0.1). To understand how pre-existing lymphatic dysfunction affects subsequent TBI, we compared the two groups that had received TBI, where one group received ablation before brain injury (Ablated + TBI) and the other received a sham procedure (Not Ablated + TBI). Interestingly, we saw that the group that had pre-existing lymphatic dysfunction before TBI had a significant upregulation in complement related genes just 24 hours post injury (Figure 2.9d,e,f). Upregulation of the complement pathway, while important for coordinating the innate immune response and for pruning synapses in development, can be highly detrimental for brain health later in life. For instance, over-activation of the complement system has been shown to be an early harbinger for neuronal loss and cognitive decline [16, 17, 158]. One quarter of the top 20 most significantly upregulated genes in the Ablated + TBI group in comparison to the Not Ablated + TBI group were related to the complement pathway, including *C1qc*, *Itgam*, *C4b*, *Ctsh*, and *Irf7* (Figure 2.9e). To further assess the overall changes in the complement system, we created a heat map of the top 20 most significantly differentially expressed complement cascade-related genes using the Broad Hallmark gene sets [159]. We found that there was substantial upregulation of many genes related

to the complement pathway in the Ablated + TBI group as compared to the Not Ablated + TBI group (Figure 2.9f).

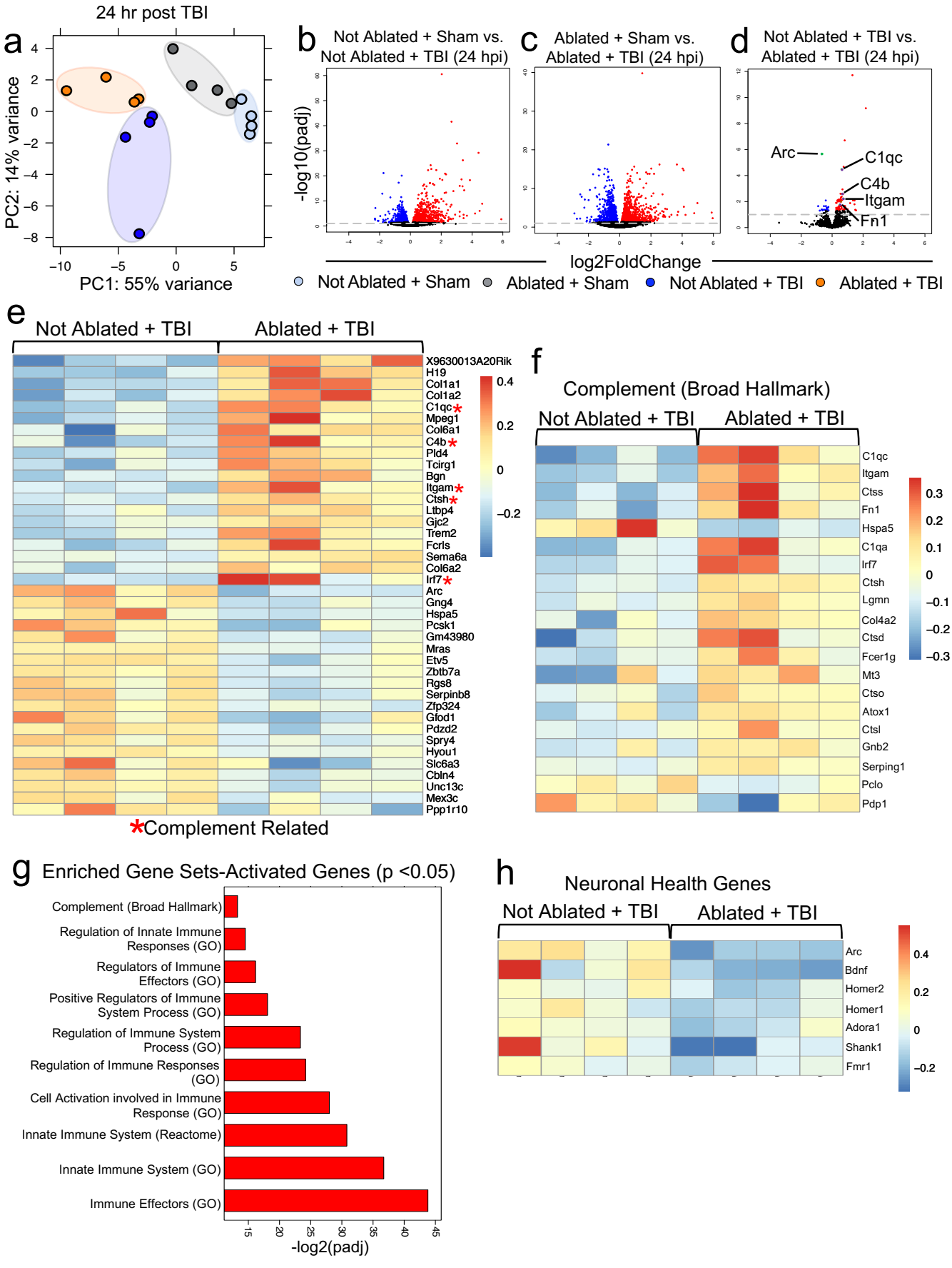
a
24 hr post TBI
PC2: 14% variance
PC1: 55% variance
b
Not Ablated + Sham vs.
Not Ablated + TBI (24 hpi)
c
Ablated + Sham vs.
Ablated + TBI (24 hpi)
d
Not Ablated + TBI vs.
Ablated + TBI (24 hpi)
-log10(padj)
Arc
C1qc
C4b
Itgam
Fn1
log2FoldChange
Not Ablated + Sham
Ablated + Sham
Not Ablated + TBI
Ablated + TBI
e
Not Ablated + TBI
Ablated + TBI
X9630013A20Rik
H19
Col1a1
Col1a2
C1qc*
Mpeg1
Col6a1
C4b*
Pld4
Tcirg1
Bgn
Itgam*
Ctsh*
Ltbp4
Gjc2
Trem2
Fcrls
Sema6a
Col6a2
Irf7*
Arc
Gng4
Hspa5
Pcsk1
Gm43980
Mras
Etv5
Zbtb7a
Rgs8
Serpinb8
Zfp324
Gfod1
Pdzd2
Spry4
Hyou1
Slc6a3
Cbln4
Unc13c
Mex3c
Ppp1r10
*Complement Related
f
Complement (Broad Hallmark)
Not Ablated + TBI
Ablated + TBI
C1qc
Itgam
Ctss
Fn1
Hspa5
C1qa
Irf7
Ctsh
Lgmn
Col4a2
Ctsd
Fcer1g
Mt3
Ctso
Atox1
Ctsl
Gnb2
Serping1
Pclo
Pdp1
g
Enriched Gene Sets-Activated Genes (p <0.05)
Complement (Broad Hallmark)
Regulation of Innate Immune Responses (GO)
Regulators of Immune Effectors (GO)
Positive Regulators of Immune System Process (GO)
Regulation of Immune System Process (GO)
Regulation of Immune Responses (GO)
Cell Activation involved in Immune Response (GO)
Innate Immune System (Reactome)
Innate Immune System (GO)
Immune Effectors (GO)
-log2(padj)
h
Neuronal Health Genes
Not Ablated + TBI
Ablated + TBI
Arc
Bdnf
Homer2
Homer1
Adora1
Shank1
Fmr1

Figure 2.9. Pre-existing meningeal lymphatic dysfunction alters gene expression 24 hours after TBI. Mice were subjected to an injection of Visudyne or vehicle i.c.m. and 15 minutes later a red laser was directed at 5 spots along the sinuses through the skull. After a week of rest, mice received TBI or a sham procedure. 24 hours after injury, RNA was isolated from homogenized brains. Bulk RNA sequencing was performed on 4 experimental groups with 4 samples per group. a) Principal component (PC) analysis showing clustering of samples. b-d) Volcano plots illustrate the number of significantly differentially expressed genes (FDR<0.1). Blue data points represent significantly downregulated genes and red data points represent significantly upregulated genes. Individual genes are highlighted in (d), where select downregulated genes are marked green and select upregulated genes are marked purple. e) Heatmap representation of the top 20 most significantly upregulated and downregulated (FDR<0.1) genes in the Not Ablated + TBI vs. Ablated + TBI groups. The red star (*) indicates genes associated with the complement signaling cascade. f) Heatmap representation of the 20 most significantly differentially expressed Broad Hallmark Complement-related genes in the Not Ablated + TBI vs. Ablated + TBI comparison. g) Gene set enrichment analysis of upregulated genes in Ablated + TBI mice compared to Not Ablated + TBI mice (uncorrected p<0.05). h) Heatmap representation of genes associated with neuronal health in the Ablated + TBI group as compared to the Not Ablated + TBI group. FDR and *P* values were calculated with DEseq2 using the Wald test for significance following fitting to a negative binomial linear model and the Benjamini-Hochberg procedure to control for false discoveries. hpi, hours post injury; padj, adjusted p-value.

To further address the question of how pre-existing lymphatic dysfunction affects subsequent TBI, we decided to take a closer look at the inflammatory pathways known to affect brain health. We found many of the upregulated genes in Ablated + TBI mice compared to Not Ablated + TBI mice were enriched in innate immune pathways (Figure 2.9g). Given this increase in inflammation with pre-existing lymphatic dysfunction before TBI, we were interested in determining whether neuronal health was affected at this early time point. Interestingly, we found multiple downregulated genes that are critical for neuronal health including *Arc, Homer1, Homer2,* and *Bdnf* (Figure 2.9h). The most significantly downregulated gene in the Ablated + TBI group when compared to the Not Ablated + TBI group was *Arc* (Figure 2.9d,e,h). *Arc*, an immediate early gene, is known to be critical for maintaining neuronal health [160]. Interestingly, even small reductions in *Arc* expression are known to be highly detrimental for learning capabilities, memory, and brain health [161].

To determine whether the changes seen in the Not Ablated + TBI vs. Ablated + TBI comparison could be attributed to the ablation procedure, we investigated the changes observed between the Not Ablated + Sham group and the Ablated + Sham group. We found that although ablation alone resulted in 338 differentially expressed genes, only 29 of these were shared with the TBI + ablation group (Figure 2.10a,b,d). Shared signatures between these two comparisons include an upregulation in genes important for collagen production (*Col1a1, Col1a2,* and *Col6a2*) and an upregulation in *H19* (important for noncoding RNA synthesis [162]) (Table 2.1). Interestingly, we found that genes related to complement (*C1qc, C4b, Ctsh, Irf7*, and *Itgam*) and neuronal health (*Arc*) were less significantly changed by orders of magnitude, or not changed in the Not Ablated + Sham vs. Ablated + Sham comparison in relation to the Not Ablated + TBI vs. Ablated + TBI comparison (Table 2.1). Therefore at 24 hours post injury, while there are changes from the ablation alone, there are important differences in the differentially regulated gene signatures and significance of these changes when compared to those seen in the Not Ablated + TBI vs. Ablated + TBI comparison (Table 2.1). Overall, these findings indicate that possessing pre-existing deficits in meningeal lymphatic function before TBI leads to elevated expression of genes associated with neuroinflammation and complement signaling at 24 hours post-injury. Moreover, we find that possessing unresolved defects in this meningeal drainage system before head injury adversely affects the expression of neuronal health genes.

Gene	Not Ablated + TBI vs. Ablated + TBI (-log2padj)	Gene Response (Not Ablated + TBI vs. Ablated + TBI)	Not Ablated + Sham vs. Ablated + Sham (-log2padj)	Gene Response (Not Ablated + Sham vs. Ablated + Sham)	Fold Change of comparisons (Column 2/ Column 4)
X9630013A20Rik	26.970626	Activated	2.815854066	Activated	9.57813344
H19	21.1141876	Activated	22.06175671	Activated	0.95704925
Col1a1	15.4302398	Activated	30.38196062	Activated	0.50787505
Col1a2	10.7553359	Activated	30.98605305	Activated	0.34710248
C1qc	10.3289388	Activated	2.391067707	Activated	4.31980187
Mpeg1	6.75743072	Activated	1.756788511	Activated	3.84646796
C4b	5.98491719	Activated	4.616960161	Activated	1.29628955
Col6a1	5.98491719	Activated	3.999476138	Activated	1.49642528
Pld4	5.94028144	Activated	6.187779078	Activated	0.96000219
Tcirg1	5.45694594	Activated	4.717892655	Activated	1.15664903
Bgn	5.360354	Activated	10.40616731	Activated	0.51511319
Ctsh	5.14985031	Activated	3.157904469	Activated	1.63078091
Itgam	5.14985031	Activated	3.936637228	Activated	1.30818514
Gjc2	4.93885587	Activated	1.674230563	Activated	2.94992577
Ltbp4	4.93885587	Activated	1.657847813	Activated	2.97907675
Trem2	4.84161903	Activated	3.181598672	Activated	1.52175668
Col6a2	4.80695313	Activated	5.819750401	Activated	0.82597239
Fcrls	4.80695313	Activated	1.824303203	Activated	2.63495296
Irf7	4.80695313	Activated	2.971062138	Activated	1.61792413
Sema6a	4.80695313	Activated	0.991155235	Activated	4.8498489
Arc	13.0384876	Repressed	0.227624649	Repressed	57.2806491
Gng4	4.79734578	Repressed	0.494613486	Repressed	9.69918109
Hspa5	3.7987826	Repressed	4.253261616	Repressed	0.89314577
Gm43980	3.79364208	Repressed	0.058467469	Repressed	64.8846637
Pcsk1	3.79364208	Repressed	2.981308322	Repressed	1.2724756
Mras	3.6452025	Repressed	2.149743978	Repressed	1.69564494
Etv5	3.49060473	Repressed	10.8326543	Repressed	0.32222986
Zbtb7a	3.49060473	Repressed	3.151038462	Repressed	1.10776329
Rgs8	3.23818268	Repressed	0.402979251	Repressed	8.03560648
Serpinb8	3.1877807	Repressed	0.046380808	Repressed	68.7305981
Zfp324	3.16803996	Repressed	0.104637618	Repressed	30.2763005
Gfod1	3.15312218	Repressed	7.999403905	Repressed	0.39416964
Pdzd2	3.14330513	Repressed	0.660051173	Repressed	4.7622143
Spry4	3.06569035	Repressed	1.54188296	Repressed	1.98827695
Hyou1	3.05247886	Repressed	0.436498851	Repressed	6.99309713
Slc6a3	3.00642093	Repressed	0.14153804	Activated	21.2410807
Cbln4	2.94477885	Repressed	0.303388055	Repressed	9.70631112
Unc13c	2.87569266	Repressed	11.36028247	Repressed	0.25313567
Mex3c	2.81167812	Repressed	0.494613486	Repressed	5.68459655
Ppp1r10	2.59057765	Repressed	0.032459754	Activated	79.8089129
Mean	6.01042697	Repressed	4.830226859	Repressed	1.24433637
Median	4.80695313	Repressed	2.603460886	Repressed	1.70710307

Table 2.1. Top 20 genes in the Not Ablated + TBI vs. Ablated + TBI group vs. Not Ablated + Sham vs. Ablated + Sham group. Mice were subjected to meningeal lymphatic photoablation after i.c.m. Visudyne injection or a control procedure. Mice were rested for one week and then underwent either TBI or a sham procedure. Bulk RNA sequencing was performed on these 4 experimental groups with 4 independent mice per group either 24 hours or 1 week post TBI. Table depicts the negative log of the adjusted p-value of the top 20 up- and down-regulated genes from the Not Ablated + TBI vs. Ablated + TBI group as compared to the Not Ablated + Sham vs. Ablated + Sham group. The fold change of the comparisons shows the negative log of the adjusted p-value from the TBI comparison divided by the negative log of the adjusted p-value from the Sham comparison. FDR and P values were calculated with DEseq2 using the Wald test for significance following fitting to a negative binomial linear model and the Benjamini-Hochberg procedure to control for false discoveries.

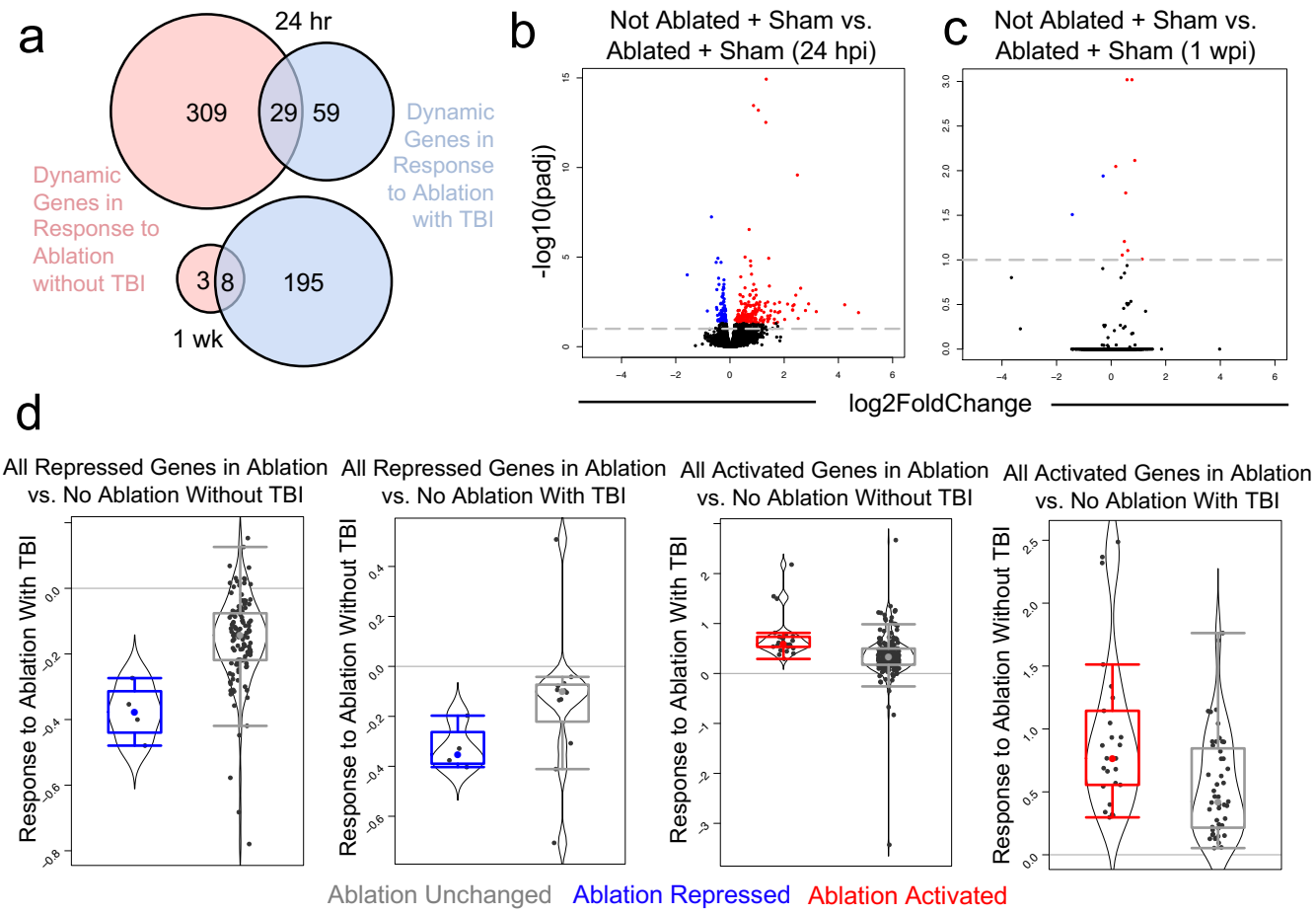

Figure 2.10. Effects of photoablation on gene expression signatures. Mice were subjected to meningeal lymphatic photoablation after i.c.m. Visudyne injection or a control procedure. Mice were rested for one week and then underwent either TBI or a sham procedure. Bulk RNA sequencing was performed on these 4 experimental groups with 4 independent mice per group either 24 hours or 1 week post TBI. a) Total numbers of differentially expressed genes in response to Ablation without TBI (pink) in comparison to the total numbers of differentially expressed genes in response to Ablation with TBI (blue) at each sequencing time point (FDR<0.1). Shared genes are in overlapping sections. b-c) Volcano plots showing differentially expressed genes at (b) 24 hours post injury and (c) 1 week post injury in the Not Ablated + Sham vs. Ablated + Sham comparison (FDR <0.1). d) Box and whisker plots at 24 hours post injury depicting activated and repressed genes in response to ablation with and without TBI (FDR<0.1). The central dot within the box plots represents the median of the data set. The upper and lower boundaries of the box represent the third (Q3) and first (Q1) quartiles respectively. The length of the box therefore represents the interquartile range (IQR). The whiskers extend to the minimum and maximum values of the set, here defined as Q1 - 1.5*IQR and Q3 + 1.5 * IQR respectively. All data points beyond the whiskers are considered outliers. The box and whisker plots are overlaid on a violin plot that encompasses the entire data set, including the outliers. The width of the violin plot represents the frequency of observations at that given y-value. Therefore, the wider the violin plot, the higher the frequency of observations. FDR values were calculated with DEseq2 using the Wald test for significance following fitting to a negative binomial linear model and the Benjamini-Hochberg procedure to control for false discoveries.

We also performed bulk RNA sequencing at 1 week post injury to investigate the effects of pre-existing lymphatic dysfunction at a more distant time point after TBI. At 1 week post injury, both the Not Ablated + Sham and the Ablated + Sham groups clustered together, indicating that the photoablation alone had very little effect at one week post injury (Figure 2.11a). Moreover, there were only 11 differentially regulated genes in the Not Ablated + Sham vs. Ablated + Sham group, indicating that at one week post injury, the ablation procedure itself is not playing a significant role in changing gene expression (Figure 2.10a,c). Interestingly, both the group with TBI alone and the group with pre-existing lymphatic dysfunction before TBI (Ablated + TBI) clustered separately (Figure 2.11a). While the TBI alone still results in many differentially regulated genes, we find that there are over 200 differentially regulated genes in the TBI group with pre-existing lymphatic dysfunction (Ablated + TBI) when compared to TBI alone (FDR< 0.1, Figure 2.11a,b). A gene set enrichment analysis with the pathways in the Reactome database for differentially expressed genes between TBI mice with pre-existing lymphatic dysfunction (Ablated + TBI) and those with TBI alone (Not Ablated + TBI) showed that the most highly enriched pathways were related to the innate and adaptive immune system and cytokine signaling (Figure 2.11c) [163]. We also used the Biocarta database [164] to determine which signaling pathways were most highly enriched in our dataset. We found that genes differentially expressed between the TBI mice with ablated meningeal lymphatics (Ablated + TBI) and TBI mice with normal lymphatics (Not Ablated + TBI) are enriched in pathways important for innate immunity (e.g. complement pathway), leukocyte recruitment (e.g. CCR5), and cytokine signaling (e.g. IL-1 and TNF signaling) (Figure 2.11d).

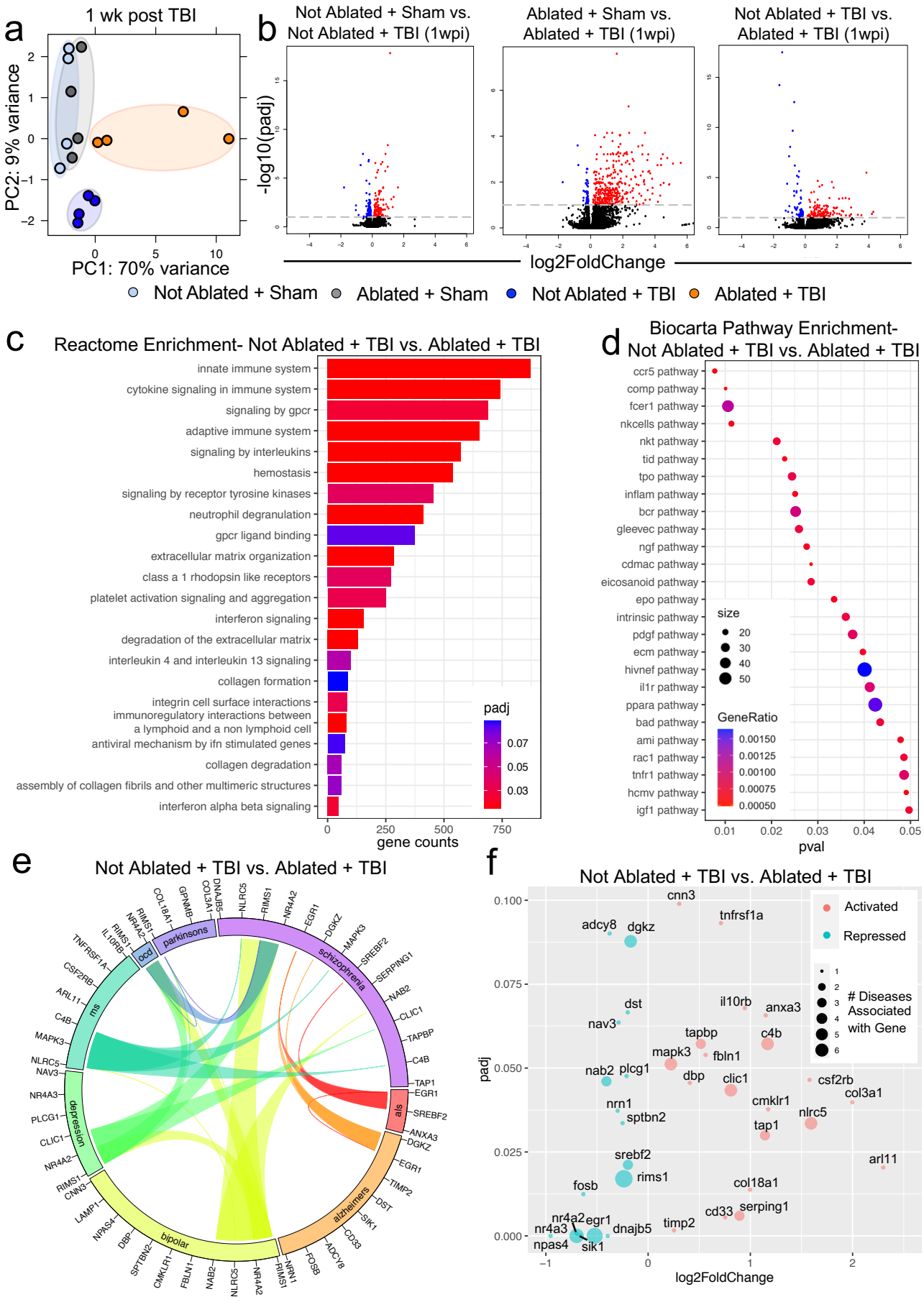
a
1 wk post TBI
PC2: 9% variance
PC1: 70% variance
b
Not Ablated + Sham vs. Not Ablated + TBI (1wpi)
Ablated + Sham vs. Ablated + TBI (1wpi)
Not Ablated + TBI vs. Ablated + TBI (1wpi)
-log10(padj)
log2FoldChange
Not Ablated + Sham
Ablated + Sham
Not Ablated + TBI
Ablated + TBI
c
Reactome Enrichment- Not Ablated + TBI vs. Ablated + TBI
innate immune system
cytokine signaling in immune system
signaling by gpcr
adaptive immune system
signaling by interleukins
hemostasis
signaling by receptor tyrosine kinases
neutrophil degranulation
gpcr ligand binding
extracellular matrix organization
class a 1 rhodopsin like receptors
platelet activation signaling and aggregation
interferon signaling
degradation of the extracellular matrix
interleukin 4 and interleukin 13 signaling
collagen formation
integrin cell surface interactions
immunoregulatory interactions between a lymphoid and a non lymphoid cell
antiviral mechanism by ifn stimulated genes
collagen degradation
assembly of collagen fibrils and other multimeric structures
interferon alpha beta signaling
padj
0.07
0.05
0.03
gene counts
d
Biocarta Pathway Enrichment- Not Ablated + TBI vs. Ablated + TBI
ccr5 pathway
comp pathway
fcer1 pathway
nkcells pathway
nkt pathway
tid pathway
tpo pathway
inflam pathway
bcr pathway
gleevec pathway
ngf pathway
cdmac pathway
eicosanoid pathway
epo pathway
intrinsic pathway
pdgf pathway
ecm pathway
hivnef pathway
il1r pathway
ppara pathway
bad pathway
ami pathway
rac1 pathway
tnfr1 pathway
hcmv pathway
igf1 pathway
size
GeneRatio
pval
e
Not Ablated + TBI vs. Ablated + TBI
parkinsons
ocd
ms
depression
bipolar
schizophrenia
als
alzheimers
f
Not Ablated + TBI vs. Ablated + TBI
Activated
Repressed
Diseases Associated with Gene
padj
log2FoldChange

Figure 2.11. TBI leads to elevated expression of disease-associated genes when the brain possesses pre-existing lymphatic deficits. Mice were subjected to an injection of Visudyne or vehicle i.c.m. and 15 minutes later a red laser was directed at 5 spots along the sinuses through the skull. After a week of rest, mice received TBI or a sham procedure. One week after injury, RNA was isolated from homogenized brains. Bulk RNA sequencing was performed on these 4 experimental groups with 4 individual mice per group. a) Principal component (PC) analysis showing clustering of samples. b) Volcano plots illustrate the number of significantly differentially expressed genes (FDR<0.1). Blue data points represent significantly downregulated genes and red data points represent significantly upregulated genes. c-d) Gene set enrichment analysis using the (c) Reactome database and (d) Biocarta pathway database shows enrichment of immune-related pathways with differentially expressed genes between TBI mice with pre-existing lymphatic dysfunction compared to mice with TBI alone. e) Circos plot depicting differentially expressed genes in TBI mice with pre-existing lymphatic dysfunction compared to mice with TBI alone (FDR<0.1) associated with neurodegenerative or psychiatric diseases. The proportion of the circle's circumference allocated to each disease represents the number of genes associated with that disease that are also differentially expressed in the Not Ablated + TBI v. Ablated + TBI comparison. The lines connecting genes within the circle indicate which genes were shared amongst disease signatures. f) Scatterplot showing the adjusted *P* value and the expression changes of genes shown in (e). padj, adjusted p-value; pval, p-value. wpi, week(s) post injury. FDR and *P* values were calculated with DEseq2 using the Wald test for significance following fitting to a negative binomial linear model and the Benjamini-Hochberg procedure to control for false discoveries.

We were next interested in investigating whether the TBI mice with pre-existing lymphatic dysfunction (Ablated + TBI) shared common genes associated with neurodegenerative or psychiatric diseases. To this end, we used the GWAS Catalog [165], a database of genome-wide association studies, to find known gene associations with several common neurodegenerative and psychiatric diseases including Parkinson's disease, schizophrenia, amyotrophic lateral sclerosis (als), Alzheimer's disease, bipolar disease, depression, multiple sclerosis (ms), and obsessive compulsive disorder (ocd). We found that the differentially expressed genes between TBI mice with pre-existing lymphatic dysfunction and mice with TBI alone were also associated with these diseases, indicating that these mice share signatures with various neurological disease states (Figure 2.11e,f).

2.3.5 Unresolved drainage defects worsen cognitive decline in TBI

The findings from the RNA-seq experiments motivated us to investigate whether there are different long-term outcomes in the TBI mice with pre-existing meningeal lymphatic dysfunction (Ablated + TBI) compared to mice with TBI alone (Not Ablated + TBI). We looked at levels of Iba1 (labels microglia and CNS infiltrating monocytes/macrophages) and GFAP (labels reactive astrocytes) immunoreactivity 2 weeks after injury or sham treatment, with or without ablation, as aggravated gliosis often correlates with worsened clinical outcomes in TBI [23, 166-168]. We found that possessing defects in the meningeal lymphatic system before TBI (Ablated + TBI) results in a significantly higher percent area of GFAP coverage (Figure 2.12a,b). While we saw an overall increase in Iba1 immunoreactivity in the Ablated + TBI group compared to the Not Ablated + Sham group, we did not see a significant increase when compared to TBI alone (Figure 2.12a,c). These initial results suggest that more severe neuroinflammation can unfold if TBI occurs in the context of pre-existing meningeal lymphatic dysfunction.

Because we saw a trend towards increased percent area Iba1 staining in Ablated + TBI mice (Figure 2.12c), we wanted to more closely examine Iba1 cell morphology in each of the experimental groups at 2 weeks post injury. We performed a Sholl analysis and found that Iba1+ cells from the pre-existing lymphatic dysfunction (Ablated + TBI) group had a lower number of dendritic branches at greater distances from the soma, indicating a less ramified, more highly activated state than in mice with TBI alone (Not Ablated + TBI), or the other control groups (Figure 2.12d,e). Additionally, the Ablated + TBI group had a higher number of Iba1+ cells (Figure 2.12f), and trends towards lower dendrite length, dendrite volume, and dendrite branch points compared to the other control groups (Figure 2.13a-c). These data suggest that brain macrophages (Iba1+ cells) in TBI mice with pre-existing lymphatic dysfunction (Ablated + TBI) are more highly activated and less ramified than Iba1+ cells in the other control groups.

Next, we sought to investigate whether possessing deficits in meningeal lymphatic function before TBI negatively affects cognitive performance, which is a common consequence of TBI in humans and animal models. Since others have shown that similar injuries to this region of the brain can lead to cognitive impairments [83, 169], we decided to investigate how pre-existing lymphatic dysfunction affects memory and motor learning following TBI. Interestingly, while all four experimental groups exhibited similar performance on the accelerating rotarod at 24 hours post-TBI, the mice possessing deficits in meningeal lymphatic function before TBI (Ablated + TBI) showed impaired motor learning over the three days of the accelerating rotarod test (Figure 2.12g). Indeed, the percent performance increase over three days in the Ablated + TBI group was lower than any of the other control groups indicating that undergoing meningeal lymphatic photoablation before TBI results in impaired motor learning (Figure 2.12g). Likewise, mice that underwent meningeal lymphatic photoablation before TBI also performed worse in the novel location recognition test (NLRT) at two weeks post-brain injury, suggesting an impairment in memory (Figure 2.12h,i). Taken together, these results indicate that TBI can cause exacerbated neuroinflammation and cognitive dysfunction when the brain possesses pre-existing defects in meningeal lymphatic function.

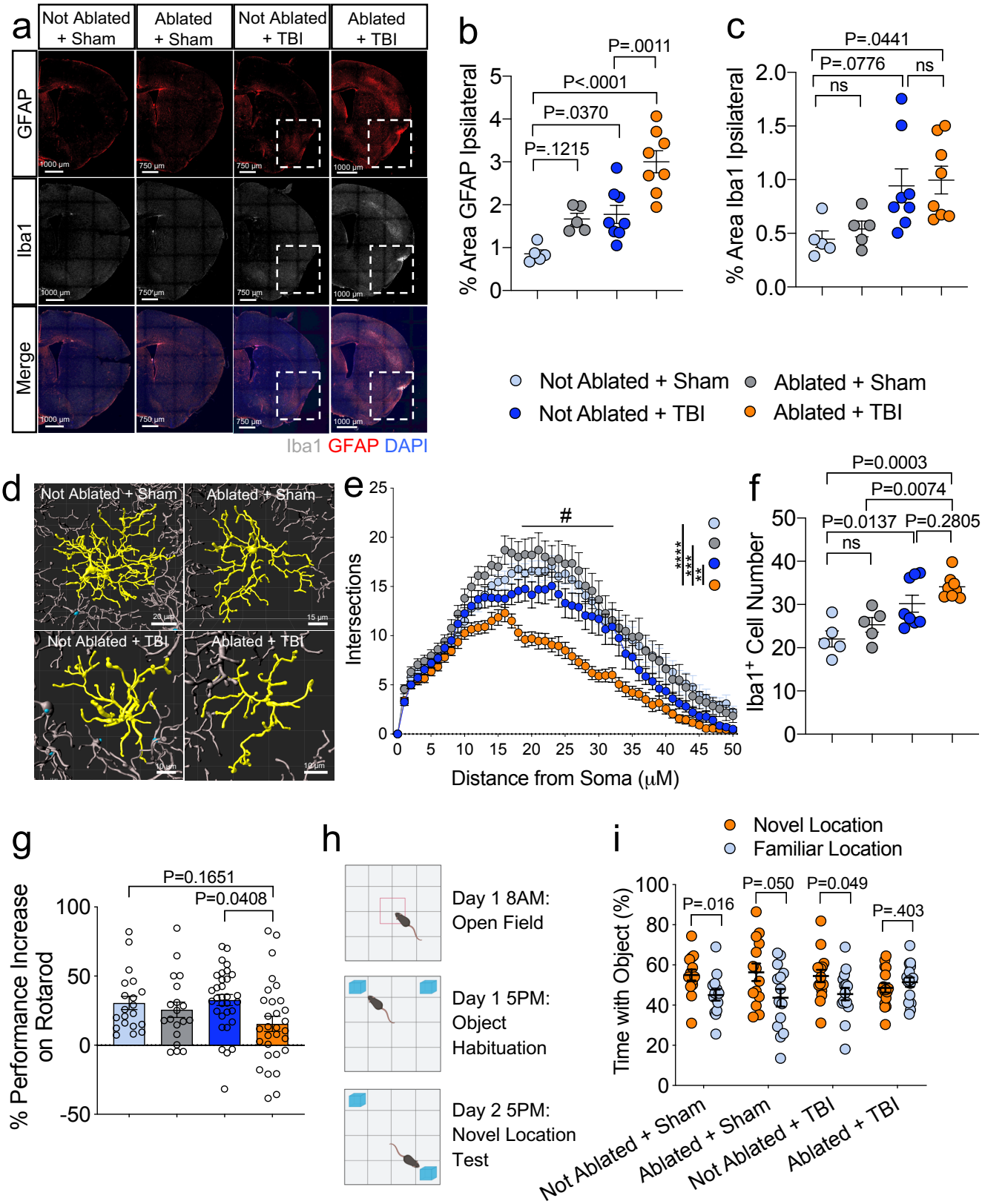
a
Not Ablated + Sham
Ablated + Sham
Not Ablated + TBI
Ablated + TBI
GFAP
Iba1
Merge
Iba1 GFAP DAPI
b
% Area GFAP Ipsilateral
P=.0011
P<.0001
P=.0370
P=.1215
c
% Area Iba1 Ipsilateral
P=.0441
P=.0776
ns
ns
Not Ablated + Sham
Ablated + Sham
Not Ablated + TBI
Ablated + TBI
d
Not Ablated + Sham
Ablated + Sham
Not Ablated + TBI
Ablated + TBI
e
Intersections
Distance from Soma (μM)
#
****
***
**
f
Iba1+ Cell Number
P=0.0003
P=0.0074
P=0.0137
P=0.2805
ns
g
% Performance Increase on Rotarod
P=0.1651
P=0.0408
h
Day 1 8AM: Open Field
Day 1 5PM: Object Habituation
Day 2 5PM: Novel Location Test
i
Novel Location
Familiar Location
Time with Object (%)
P=.016
P=.050
P=.049
P=.403
Not Ablated + Sham
Ablated + Sham
Not Ablated + TBI
Ablated + TBI

Figure 2.12. Prior lymphatic defects lead to exacerbated TBI-induced inflammation and cognitive decline. Mice were subjected to meningeal lymphatic photoablation or a control procedure and then to TBI or a sham procedure 1 week later. a-f) Brains were harvested 2 weeks after TBI. a) Representative images of the brain hemisphere ipsilateral to the injury and quantification of the percent area of (b) GFAP (red) and (c) Iba1 (grey) immunoreactivity in all experimental groups (Sham groups n=5, TBI groups n=8). Dashed boxes denote the injury site. d) Representative reconstructions of morphology of Iba1+ cells and (e) Sholl analysis. Each data point represents the number of Iba1+ branches intersecting with a radius of 0-50 μm from the soma, calculated by the average of 20 microglia per group (4 Iba1+ cells per section, 5 mice per group; data from one experiment). Number sign (#) indicates that all control groups were significantly different from the Ablated + TBI group from 18-32 μm; ****P<.0001, ***P=.0003, **P=.0034 (calculated at 23 μm). f) Quantification of the average number of Iba1+ cells per field of view (Sham groups n=5, TBI groups n=8). g) The percent performance increase on the accelerating rotarod from day 1 to day 3 post TBI or sham procedure (Not Ablated + Sham n=20, Not Ablated + TBI n=32, Ablated + Sham n=19, Ablated + TBI n=30; pooled data from 4 independent experiments). h) Schematic depicting the experimental setup of the NLRT and the i) percent time the mouse spent investigating each object over the total time investigating both objects (Not Ablated + Sham n=14, Not Ablated + TBI n=15, Ablated + Sham n=14, Ablated + TBI n=16; pooled data from two independent experiments). Each point represents the percent time one mouse spent with either the novel location object (orange) or the familiar location object (blue). All other n values refer to the number of mice used and the error bars depict mean ± s.e.m. *P* values calculated by two-way ANOVA with Tukey's multiple comparison correction (b,c,e,f,g) and mixed two-tailed unpaired Student's t-test with Holm-Sidak multiple comparison correction (i).

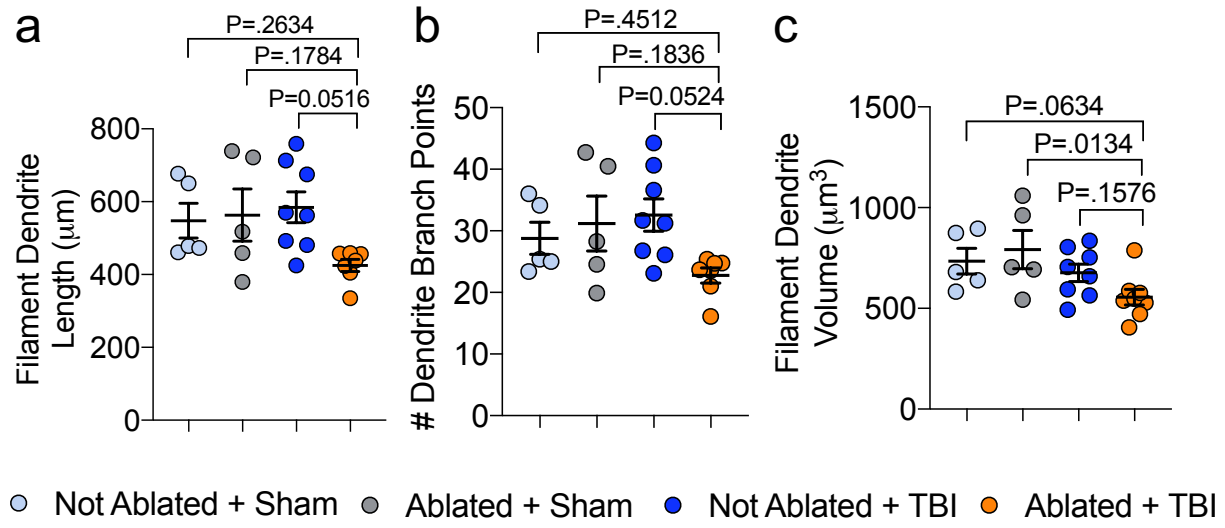

Figure 2.13. The effect of pre-existing lymphatic dysfunction on Iba1+ cells. Mice were subjected to meningeal lymphatic photoablation after i.c.m. Visudyne injection or a control procedure and then to TBI or a sham procedure 1 week later. a-c) Brains were harvested 2 weeks after TBI, sectioned, and stained for Iba1. Quantification of the (a) average filament dendrite length (μm), (b) average number of dendrite branch points, and (c) average filament dendrite volume (μm^3) (Not Ablated+Sham n=5, Ablated+Sham n=5, Not Ablated+TBI n=8, Ablated+TBI n=7; data from one experiment). All n values refer to the number of mice used and the error bars depict mean ± s.e.m. *P* values calculated by two-way ANOVA with Tukey's multiple comparison correction (a-c).

2.3.6 Lymphatic rejuvenation mitigates TBI-driven inflammation

To better understand the functional consequences of impaired meningeal lymphatic function in TBI, we next explored whether boosting CNS lymphatic drainage is effective in attenuating TBI disease pathogenesis. Multiple recent studies have shown that aging leads to severe impairments in meningeal lymphatic function [139-141]. Moreover, it is also known that even mild-to-moderate forms of brain trauma can have especially devastating consequences in elderly individuals [104, 132, 151-153]. Therefore, we were interested in investigating whether recuperating meningeal lymphatic function in aged mice would be effective in limiting TBI disease pathogenesis. To this end, we utilized viral delivery of VEGF-C, which has previously been shown to successfully increase the diameter of the meningeal lymphatic vessels [76, 90, 139]. Importantly, delivery of VEGF-C to the meningeal lymphatic vessels in aged mice has also been reported to rejuvenate meningeal lymphatic draining function [139]. Accordingly, we subjected aged mice (18-24 months of age) or young mice (8-10 weeks of age) to an i.c.m injection with either AAV1-CMV-mVEGF-C or control AAV1-CMV-eGFP. We observed stable expression of the viral vector along the transverse sinus (TS) and superior sagittal sinus (SSS) in the aged meninges 1 month after injection (Figure 2.14a). Two weeks after viral vector delivery, we subjected these mice to TBI or sham treatment. Not surprisingly, the aged mice who experienced head trauma had a significantly longer loss-of-consciousness and performed significantly worse on the neuroscore behavioral tests than their younger counterparts with the same injury parameters (Figure 2.14b,c). There were, however, no differences in righting time or neuroscore between the aged TBI groups that had received AAV1-CMV-mVEGF-C or AAV1-CMV-eGFP delivery (Figure 2.14b,c). Mice that received sham procedures instead of a TBI and either AAV1-CMV-mVEGF-C or AAV1-CMV-eGFP delivery also showed no differences in the righting times or neuroscore behavioral tests, although predictably, both measurements were lower than in mice that had received TBI (Figure 2.15a,b and Figure 2.14b,c). Two weeks after injury and one month after viral vector delivery, we

measured GFAP and Iba1 immunoreactivity to assess gliosis and determine whether treatment with VEGF-C improved neuroinflammatory measures in the injured brains. Interestingly, we saw that aged TBI mice that received viral-mediated VEGF-C treatment (Aged- VEGFC + TBI) had significantly lower levels of Iba1 in the hemisphere contralateral to the injury site, and a trend towards lower levels of Iba1 in the hemisphere ipsilateral to the injury site when compared to mice that had received the control viral vector (Aged- GFP + TBI) (Figure 2.14d-f). Notably, the levels of Iba1 in the aged TBI mice that were treated with VEGF-C (Aged- VEGFC + TBI) were more similar to the levels of Iba1 immunoreactivity in a young TBI mouse (Young- GFP + TBI) (Figure 2.14d-f and Figure 2.15d,f). In contrast, VEGF-C pretreatment was not found to influence GFAP immunoreactivity in aged mice following head trauma (Figure 2.14d,g,h and Figure 2.15c,e). These data indicate that boosting meningeal lymphatic function after TBI may aid in decreasing levels of Iba1 gliosis in aged mice.

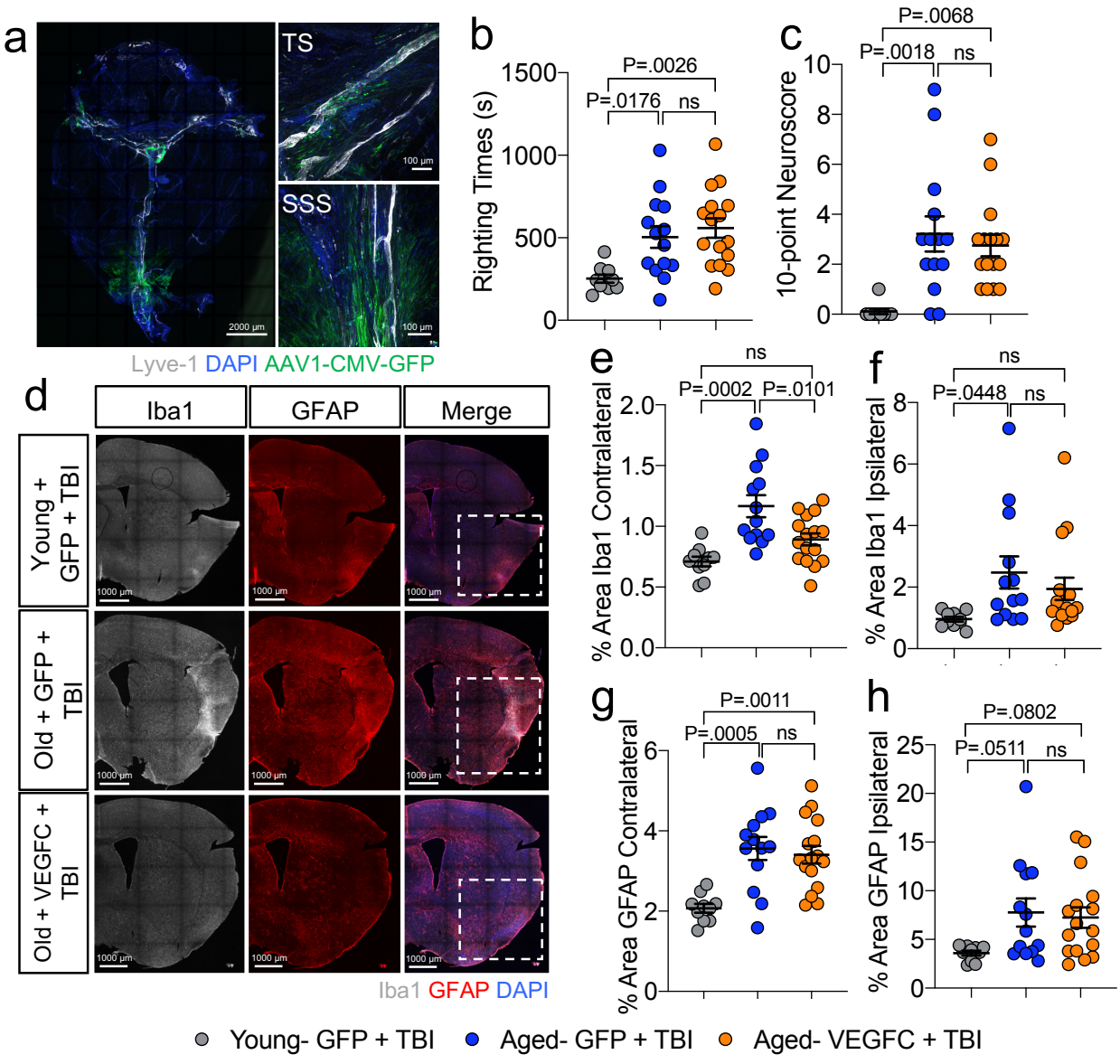
a
TS
SSS
2000 µm
100 µm
100 µm
Lyve-1 DAPI AAV1-CMV-GFP
b
Righting Times (s)
1500
1000
500
0
P=.0026
P=.0176
ns
c
10-point Neuroscore
10
8
6
4
2
0
P=.0068
P=.0018
ns
d
Iba1
GFAP
Merge
Young + GFP + TBI
Old + GFP + TBI
Old + VEGFC + TBI
1000 µm
Iba1 GFAP DAPI
e
% Area Iba1 Contralateral
2.0
1.5
1.0
0.5
0.0
ns
P=.0002
P=.0101
f
% Area Iba1 Ipsilateral
8
6
4
2
0
ns
P=.0448
ns
g
% Area GFAP Contralateral
6
4
2
0
P=.0011
P=.0005
ns
h
% Area GFAP Ipsilateral
25
20
15
10
5
0
P=.0802
P=.0511
ns
Young- GFP + TBI
Aged- GFP + TBI
Aged- VEGFC + TBI

Figure 2.14. VEGF-C treatment of aged mice results in decreased neuroinflammation after TBI. Aged mice (18-20 months old) received 2 µl of artificial CSF containing 10^{13} genome copies per ml of either AAV1-CMV-mVEGF-C or control AAV1-CMV-eGFP by i.c.m. injection to rejuvenate meningeal lymphatic drainage function. Young mice (8-10 weeks of age) received 2 µl of artificial CSF containing 10^{13} genome copies per ml of control AAV1-CMV-eGFP by i.c.m. injection. Mice were rested for two weeks and then were subjected to either TBI or sham procedures. Two weeks after injury, brains were harvested, sectioned and stained for markers of gliosis. a) Representative image of a meningeal whole mount 1 month after viral vector administration showing Lyve-1 (grey), DAPI (blue), and AAV1-CMV-eGFP (green). b) Righting times (Young-GFP+TBI n=10, Aged-GFP+TBI n=14, Aged-VEGFC+TBI n=16; pooled data from 2 independent experiments) and c) 10-point gross neuroscore of mice at 1 hour after TBI (Young-GFP+TBI n=9, Aged-GFP+TBI n=14, Aged-VEGFC+TBI n=16; pooled data from 2 independent experiments). d) Representative images of hemisphere ipsilateral to the site of injury stained with Iba1 (grey), GFAP (red) and DAPI (blue). Dashed boxes in merge column indicate lesion site. e-h) Quantification of the percent area of (e-f) Iba1 and (g-h) GFAP immunoreactivity in the hemispheres contralateral and ipsilateral to the site of injury. (Young-GFP+TBI n=10, Aged-GFP+TBI n=13, Aged-VEGFC+TBI n=16; pooled data from 2 independent experiments). All n values refer to the number of mice used and the error bars depict mean ± s.e.m. *P* values calculated by one-way ANOVA with Tukey's multiple comparison correction (b,c,e,f,g,h). SSS, superior sagittal sinus; TS, transverse sinus.

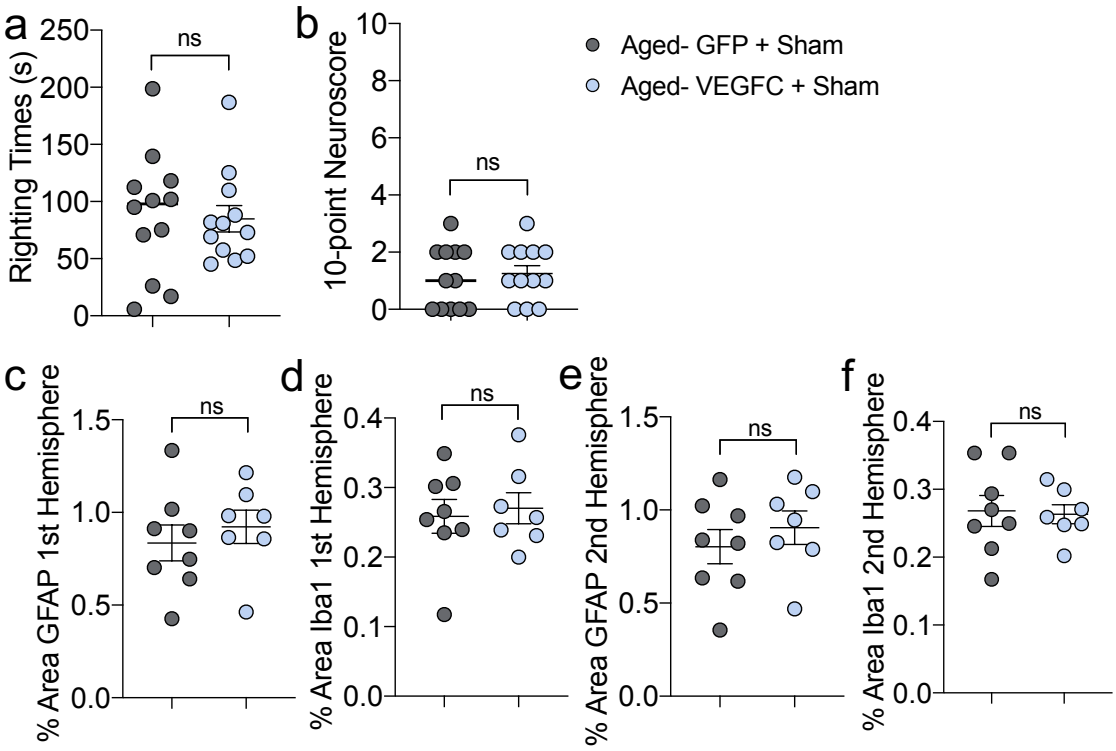

Figure 2.15. Treatment of uninjured aged mice with VEGF-C does not influence righting time, neuroscore, or gliosis measures. Aged mice (18-20 months old) received 2 µl of artificial CSF containing 10^{13} genome copies per ml of either AAV1-CMV-mVEGF-C or control AAV1-CMV-eGFP by i.c.m. injection and then mice were subjected to sham treatment 2 weeks later. a) Righting times and b) 10-point gross neuroscore of mice at 1 hour post sham procedure (n=12 mice/group; pooled data from 2 independent experiments). Two weeks after sham procedure, brains were harvested, sectioned, and stained for markers of gliosis. c-f) Quantification of the percent area of Iba1 and GFAP immunoreactivity in both hemispheres of the brain (Aged-GFP+Sham n=8, Aged-VEGFC+Sham n=7). All n values refer to the number of mice used and the error bars depict mean ± s.e.m. *P* values were calculated using two-tailed Student's t-test.

2.4 Discussion

Despite being a significant medical issue, the biological factors that promote CNS pathology and neurological dysfunction following TBI remain poorly characterized. Recently, the meningeal lymphatic system was identified as a critical mediator of drainage from the CNS. In comparison to other peripheral organs, our understanding of how defects in lymphatic drainage from the CNS contribute to disease is limited. Here, we report that meningeal lymphatic function is impaired after TBI and that this disruption begins almost immediately and may take months to fully return to pre-injury levels. We further show that ICP is significantly elevated at two hours post-brain injury, and that this increase in ICP can promote hotspot dysfunction in the uptake of CSF from the subarachnoid space. Moreover, we find that increased ICP is sufficient to cause meningeal lymphatic dysfunction. Our work also provides evidence that pre-existing lymphatic dysfunction, as may occur with repetitive head injury and aging, predisposes the brain to more severe neuroinflammation and cognitive deficits.

Several recent studies in other models of disease have shown that the meningeal lymphatic system is critical for modulating immune responses and inflammation in the CNS [90, 91, 139]. Whether CNS lymphatic drainage is involved in promoting or resolving inflammation is likely specific to individual disease settings. For instance, mounting evidence indicates that lymphatic drainage plays a role in promoting autoimmunity by facilitating drainage of brain antigens to the peripheral dCLN. In the context of experimental autoimmune encephalomyelitis (EAE), ablation of the meningeal lymphatic vasculature was found to decrease disease severity by limiting $CD4^+$ T cell infiltration into the spinal cord [91]. Consistent with a disease-promoting role for CNS lymphatic drainage in EAE, other studies have shown that lymphangiogenesis near the cribriform plate is a hallmark of disease progression and suggest that this may augment the peripheral adaptive immune response to myelin peptides [92]. In other instances, drainage of

macromolecules and protein aggregates from the brain through the meningeal lymphatics is essential to maintain CNS health, as was recently shown to be the case in mouse models of Alzheimer's disease [139]. In this study by Da Mesquita *et al.*, it was shown that blocking lymphatic drainage with Visudyne photoablation results in the accumulation of amyloid beta aggregates in the meninges and hippocampus. Furthermore, recent evidence also suggests that having proper meningeal lymphatic drainage is critical for mounting protective immune responses to invasive and hard-to-target brain cancers [90].

Neuroinflammation and gliosis can often persist for months or even years post-brain trauma [10, 12], and interventions aimed at attenuating this neuroinflammation have proven successful in modulating cognitive outcomes [43, 49]. Yet, the physiological processes involved in the prolonged inflammatory state of the TBI brain remain poorly defined. Based on our findings presented here, it is possible that impaired drainage of DAMPs such as amyloid beta, necrotic cells, and cellular debris from the brain could incite prolonged immune activation in the injured brain. Therefore, therapeutic approaches that promote functional recovery of the meningeal lymphatic system could provide strategies to help curtail the persistent neuroinflammation that is a hallmark of TBI.

An acute rise in ICP after head trauma is a poor prognostic indicator in TBI patients and is estimated to account for nearly half of all TBI mortalities [147, 148]. We found that the rise in ICP seen after TBI or jugular vein ligation results in decreased meningeal lymphatic drainage, indicating that changes in the CNS environment can rapidly impact lymphatic function. While acute rises in ICP after injury, caused by brain edema and swelling, may result in decreased drainage [147], it still remains to be seen how longer-lasting alterations in ICP affect the meningeal lymphatic vasculature. It is possible that preventing exorbitant rises in ICP after brain injury may

allow for a more succinct immune response due to more efficient drainage of neurotoxic DAMPs from the CNS.

The mechanism of how CSF is taken up into meningeal lymphatics and removed from the CNS is still widely debated. Before the recent characterization of the meningeal lymphatic system, it was thought that arachnoid granulations were the main mechanism through which CSF was removed from the brain [170]. The arachnoid granulations are areas of the arachnoid layer in the meninges that project through the meningeal layers into the venous sinuses, where they are thought to absorb CSF. However, evidence for arachnoid granulations in mice has been scarce [170]. With the recent findings that the meningeal lymphatic system is capable of transporting CSF to the periphery, the term hotspots was coined to describe areas along this lymphatic network in which CSF appears to be taken more readily into the lymphatic pathways. These hotspots have been reported both in the dorsal and basal meningeal lymphatic network [91, 140]. How these hotspots take up CSF and solutes from the CNS is still not clear. It has been proposed that the lymphatics may send extensions into the sub-arachnoid space where CSF can be taken up, but this has not been further substantiated [91]. Further research is needed to understand the anatomy of the lymphatic vasculature at the hotspots and to determine which macromolecules and cells are capable of trafficking through the meningeal lymphatic vasculature in homeostasis and various disease states. Furthermore, additional studies are also needed to delineate the contributions of the recently identified basal CNS lymphatics in TBI pathogenesis [140].

Because clearance of ISF containing solutes and macromolecules from the brain parenchyma relies on perivascular routes, termed the glymphatic system [81, 83, 84, 171], we anticipate that changes in ICP would also affect glymphatic function. Indeed, our findings are consistent with data showing that the glymphatic system is impaired after TBI [80, 83]. The glymphatic system and lymphatic system are inherently linked [81, 85]. The glymphatic system is responsible for

transport of ISF to the CSF surrounding the brain, and the lymphatic system takes up CSF/ISF for transport into the periphery [83, 85, 171]. While decreased ISF transport from the parenchyma to the sub-arachnoid space may lead to decreased lymphatic drainage [83, 84], it has also been shown that impaired lymphatic drainage decreases recirculation of macromolecules through the glymphatic route [139]. Our findings indicate that, in addition to the previously described glymphatic dysfunction, there is also lymphatic dysfunction after TBI. By directly targeting the meningeal lymphatic vasculature through pharmacologic photoablation in our studies, we highlight that pre-existing lymphatic dysfunction results in increased TBI-mediated neuroinflammation and cognitive dysfunction. Additionally, injections into the cisterna magna, as was done in our studies, largely bypass the need for glymphatic clearance, as the meningeal lymphatic network takes up CSF directly from this compartment. Therefore, impairment in both systems likely coalesce to cause defective clearance of toxins, protein aggregates, and macromolecules from the brain after TBI. Preventing the rapid rise in ICP seen after TBI may provide a route in which to address both the glymphatic and lymphatic dysfunction that persists after brain trauma; however, future studies are needed to definitively test this.

Interestingly, TBI has been strongly linked to an increased risk of developing numerous other neurological disorders later in life including CTE, Alzheimer's disease, amyotrophic lateral sclerosis, and other psychiatric disorders [4-7, 9]. Our understanding of how brain trauma contributes to the development of these other neurological disorders at the mechanistic level is currently limited. Like TBI, the majority of these CNS disorders are also characterized by neuroinflammation and impaired clearance of DAMPs (e.g. protein aggregates and neurotoxic debris). One could envision that TBI-induced disruptions in meningeal lymphatic function and the resulting buildup of DAMPs in the brain could set off a series of events that ultimately lead to other forms of neurological disease down the road, although future studies are needed to formally test this hypothesis. One approach to test this hypothesis is to investigate whether rejuvenation of

meningeal lymphatic function after TBI limits the risk of disease sequelae later in life. As a proof of principle, we show here that rejuvenating meningeal lymphatic vasculature in aged mice with viral delivery of VEGF-C is effective in preventing excessive Iba1 gliosis following brain trauma.

For reasons that remain poorly understood, sustaining a second head injury before the brain has recuperated from prior head trauma can have devastating consequences. Furthermore, it has been shown that repetitive TBIs result in more serious long-term outcomes when compared to a single TBI [32, 33, 154, 156, 172]. Indeed, recent reports in the scientific literature and media have highlighted several high-profile cases of repetitive TBI and its devastating consequences that can include CTE and suicide [28, 36, 156]. Improved understanding of what makes the injured brain more vulnerable to more severe pathology and neurological demise following secondary head trauma will lead to improved treatment practices. Our findings presented in this paper suggest that disruptions in meningeal lymphatic function may contribute at some level to the more severe neuroinflammation and neurological dysfunction commonly observed in repetitive TBI. The lack of defined guidelines for when individuals can safely return to high-risk activities following TBI is a significant problem for caregivers. Our work suggests that evaluating meningeal lymphatic drainage recovery post-injury might provide clinicians with a much-needed empirical test to inform athletes and military personnel of when it is safe to return to action. However, improved diagnostics must first be developed in order to accurately measure meningeal lymphatic function in humans.

While our studies on pre-existing lymphatic dysfunction before TBI provide important insights into how lymphatic dysfunction may contribute to a higher neuroinflammatory state, additional studies are required to more fully understand the role that each CNS-resident cell population is playing in this inflammatory environment. While we see an increase in GFAP immunoreactivity in the brain after Ablation + TBI as compared to other control groups alone two weeks after injury (Figure

2.12a,b), this same change is not apparent in the sequencing data at one week post injury. We would expect the inflammatory environment to be dynamically changing throughout this time and believe that following up on these studies with other techniques including single cell RNA sequencing would be incredibly valuable to understand how cells such as microglia and astrocytes are changing in response to injury, and how they might be influencing the inflammatory environment after TBI.

TBI is an especially serious threat to health in the elderly, where it is a leading cause of death and disability [152, 153, 155]. Even though the elderly only account for 10% of all TBI cases, over 50% of all TBI-related death occurs in individuals over the age of 65 [173]. It has been extensively shown that similar injuries result in more severe pathology and neurological impairment in the elderly than in other age groups [151, 155]; however, the cause for this is currently not well understood. Interestingly, several recent studies have shown that the meningeal lymphatics are impaired with aging [139-141]. Moreover, boosting lymphatic function with VEGF-C treatment can mitigate the cognitive deficits seen in aged mice [91]. In our studies presented here, we show that photoablation of meningeal lymphatic vessels before head injury leads to more severe neuroinflammatory outcomes and decreased performance in cognitive tests following TBI. Therefore, it is feasible that aging-associated deterioration of CNS lymphatic function may contribute at some level to the especially devastating consequences of TBI in the elderly. Indeed, our data demonstrating that viral delivery of VEGF-C to aged mice improves neuroinflammatory outcomes after TBI provides further evidence that the lymphatic system may be involved in the particularly devastating outcomes the elderly experience after TBI. Furthermore, it suggests that boosting meningeal lymphatic drainage may serve as a viable therapeutic option to limit TBI pathogenesis.

Overall, the work described here provides insights into how the meningeal lymphatic system is impacted by TBI and also how pre-existing defects in this drainage system can predispose the brain to exacerbated neuroinflammation and cognitive outcomes following brain injury. We show that even mild forms of TBI can result in pronounced defects in meningeal lymphatic function that can last for weeks post-injury. Mechanistically, we demonstrate that closed-skull TBI is associated with elevated ICP and that this can contribute to disruptions in meningeal lymphatic drainage function. Finally, we provide evidence that boosting meningeal lymphatic function through delivery of VEGF-C may serve to decrease neuroinflammation after TBI. Importantly, improved understanding of the contributions of the meningeal lymphatic system in brain injury and recovery may help provide opportunities for therapeutic approaches to treat TBI.

2.5 Methods

Mice

All mouse experiments were performed in accordance with the relevant guidelines and regulations of the University of Virginia and approved by the University of Virginia Animal Care and Use Committee. C57BL/6J mice were obtained from Jackson Laboratories. Mice were housed and behavior was conducted in specific pathogen-free conditions under standard 12-hour light/dark cycle conditions in rooms equipped with control for temperature (21 ± 1.5°C) and humidity (50 ± 10%). Mice matched for sex and age were assigned to experimental groups and all adult mice used were between 8-10 weeks of age. Males and females were used for drainage and lymphangiogenesis studies, as sex has not been shown to influence lymphatic drainage at baseline [139]. Both males and females were also used to study the effects of increased ICP on lymphatic flow. Males were used for all pre-existing lymphatic dysfunction studies (Figures 2.8-2.13) for consistency with behavioral readouts and for consistency within the RNA sequencing data, as sex can influence both of these readouts. Male mice were also used for the aged mice

experiments. All aged mice (used for experiments in Figures 2.14-2.15) were between 18 and 24 months of age and were obtained from Jackson Laboratories and the National Institute on Aging (NIA) Aged Rodent Colonies.

Traumatic brain injury

This injury paradigm was adapted from the published Hit and Run model [169]. Mice were anesthetized by 4% isoflurane with 0.3 kPa O_2 for 2 minutes and then the right preauricular area was shaved. The mouse was placed prone on an 8 x 4 x 4-inch foam bed (type E bedding, open-cell flexible polyurethane foam with a density of approximately 0.86 pounds per cubic feet and a spring constant of approximately 4.0 Newtons per meter) with its nose in a nosecone delivering 1.5% isoflurane (purchased from Foam to Size, Ashland VA). The head was otherwise unsecured. The device used to deliver TBI was a Controlled Cortical Impact Device (Leica Biosystems, 39463920). A 3 mm impact probe was attached to the impactor device which was secured to a stereotaxic frame and positioned at 45 degrees from vertical. In this study, we used a strike depth of 2 mm, 0.1 s of contact time and an impact velocity of 5.2 meters (m) per second (s). An impact velocity of 6.2 m per s was used for the TBI severity studies in Figure 2.4. The impactor was positioned at the posterior corner of the eye, moved 3 mm towards the ear and adjusted to the specified depth using the stereotaxic frame. A cotton swab was used to apply water to the injury site and the tail in order to establish contact sensing. To induce TBI, the impactor was retracted and dispensed once correctly positioned. The impact was delivered to the piriform region of the brain. Following impact, the mouse was placed supine on a heating pad and allowed to regain consciousness. After anesthesia induction, the delivery of the injuries took less than 1 minute. The time until the mouse returned to the prone position was recorded as the righting time. Upon resuming the prone position, mice were returned to their home cages to recover on a heating pad for six hours with soft food. For sham procedures, mice were anesthetized by 4% isoflurane with 0.3 kPa O_2 for 2 minutes and then the right preauricular area was shaved. The mouse was placed

prone on a foam bed with its nose secured in a nosecone delivering 1.5% isoflurane. The impactor was positioned at the posterior corner of the eye, moved 3 mm towards the ear and adjusted to the specified depth using the stereotaxic frame. A cotton swab was used to apply water to the injury site and the tail in order to establish contact sensing. Then, the impactor was adjusted to a height where no impact would occur, and was retracted and dispensed. Following the sham procedure, the mouse was placed supine on a heating pad and allowed to regain consciousness. Mice were allowed to recover on the heating pad in their home cages for 6 hours with soft food before being returned to the housing facilities.

Intra-cisterna magna injections

Mice were anaesthetized by intraperitoneal (i.p.) injection of a mixed solution of ketamine (100 mg per kg) and xylazine (10 mg per kg) in sterile saline. The skin of the neck was shaved and cleaned with iodine and 70% ethanol, and ophthalmic solution (Puralube Vet Ointment, Dechra) was placed on the eyes to prevent drying. The head of the mouse was secured in a stereotaxic frame and an incision in the skin was made at midline. The muscle layers were retracted and the cisterna magna exposed. Using a Hamilton syringe (coupled to a 33-gauge needle), the volume of the desired solution was injected into the cerebrospinal fluid (CSF)-filled cisterna magna compartment. For the bead experiments, 2 µl of FluoSpheres carboxylate 0.5 µm-beads 505/515 (Invitrogen, F8813) in artificial CSF (597316, Harvard Apparatus UK) were injected at a rate of 2 µl per minute. For Visudyne experiments, 5 µl of Visudyne (verteporforin for injection, Valeant Ophthalmics) was injected at a rate of 2.5 µl per minute. For Lyve-1 labeling experiments, 2 µl of anti-mouse Lyve-1 488 (Invitrogen, 53044382, undiluted) was injected at a rate of 2 µl per minute. For experiments with aged mice, 2 µl of artificial CSF containing 10^{13} genome copies per ml of AAV1-CMV-mVEGF-C, or control AAV1-CMV-eGFP (AAV1, adeno-associated virus serotype 1; CMV, cytomegalovirus promoter; eGFP, enhanced green fluorescent protein; purchased from

Vector BioLabs, Philadelphia), were injected into the cisterna magna CSF at a rate of 2 µl per minute. The needle was inserted into the cisterna magna through retracted muscle in order to prevent backflow upon needle removal. The neck skin was then sutured, after which the mice were subcutaneously injected with ketoprofen (1 mg per kg) and allowed to recover on a heating pad until fully awake.

Pharmacologic meningeal lymphatic vessel ablation

Visudyne treatment was adapted from published protocols [91, 139, 157]. Selective ablation of the meningeal lymphatic vessels was achieved by i.c.m. injection and transcranial photoconversion of Visudyne (verteporfin for injection, Valeant Ophthalmics). Visudyne was reconstituted following the manufacturer's instructions and 5 µl was injected i.c.m. following the procedure described above in the intra-cisterna magna injections methods section. After 15 minutes, a midline incision was created in the skin to expose the skull and visudyne was photoconverted by pointing a 689-nm-wavelength non-thermal red light (Coherent Opal Photoactivator, Lumenis) to five different locations above the intact skull (1 at the injection site, 1 at the superior sagittal sinus, 1 at the confluence of the sinuses and 2 at the transverse sinuses). This experimental group is labeled as Ablated or Visudyne + laser. Each location was irradiated with a light dose of 50 J per cm^2 at an intensity of 600 mW per cm^2 for a total of 83 seconds. Controls were injected with the same volume of Visudyne (without the photoconversion step; labeled as Visudyne or Not Ablated) or sterile saline plus laser treatment (labeled as Vehicle + laser). The scalp skin was then sutured, after which the mice were subcutaneously injected with ketoprofen (1 mg per kg) and allowed to recover on a heating pad until fully awake.

Intracranial pressure measurements

Intracranial pressure (ICP) was measured according to published protocols [91, 139]. Mice were anaesthetized by i.p. injection with ketamine (100 mg per kg) and xylazine (10 mg per kg) in saline

and the skin was incised to expose the skull. A 0.5-mm diameter hole was drilled in the skull above the left parietal lobe. Using a stereotaxic frame, a pressure sensor catheter (model SPR100, Millar) was inserted perpendicularly into the cortex at a depth of 1 mm. To record changes in ICP, the pressure sensor was connected to the PCU-2000 pressure control unit (Millar). For measurements in mice after TBI (30 minutes, 2 hours, 6 hours, 24 hours, 3 day, 4 day and 1 week post injury) or after jugular venous ligation (3 hours and 24 hours) ICP was recorded for 6 minutes after stabilization of the signal and the average pressure was calculated over the last 3 minutes of recording. Mice were euthanized following the procedure.

Jugular venous ligation

Mice were anaesthetized by i.p. injection with ketamine (100 mg per kg) and xylazine (10 mg per kg) in saline. The left and right preauricular area and the skin between the ears was shaved and prepped with iodine and 70% ethanol. Ophthalmic ointment (Puralube Vet Ointment, Dechra) was applied to the eyes to prevent drying. The mouse was secured onto a surgical plane in the lateral position and a lateral incision was created between the two mouse ears. The incision site was retracted to reveal the left temporalis muscle. The left temporalis muscle was retracted to reveal the infratemporal fossa, where the left internal jugular vein can be identified. The left internal jugular vein was ligated using 8-0 Nylon Suture (AD surgical, XXS-N808T6), and then the same procedure was performed on the opposite side to ligate the right jugular vein. The incision was then sutured and the mice were subcutaneously injected with ketoprofen (1 mg per kg) and were allowed to recover on the heating pad until awake. Sham mice received the incision and the jugular veins were exposed bilaterally, but they did not undergo ligation. The intracranial pressure on these mice was recorded as described in the intracranial pressure measurements methods section 3 and 24 hours after ligation.

RNA extraction and sequencing

For RNA extraction, the brain hemisphere ipsilateral to the brain injury was harvested, the cerebellum and olfactory bulbs were removed, and the hemisphere was immediately snap-frozen in dry ice and stored at −80 °C until further use. After defrosting on ice, samples were mechanically homogenized in 500 μl extraction buffer comprised of T-PER Tissue Protein Extraction Reagent (78510, Thermo Scientific) supplemented with PhosSTOP phosphatase inhibitor cocktail (04906845001, Roche) and cOmplete protease inhibitor cocktail (11873580001, Roche). 100 μl of the homogenate was transferred to a tube containing 1.1 ml TRIzol Reagent (15596018, Life Technologies) and vortexed. 200 μl chloroform (BP1145-1, Fisher Scientific) was added to the samples, was vortexed, and was allowed to incubate for 5 minutes at room temperature. Samples were then spun at 18,400 RCF at 4 °C for 15 minutes. The top aqueous phase was transferred into a new Eppendorf tube and 300 μl isopropanol (I9516, Sigma) was added, vortexed, and allowed to incubate at room temperature for 10 minutes. Samples were then spun down at 13,500 RCF at 4 °C for 12 minutes. The RNA pellet was washed 2 times with 70% ethanol and resuspended in DNAse/RNAse free water. Sample quality and RNA concentration were assessed using the NanoDrop 2000 Spectrophotometer (Thermo Scientific) and samples were frozen at -80 °C until further use. For sequencing, total RNA samples were sent to GENEWIZ for library preparation and paired end sequencing.

RNA-seq analysis

The raw sequencing reads (FASTQ files) were aligned to the UCSC mm10 mouse genome build using the splice-aware read aligner HISAT2 [174]. Samtools was used for quality control filtering[175]. Reads were sorted into feature counts with HTSeq [176]. DESeq2 was used to normalize the raw counts based on read depth and perform principal component analysis and differential expression analysis [177]. The p-values were corrected with the Benjamini-Hochberg procedure to limit false positives arising from multiple testing. The gene set collections from

MSigDB were used for differential gene set enrichment analysis [159]. The analysis itself was performed using the Seq2Pathway, fgsea, tidyverse, and dplyr software packages. Heatmaps were generated using the pheatmap R package [https://github.com/raivokolde/pheatmap] while other plots were made with the lattice (http://lattice.r-forge.r-project.org/) or ggplot2 [https://ggplot2.tidyverse.org] packages. The GWAS Catalog was used to find genes associated with neurodegenerative or psychiatric diseases [https://www.ebi.ac.uk/gwas/home][165], and the circos plot including these data was generated using the circlize R package[178]. All code used for analysis is available at [https://github.com/arun-b-dutta/TBI_Lymphatics_RNAseq-Analysis]. Raw and processed sequencing data can be accessed through the Gene Expression Omnibus (GEO) at [https://www.ncbi.nlm.nih.gov/geo/query/acc.cgi?acc=GSE155063].

Behavioral testing

All behavioral experiments were carried out during daylight hours (except the Novel Location Recognition test, which was performed at 5:00PM) in a blinded fashion.

Gross Neuroscore

The gross neuroscore was performed following a published protocol with modifications [179]. Briefly, mice performed 10 individual tasks to assess behaviors including seeking/exploring tendencies, the startle reflex, and balance/motor coordination. The ability to cross different width beams, to react to a loud noise, to balance on a beam, and to explore the surroundings were assessed and scored by a blinded experimenter 1 hour after TBI. If the mouse was able to adequately perform the task, a score of 0 was given. If the mouse failed to adequately perform the test, a score of 1 was given. Scores for the 10 tasks were summed for a total minimum score of 0 and a total maximum score of 10.

Rotarod test

The mice were transported to the behavior room and allowed to habituate for 1 hour before each day of testing. The experimental apparatus used in this test contained 5 separate compartments on a rotating rod to accommodate 5 mice per trial (MED Associates Inc, ENV-575M). The rod was programmed to turn starting at 4 rotations per minute (rpm) and to accelerate to 40 rpm over a span of 5 minutes. Each mouse was placed on the rod and allowed to ambulate until it either fell off, hung without effort on the rod for a total of 5 rotations, or reached the trial endpoint (6 minutes). When a mouse fell from the rotarod, it disrupted a laser sensor to stop recording. The time spent on the rod and the speed at which the mouse fell or the trial ended was recorded (RotaRod Version 1.4.1, MED associates inc). Three trials were performed each day for 3 days. The 3 trials per day were averaged, and latency to fall and percent performance increase were calculated based off of the average time of trial per mouse per day.

Novel Location Recognition Test (NLRT)

The novel location recognition test was performed following a published protocol with modifications [139]. The mice were transported to the behavior room and allowed to habituate for 1 hour before each trial of the test. The experimental apparatus used in this study was a square box made of opaque white plastic (35 cm × 35 cm). The mice were first habituated to the square apparatus for 10 minutes by allowing for free exploration within the open field. Eight hours later, after 5:00PM, two identical objects were then positioned in the two far corners of the arena at distances of 5 cm away from the adjacent arena wall (familiar locations). Mice were then placed in the arena facing the wall furthest away from the objects and allowed to explore the arena and objects for 10 minutes. Time spent investigating the objects was measured and was considered the training phase of the test. After 24 hours, the mice were placed in the same box but one object was moved down to a diagonal position (novel location). The time spent exploring the objects in the familiar or novel location was measured for 10 minutes and was considered the test phase. Exploration of an object was recorded when the mouse approached an object and touched it with

its vibrissae, snout, or forepaws and was measured using a video tracking software (Noldus Ethovision XT). The preference for either the novel or familiar object was calculated as the percent of time the mouse spent with one object divided by the total time the mouse spent investigating either object.

Tissue collection

Mice were euthanized with CO_2 and then transcardially perfused with 20 ml 1x PBS. Deep cervical lymph nodes were dissected and drop-fixed in 4% paraformaldehyde (PFA) for 2 hours at 4 °C and then the CUBIC clearance protocol was performed as described below in the dCLN clearance methods sections [180]. For meningeal whole mount collection, skin and muscle were stripped from the outer skull and the skullcap was removed with surgical scissors and fixed in 2% PFA for 12 hours at 4 °C. Then the meninges (dura mater and arachnoid mater) were carefully dissected from the skullcaps with Dumont #5 forceps (Fine Science Tools). Meningeal whole-mounts were then moved to PBS and 0.05% azide at 4 °C until further use. Brains were removed and kept in 4% PFA for 24 hours and cryoprotected with 30% sucrose for 3 days. A 4 mm coronal section of brain tissue that surrounded the site of the lesion was removed using a brain sectioning device and then frozen in Tissue-Plus OCT compound (Thermo Fisher Scientific). Fixed and frozen brains were sliced (50 µm thick sections) with a cryostat (Leica) and kept in PBS + 0.05% azide at 4 °C until further use.

dCLN clearance

dCLN clearance was performed following the published CUBIC protocol with modifications [180]. Briefly, nodes were incubated in 50% reagent 1 (prepared 1:1 with dH2O) for 1 day at 37 °C, shaking, with DAPI (1:1000). Nodes were then transferred to reagent 1 for 1 day at 37 °C, shaking, with DAPI (1:1000). Nodes were washed 2 times in PBS + 0.01% sodium azide for 2 hours and overnight with DAPI (1:1000) at 37 °C. Then nodes were incubated with 50% reagent 2 (prepared

1:1 with dH2O) for 1 day at 37 °C with DAPI (1:1000). Finally, nodes were incubated with reagent 2 for 1 day at 37 °C. Nodes were placed in 8 well chambers (155411, Thermo Fisher) with mineral oil and imaged with confocal microscopy.

Immunohistochemistry, imaging and quantification

For immunofluorescence staining, floating brain sections and meningeal whole-mounts in PBS and 0.05% azide were blocked with either 2% donkey serum or 2% goat serum, 1% bovine serum albumin, 0.1% triton, 0.05% tween-20, and 0.05% sodium azide in PBS for 1.5 hours at room temperature. This blocking step was followed by incubation with appropriate dilutions of primary antibodies: anti-Lyve-1–eFluor 660 & eFluor 488 (eBioscience, clone ALY7, 1:200), anti-CD31 (Millipore Sigma, MAB1398Z, clone 2H8, 1:200), anti-Iba1 (Abcam, ab5076, 1:300) and anti-GFAP (Thermo Fisher Scientific, 2.2B10, 1:1000) in the same solution used for blocking overnight at 4°C or for 3 hours at room temperature. Meningeal whole-mounts or brain tissue sections were then washed 3 times for 10 minutes at room temperature in PBS and 0.05% tween-20, followed by incubation with the appropriate goat or donkey Alexa Fluor 594 or 647 anti-rat, -goat (Thermo Fisher Scientific, 1:1000) or -Armenian hamster (Jackson ImmunoResearch, 1:1000) IgG antibodies for 2 hours at RT in the same solution used for blocking. The sections or whole-mounts were then washed 3 times for 10 minutes at RT before incubation for 10 minutes with 1:1000 DAPI in PBS. The tissue was then transferred to PBS and mounted with ProLong Gold antifade reagent (Invitrogen, P36930) on glass slides with coverslips. Slide preparations were stored at 4°C and imaged using a Lecia TCS SP8 confocal microscope and LAS AF software (Leica Microsystems) within one week of staining. Quantitative analysis of the acquired images was performed using Fiji software. For the assessment of gliosis in the injured and uninjured brains, 2 representative brain sections from the site of the lesion (approximately -0.74 to 0 bregma) or the corresponding area in sham animals were fully imaged and at least 5 animals were included per experimental group. The full brain section was adjusted for brightness/contrast uniformly for each

experiment (Experiments in Figure 2.12a-c: b/c- GFAP-32/190, b/c- Iba1-51/158, experiments in Figure 2.14h-j: b/c- GFAP- 41/224, b/c- Iba1-40/174), and the percent area of coverage of each immunohistochemical markers was calculated per hemisphere for each brain section. Each hemisphere was traced, and then the threshold was uniformly set for each experiment to select for stained cells (Experiments in Figure 2.12a-c: thresh- GFAP-90/255, b/c- Iba1-115/255, Experiments in Figure 2.14h-j: b/c- GFAP- 115/255, b/c- Iba1-139/255). The mean percent area fraction was calculated using Microsoft Excel. For Figure 2.2, high magnification images (20x and 63x) were taken directly adjacent to the site of the injury and the entire hemisphere ipsilateral to the injury was quantified for the levels of gliosis at each timepoint as specified above. For lymph nodes, the percent volume of microbead coverage in cleared dCLN was assessed by creating a 3D reconstruction of the node and then calculating the volume covered by beads divided by the total volume of the node using Fiji. The right and the left dCLN percent volume were averaged together for each mouse. For assessment of meningeal lymphatic vessel coverage and complexity, images of meningeal whole-mounts were acquired using a confocal microscope and Fiji was used for quantifications. The entire meningeal whole-mount (overlying both the injured and uninjured hemisphere) was traced and used for quantification. The percent area coverage of Lyve-1 was used to determine the coverage of the lymphatic vessels. When applicable, the same images were used to assess the percentage of field coverage by Lyve-1^{-}CD31^{+} vessels. To assess lymphatic vessel diameter, 70 measurements per meningeal whole-mount were taken by a blinded experimenter (40 along the transverse sinus and 30 along the superior sagittal sinus) and were averaged together. Lymphatic vessel loops and sprouts were calculated along both the transverse sinus and superior sagittal sinus by two independent blinded experimenters. Areas along the edge of the transverse sinuses were excluded for sprout quantification to avoid counting any lymphatic ends created by removal of the whole-mount. All meningeal whole mounts used for quantification of lymphatic morphology were imaged with identical confocal settings and Fiji parameters (b/c-Lyve-1-18/149, thresh-Lyve-1-102/255). For microglia morphology analysis, high

magnification (63x) images of microglia were taken and the filament function in Imaris software (9.5.1 Bitplane) was used to identify Iba1+ cells with their dendritic processes. Three fields of view in the peri-lesional area were imaged for each section, and two sections were imaged for each mouse. The microglia parameters for each section and field of view (cell number, filament dendrite length, filament dendrite volume, and number of dendritic branch points) were averaged together and plotted as one point per mouse. For the Sholl analysis, 4 microglia per field of view were quantified for 5 mice.

Flow cytometry

Mice were euthanized and blood was collected with cardiac puncture. Red blood cells were lysed, and then cells were then centrifuged for 5 minutes at 400 RCF and resuspended in 200 μl FACS buffer (pH 7.4; 0.1 M PBS; 1 mM EDTA, and 1% BSA). Fluorescence data were collected with a Gallios (Beckman Coulter), then analyzed using FlowJo software (Treestar). Single cells were gated using the height, area, and pulse-width of the forward and side scatter. Beads were gated based on their size and fluorescence.

eGFP or VEGF-C AAV delivery

For experiments using viral-mediated expression of mVEGF-C to enhance meningeal lymphatic vasculature growth, 2 μl of artificial CSF containing 10^{13} genome copies per ml of AAV1-CMV-mVEGF-C or control AAV1-CMV-eGFP (AAV1, adeno-associated virus serotype 1; CMV, cytomegalovirus promoter; eGFP, enhanced green fluorescent protein; purchased from Vector BioLabs, Philadelphia) were injected into the cisterna magna CSF at a rate of 2 μl per minute, following the procedure described in the intra-cisterna magna injections methods section.

Statistical analysis and reproducibility

Sample sizes were chosen on the basis of standard power calculations (with $\alpha = 0.05$ and power of 0.8). Experimenters were blinded to the identity of experimental groups from the time of euthanasia until the end of data collection and analysis. One-way ANOVA, with Bonferroni's multiple comparison test, Tukey's multiple comparison test, Dunnett's multiple comparison test, or Holm-Sidak's post hoc test, were used to compare multiple independent groups. Two-group comparisons were made using unpaired Student's t-test. For comparisons of multiple factors (for example, age versus treatment), two-way ANOVA with Bonferroni's post hoc test or Tukey's multiple comparison test was used. Repeated-measures two-way ANOVA with Bonferroni's post hoc test was used for day versus treatment comparisons with repeated observations. Statistical analysis (data are always presented as mean ± s.e.m.) was performed using Prism 8.0 (GraphPad Software, Inc.).

Data availability

All data and genetic material used for this paper are available from the authors on request. Raw and processed sequencing data can be accessed through the Gene Expression Omnibus (GEO) at [https://www.ncbi.nlm.nih.gov/geo/query/acc.cgi?acc=GSE155063]. Source data for all figures are provided with this paper.

Code availability

All code used for analysis is available at [https://github.com/arun-b-dutta/TBI_Lymphatics_RNAseq-Analysis].

Chapter 3

Discussion and Future Directions

3.1 Dissertation discussion

This dissertation focused on how brain injury affects the meningeal lymphatic vessels and how this lymphatic network shapes subsequent neuroinflammation. We presented data showing that the meningeal lymphatic system is impaired after even mild brain injuries and that this may stem from increases in intracranial pressure (ICP) (Chapter 2). We also demonstrated that TBI leads to more severe neuroinflammation and cognitive dysfunction when the brain possesses pre-existing impairments in the meningeal lymphatic system before head trauma (Chapter 2). Finally, we determined that administration of VEGF-C to boost the meningeal lymphatic pathways can decrease TBI-induced neuroinflammation in aged mice (Chapter 2). Emerging evidence points to extensive crosstalk between the immune system and the brain both under homeostatic conditions and following brain injury [181-184]. This dissertation has contributed to the knowledge on how the meninges serve a unique role in facilitating this crosstalk. While our studies have helped to uncover previously undescribed roles for the meningeal lymphatic system in head trauma, we have only just begun to scratch the surface in our understanding of how this drainage pathway influences TBI pathogenesis. In this discussion section, I highlight some of the future directions that I believe will be important to explore in an effort to further define how TBI-induced meningeal dysfunction mechanistically contributes to neurological disease.

3.1.1. Alterations of the meningeal lymphatic system and the contribution of increased ICP following TBI.

The studies presented in this dissertation show that lymphatic drainage, following a single mild TBI, is decreased out to a month post injury, and that increased ICP may contribute to this decrease in drainage (Figure 3.1). Increased ICP, or intracranial hypertension, is a main driver of morbidity and mortality post TBI [148, 185]. Current management recommendations for intracranial hypertension following a TBI include sedation, head elevation, and control of other factors including hypertension and seizures [186]. More severe and persistent increases in ICP can require hyperosmolar therapy, hyperventilation and/or hypothermia [186]. In the case that these initial methods are unsuccessful, surgical methods including CSF drainage and decompressive craniectomy can be used to address uncontrollable ICP [186]. While these interventions are utilized as life-saving measures, our findings suggest that early management of increased intracranial pressure may prevent severe lymphatic damage and therefore have more long-term benefits as well. Preventing a drastic rise in intracranial pressure following TBI may allow for better lymphatic drainage and prevent long-term inflammatory consequences. However, more studies are required to fully address this. For instance, one experiment that we hope to perform in the future is to deliver a TBI and then take surgical measures to prevent a rise in intracranial pressure within 30 minutes of injury. In one cohort of mice, intracranial pressure would be measured before and after this surgical intervention to determine whether it was successful in preventing the ICP rise. Specifically, we will drill two holes in the right and left parietal bones in the skull to stimulate decompressive craniectomy, which is used to relieve increased ICP in humans with refractory intracranial hypertension [187]. We would like to avoid doing a complete craniectomy, as we believe this will more greatly disturb the meningeal anatomy. In a second cohort of mice, following surgical intervention, we could then assess bead drainage to determine whether surgical intervention prevented the decrease in bead drainage we see after TBI. This would more fully address whether aggressive management of ICP could prevent the deficits we see in lymphatic drainage post TBI.

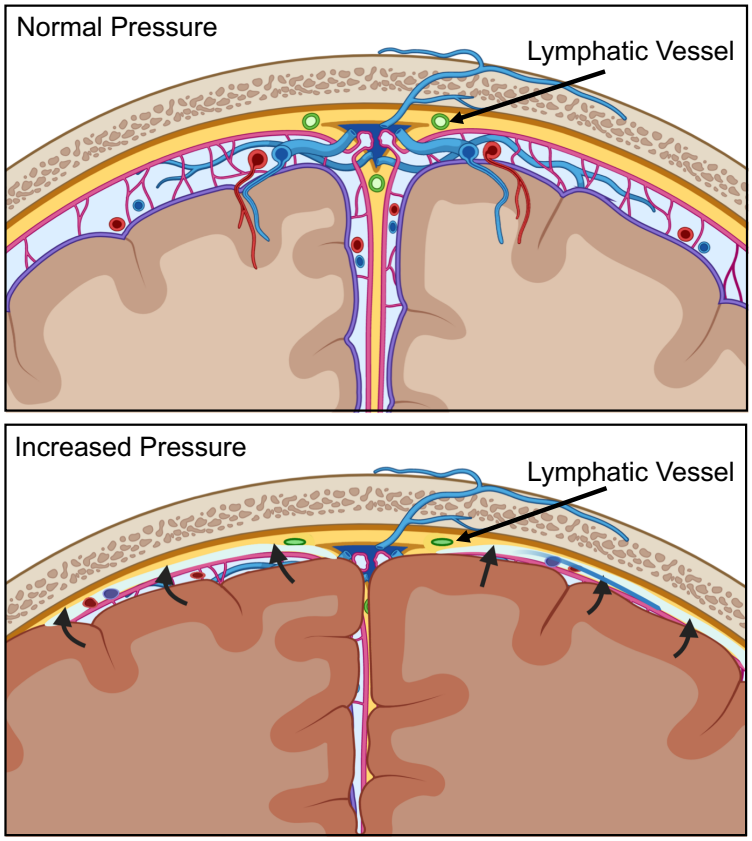

Figure 3.1. Increased intracranial pressure contributes to lymphatic dysfunction. Schematic depicting a potential mechanism behind how ICP may contribute to meningeal lymphatic dysfunction following brain injury. Cerebral edema and brain swelling against the fixed area of the skull may result in compression or damage of the meningeal lymphatic vessels.

While we see rapid reductions in lymphatic drainage immediately following brain injury, we show changes in the lymphatic vasculature morphology one- and two-weeks following injury. The mechanistic driver of these morphological changes is not fully understood. Moreover, the significance of these changes in either promoting or inhibiting drainage is not known. One possibility is that increased ICP seen after injury drives this response through initial damage to the lymphatic vasculature, which then promotes a lymphangiogenic healing response. A second possibility is that cytokines such as TNF and IL-6, both of which are known to increase in the CNS following TBI and promote lymphangiogenesis, may orchestrate these changes in lymphatic morphology post-TBI. Most likely, a combination of factors promotes this response. While it is not fully clear whether this transient lymphangiogenic response is beneficial or not, lymphatic drainage does appear to improve at one- and two-weeks following injury, suggesting that it may aid in the functional recovery of drainage.

Collectively, the rise in pressure following TBI likely contributes to a multitude of changes both in the brain and the meninges. However, while we believe increased ICP likely contributes to the meningeal lymphatic dysfunction seen after TBI, we do not anticipate that it is the sole cause of this deficit. For instance, we know that there is substantial cell death within the brain and meninges following brain injury, and likely some of the lymphatic endothelial cells involved in lymphatic drainage are either initially damaged by the injury, or secondarily damaged by the resulting inflammation. Moreover, the damaged blood brain barrier (BBB) allows for a massive influx of inflammatory cells that respond to the injury into both the brain and meninges. Whether this influx and eventual efflux of immune cells “clogs” the meningeal lymphatic system remains unknown. Further experiments to address how different CNS components (immune cells, protein aggregates) drain through the lymphatic system following injury are required.

Overall, cell death, increased ICP, and the massive immune influx likely all contribute to the decreased drainage capacities seen following injury. Aggressive management of increased ICP may not only be a life saving measure, but may also prevent more nuanced negative long-term consequences following injury including the heightened risk for neurodegenerative and psychiatric diseases. Additional murine and clinical studies are required to further study long-term outcomes following TBI with different levels of ICP control, to determine how important these initial steps are for controlling inflammation in the brain and meninges.

3.1.2 Pre-existing lymphatic dysfunction and opportunities for therapeutic intervention.

While the meningeal lymphatic network has not been studied in many disease contexts to date, it is clear that dysfunction in meningeal lymphatic drainage exists across several disease/degenerative contexts including aging, TBI and sub-arachnoid hemorrhage (SAH) [89, 139-141, 188]. Moreover, several studies, including our own, have indicated that having lymphatic dysfunction prior to a brain injury can worsen inflammation and behavioral outcomes [88, 89]. We believe that instances of pre-existing lymphatic dysfunction prior to brain injury may occur in several contexts, including in the elderly who experience a fall and TBI, or in athletes that may experience multiple concussions within close proximity. In the case of athletics, it would be important to understand when the lymphatic system has returned to baseline in order to determine when the risk is at its lowest for athletes to return to play after a concussion. While the lymphatic system has been successfully imaged in humans [86], there is still no known reliable way to measure meningeal lymphatic flow or function outside of murine models. Accordingly, it has not been established whether humans experience the same reduction in meningeal lymphatic drainage in aging or following head trauma. Further advances in imaging techniques are needed to assess whether the meningeal lymphatic system is indeed impaired in the same contexts as seen in mice. If this proves to be the case, these same imaging techniques could be used for

diagnostic purposes to assess the health of the meningeal lymphatic system in multiple contexts including brain injury, aging, and brain cancers.

While diagnostic imaging may be useful to empirically evaluate defects in meningeal lymphatic drainage function, it will be even more important to design ways to improve lymphatic function in those that have impairments. One exciting option, treatment with vascular endothelial growth factor C (VEGF-C), has been shown to improve meningeal lymphatic flow and improve outcomes in multiple contexts [89, 90, 139]. In aged mice, administration of VEGF-C to the meningeal lymphatic system was shown to improve memory as assessed by both the Morris Water Maze (MWM) and the Novel Location Recognition Test (NLRT) [139]. In a murine model of glioblastoma, VEGF-C was shown to increase the amount of T cells responding to the tumor [90]. This enhanced T cell response resulted in survival of these mice and improved the efficacy of PD-1/PD-L1 checkpoint blockade therapy [90]. In an almost certainly deadly disease, advances like this provide hope that the immune system can be modulated in a way to promote healing. Finally, my thesis studies demonstrated that administration of VEGF-C to the meningeal lymphatic vasculature in aged mice prior to TBI resulted in decreased gliosis in the brain parenchyma following injury (Chapter 2) [89]. While a promising candidate for therapy in multiple contexts, further research is required in both mice and humans to determine if VEGF-C administration is a viable option in these various conditions.

Research on the meningeal lymphatic system is still in its infancy; multiple diseases have not been studied in relation to this system, and we are just beginning to scratch at the surface of the ones that have. Many questions remain concerning how this system functions in humans and whether it could be manipulated to modulate disease progression. The burgeoning field of neuroimmunology has exposed novel opportunities for understanding diseases of the brain that have devastating outcomes and few therapeutic options. The meningeal lymphatic system lies at

the interface of the brain and the immune system, and understanding how it influences the progression and outcomes of neurodegenerative and psychiatric diseases may shed light on new treatment possibilities.

3.2 Future directions for study

In Chapter 2, we demonstrated that the meningeal lymphatic system plays an important role in the pathogenesis of TBI, however there is still much that is unknown about this system both in the context of brain injury and more broadly. Beyond the lymphatic system, little is currently known about how the meninges as a whole respond to and heal from TBI, and how this impacts neurological function and behavior. Below, I will present plans for future studies and ideas for follow-up work.

3.2.1 *Investigate whether meningeal lymphatic dysfunction in TBI contributes to premature amyloid beta (Aβ) buildup in Alzheimer's disease (AD) mouse models.*

Experiencing one or multiple TBIs results in a heightened risk for developing AD as well as an earlier age of AD onset [29, 36, 130, 189]. Moreover, TBI is associated with a higher Aβ and tau load in the brain in both humans and mouse models of AD [28, 30, 36]. The mechanisms behind this elevated risk for neurodegenerative disease following TBI has not yet been elucidated. Recent findings highlight that the CNS lymphatic system is impaired in aged mice, and that this impairment can result in exacerbated accumulation of Aβ within the meninges in mouse models of AD [139, 140, 144]. Moreover, our findings discussed in this thesis dissertation highlight a rapid and long-lasting impairment in the meningeal lymphatic system following brain injury (Figure 2.1). Whether brain injury induced lymphatic dysfunction contributes to the increased risk of AD and other sequelae following TBI remains unknown. For this future project, we hope to delineate how

dysregulation or rejuvenation of the meningeal lymphatic system influences neurodegenerative disease progression.

First, we will evaluate the contribution of meningeal lymphatic dysfunction to Aβ buildup after TBI, which may shed light on why TBI is a risk factor for AD. To this end, we will utilize the 5xFAD mouse model of AD, which expresses human APP and PSEN1 with 5 AD-linked mutations that overexpress Aβ, to assess whether TBI results in a more rapid buildup of Aβ in the brain and meninges [190]. While increased Aβ plaque load in the brain parenchyma has been reported after TBI [30, 36], it is not known whether TBI also results in seeding of Aβ in the meninges. We have begun to interrogate which age, injury severity, sex, and time after injury results in Aβ buildup. For a pilot experiment, we injured 5xFAD male mice at 8 weeks of age, and waited until 15 weeks of age to harvest the brains and meninges. We found that there is a trend towards increased Aβ load in the meninges after TBI that correlates with the righting time, which is a measure of the injury severity (Figure 3.2a-c). However, we did not see this same trend in the brain parenchyma (Figure 3.2d,e). In order to make more concrete conclusions, this experiment must be repeated. Additionally, the age of injury and/or harvest, in addition to the injury severity, quality and frequency may need to be optimized in order to reliably detect changes in Aβ accumulation following TBI. We hope to follow up with additional experiments in the future.

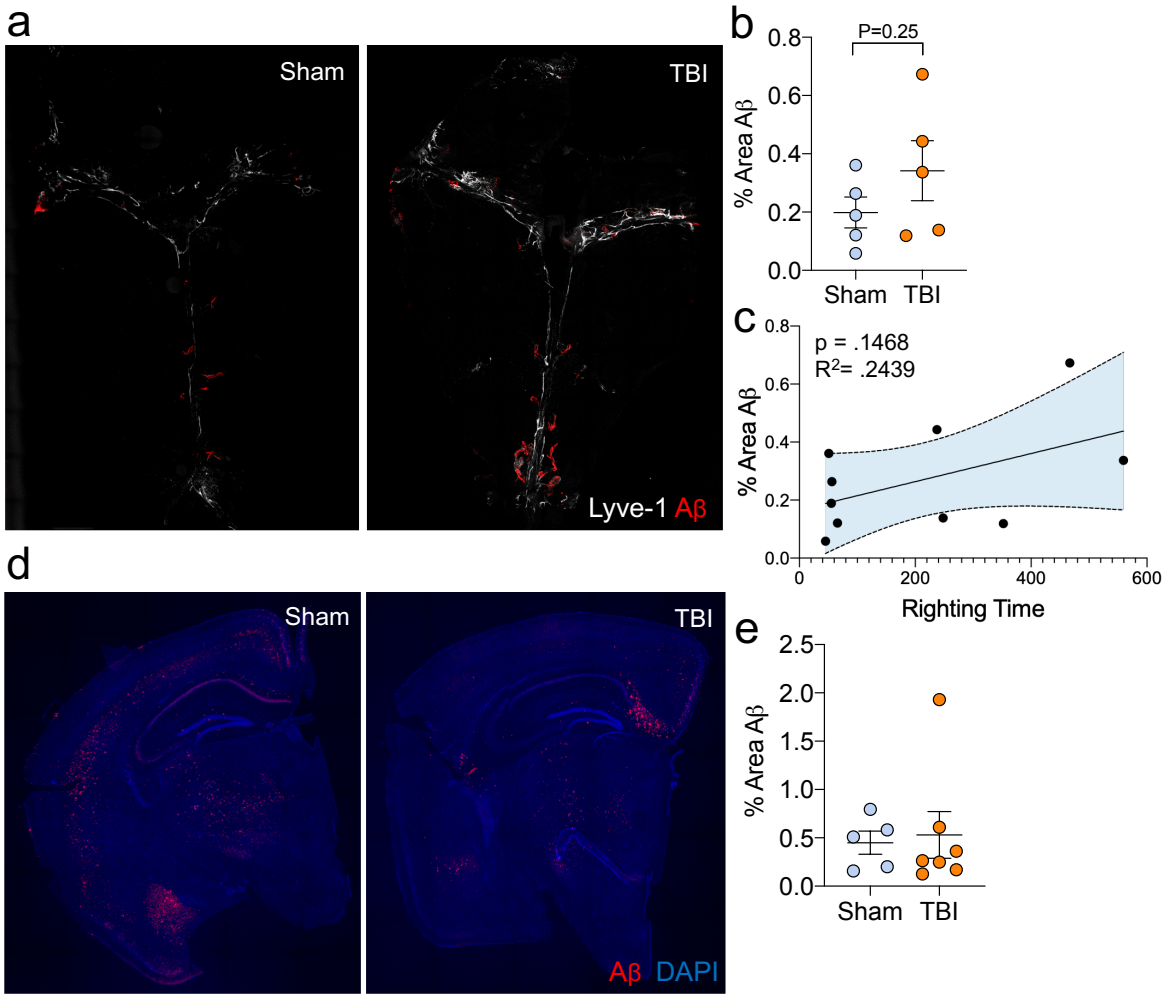

Figure 3.2. The effect of TBI in male 5xFAD mice on Aβ buildup in the brain and meninges. Male 5xFAD mice received TBI or sham treatment at 8 weeks of age and then were harvested at 15 weeks of age. Meningeal whole mounts and brains were harvested. a) Representative images of meningeal whole mounts stained with Lyve-1 660 (grey) and Aβ (red) after TBI or a sham procedure. b) Quantification of percent area of Aβ in the meningeal whole mount (Sham n=5, TBI n=5; data from one experiment). c) Correlation of percent area Aβ with the righting time of the mice. d) Representative images of coronal brain sections from the right hemisphere stained for Aβ (red) and DAPI (blue). The right hemisphere is the hemisphere that is impacted in the TBI mice. e) Quantification of percent area of Aβ in the right hemisphere of the brain (Sham n=5, TBI n=7; data from one experiment). All n values refer to the number of mice used and the error bars depict mean

Once we have established a system in the lab where we can consistently demonstrate that TBI results in more rapid accumulation of Aβ, we can then manipulate the lymphatic system to determine whether impairments or improvements in this system can block or facilitate Aβ clearance, respectively. Using viral delivery of VEGF-C, which will enhance lymphatic growth and function (Figure 3.3), we will assess whether boosting lymphatic drainage after TBI helps to limit TBI-induced Aβ deposition. Prevention of Aβ seeding early after injury with VEGF-C treatment may help reduce the risk of developing AD and other diseases later in life. In addition to measuring Aβ levels, we also hope to use behavioral tests for memory and learning to assess whether VEGF-C delivery can improve functional outcomes after TBI in an Aβ-mediated mouse model of AD. There are several behavioral tests that are commonly used to assess memory function in the 5xFAD mouse model of AD including the MWM and the Novel Object Recognition Test (NORT) [191]. We will use the MWM to assess learning memory function and the NORT to assess the ability of a mouse to remember a previously-encountered object. These tests will allow us to evaluate if boosting meningeal lymphatic drainage function with VEGF-C treatment following TBI is effective in limiting memory deficits associated with AD.

In addition to rejuvenation of the lymphatic system, we will also disrupt the lymphatic system by performing the same Visudyne technique discussed in Chapter 2 (Figure 2.8). We will assess whether disruption of the lymphatic drainage before TBI results in increased Aβ deposition in both the brain and meninges, and whether this contributes to worsened neurologic function.

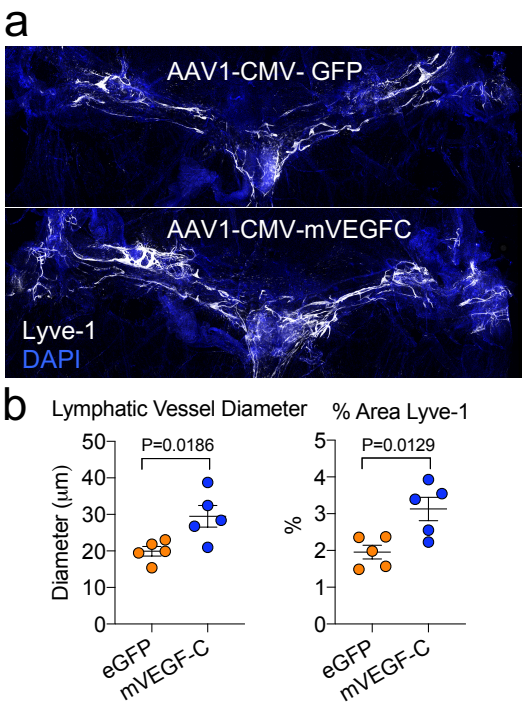

Figure 3.3. VEGF-C administration after TBI results in lymphangiogenesis. Mice received a TBI and then 24 hours later, either VEGF-C or a control viral construct was administered. a) Representative images and b) lymphatic vessel diameter and percent area of Lyve-1 coverage in meningeal whole mounts 2 weeks after TBI (Sham n=5, TBI n=5; data from one experiment). All n values refer to the number of mice used and the error bars depict mean ± s.e.m.

Overall, these proposed experiments will address the knowledge gap of how TBI contributes to the increased risk for neurodegenerative diseases, and whether the meningeal lymphatic system is implicated in this risk. Understanding how the CNS lymphatic system contributes to disease pathogenesis may allow us to devise novel treatment options to protect against sustained and unchecked inflammation in the brain both after injury and during neurodegeneration.

3.2.2 *Interrogate the meningeal response to TBI.*

The brain was originally thought to be immune-privileged, and indeed, recent studies indicate that relatively few immune cells are present within the brain parenchyma under homeostatic conditions [192]. However, despite the paucity of immune cells in the parenchyma, there is still constant immune signaling that occurs throughout the lifetime [181-183, 192]. Interestingly, the meninges serve as an important source of cytokine signaling, often from immune cells that are not present in the brain parenchyma in appreciable amounts under homeostatic conditions [63, 64]. The meninges reside in the layer between the brain and the skull and serve as both a barrier and an interface between the brain and the immune system. The meninges consist of three layers: the pia, the arachnoid, and the dura mater, which contain different cell populations including fibroblasts, immune cells, blood vasculature, and endothelial cells [56], however the full cellular heterogeneity of the meninges is still unknown. Furthermore, the sub-arachnoid space, located between the pia and the arachnoid, contains cerebrospinal fluid (CSF) which contains immune cells as well. The most current complete picture of the meninges is a CyTOF dataset of the meninges at steady state, however, CyTOF requires the selection of antibodies for known cell populations [65]. While the current understanding of the meninges is rudimentary, it is known that they play roles in facilitating proper CNS development, modulating behavior, and regulating disease progression [57, 58].

For instance, some cytokine signaling, including production of IFN-γ, IL-4, and IL-17a by resident T cells in the meninges, has been shown to be important for normal behaviors. IFN-γ is important in maintaining social behavior networks, whereas IL-4 has been implicated in positive performance in learning and memory cognitive tests [63, 64]. Meningeal γδ T cell production of IL-17a is important for modulating anxiety-like behaviors and memory [65, 66].

In addition to meningeal T cell production of cytokines, it is known that immune cells within the CSF in the subarachnoid space can also produce signaling molecules and interact with brain-derived products and antigens [193, 194]. Brain interstitial fluid (ISF) and CSF intermix in the subarachnoid space and both recirculate throughout the brain and drain through the lymphatic network to the periphery [77, 80, 85, 171, 195]. The glymphatic system is the pathway in which ISF is evacuated from the brain parenchyma and recirculated along arterial and venous routes [80-83, 85, 196]. This system provides the meningeal cells and cells within the CSF with access to brain antigens and proteins. Despite this rich immune environment and its proximity to the brain, very little is known about the meningeal response to injury or other disease conditions.

One of the first indications implicating the meninges in the response to brain injury is the finding that meningeal enhancement with post-contrast fluid attenuated inversion MRI can be seen in 50% of patients with mild TBIs and no apparent parenchymal damage; one of the few signs of mild TBI that can be detected by modern imaging techniques in human patients [15]. This enhancement seen on contrast-enhanced MRI has been shown to occur within minutes of injury [69]. Moreover, many individuals who experienced mild TBIs still experienced extravasation of contrast into the sub-arachnoid space, indicating that the blood-brain-barrier is compromised [69]. While 83% of patients experienced resolution in meningeal enhancement 19 days after injury, 17% had persistent enhancement 3 months post-injury, indicating that some patients experienced

prolonged periods without complete meningeal repair in mild TBI [70]. The factors that influence this differential response to mild head injury are just beginning to be understood.

In order to better define how mild TBI affects meningeal immunity, we performed single cell RNA sequencing (scRNA-seq) on the meninges one week post injury (Figure 3.4a). This approach offers an unbiased and comprehensive assessment of how the different cell populations within the meningeal environment respond to or are altered by head trauma. Before filtering and processing of the data, we sequenced 2,703 cells in the Sham group with a median of 981 genes per cell, and 4,345 cells in the TBI group with a median of 1,192 genes per cell. In order to assess the cell populations present in the meninges, we reduced the dimensionality of the dataset and displayed the data through Uniform Manifold Approximation and Progression (UMAP). Clustering of both the Sham and TBI meninges together revealed 21 unique cell populations including endothelial cells, fibroblasts, and ciliated ependymal cells from the pia. Additionally, the meninges include a full repertoire of immune cells including macrophages, B cells, T cells, NK cells, dendritic cells, plasmacytoid dendritic cells, and neutrophils (Figure 3.4b,c). When separated out by Sham and TBI treatments, all 21 populations are still present in both groups (Figure 3.5a), however the frequencies are varied (Figure 3.5b). Most notably, brain injury was characterized by increased frequencies of fibroblasts and a distinct subset of macrophages that express high expression of levels of complement-related proteins (referred to as “Activated Macrophages 1”). While there is a reduction in frequency of some other cell types (mainly the B cell populations) it is unclear whether this is relative to the expansion of the other subsets or an actual decrease in number (Figure 3.5b,c). These data indicate that the meninges are a heterogenous tissue at the cellular level that undergo alterations in macrophage and fibroblast populations one week following TBI.

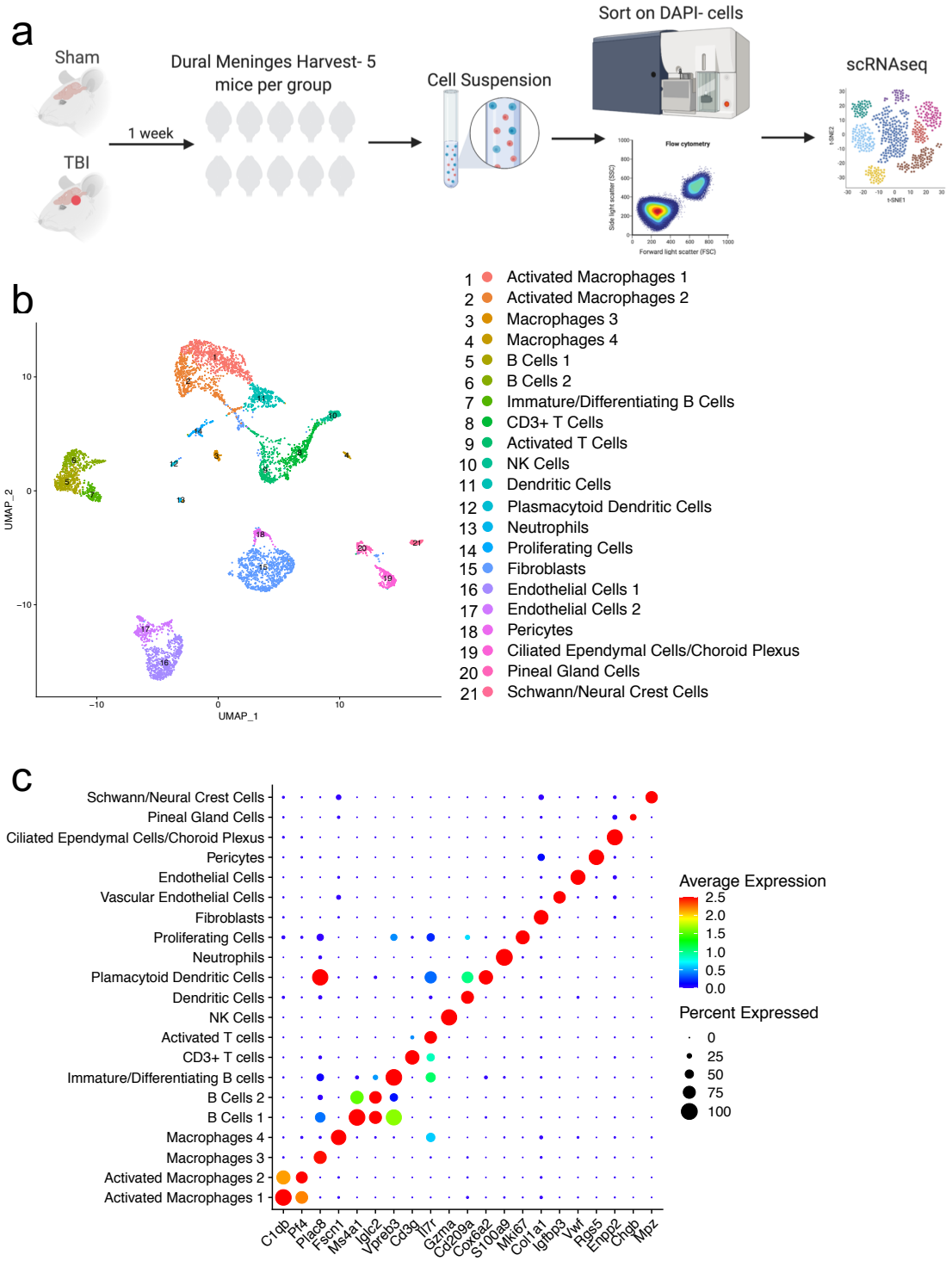

Figure 3.4. The meninges are a heterogeneous tissue. Male mice at 10 weeks of age received a TBI or sham procedure. One week later, the meninges from 5 mice per group were harvested, pooled, and processed for single cell RNA sequencing (scRNA-seq). a) Schematic of scRNA-seq protocol. b) UMAP representation of the cell populations present in the meninges where both Sham and TBI groups are included. c) Dot plot representation of cluster defining genes for each cell population. Graphs were calculated with Seurat by normalizing the dataset, finding the variable features of the dataset, scaling the data and then reducing the dimensionality.

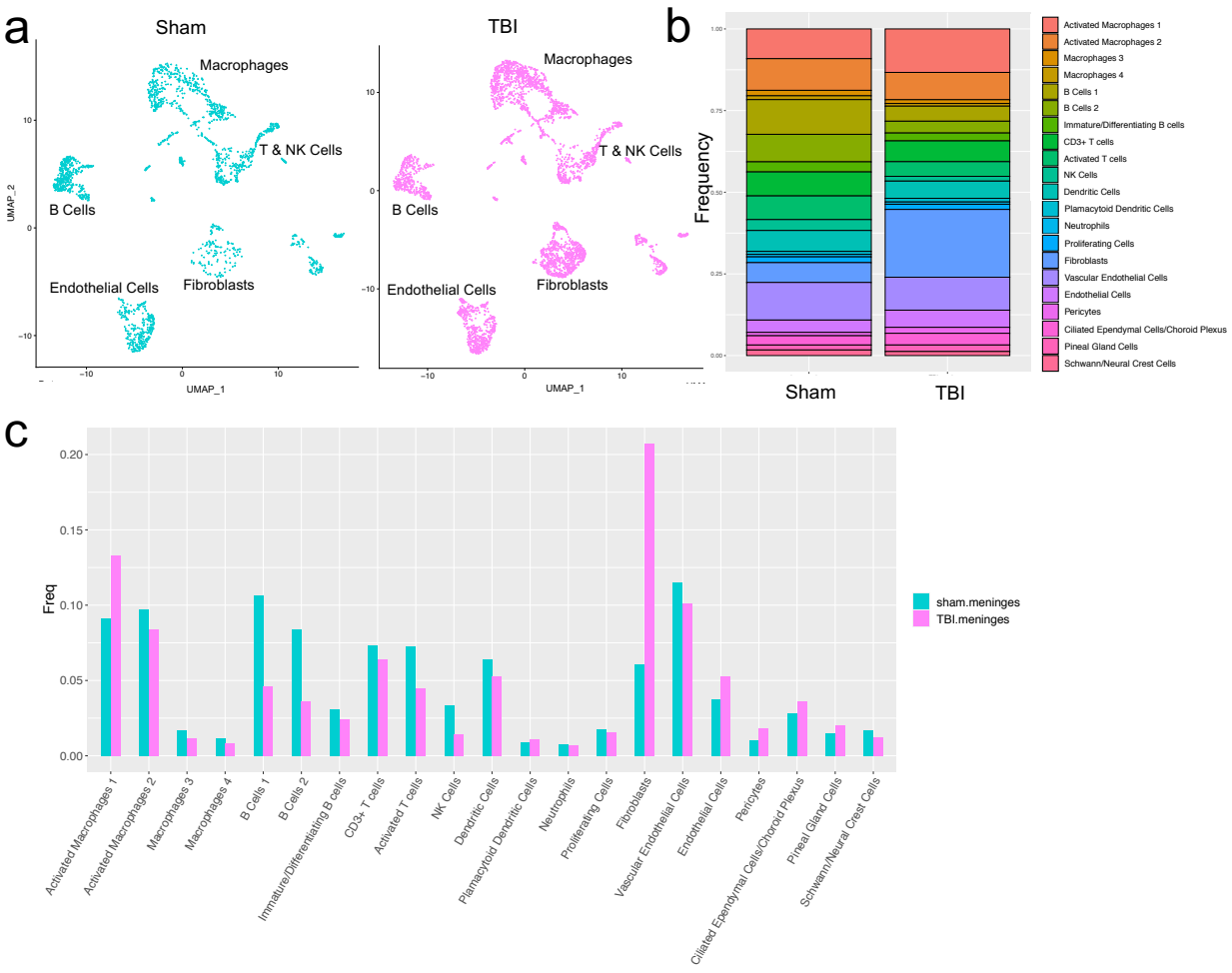

Figure 3.5. Cell specific alterations in meningeal populations following brain injury. Male mice at 10 weeks of age received a TBI or sham procedure. One week later, the meninges from 5 mice per group were harvested, pooled, and processed for scRNA-seq. a) UMAP representation of the cell populations present in the meninges separated by Sham (blue) and TBI (pink). b-c) Frequencies of cell populations in Sham v. TBI samples represented as a (b) gradient bar chart and (c) bar graph. Graphs were calculated with Seurat by normalizing the dataset, finding the variable features of the dataset, scaling the data and then reducing the dimensionality.

Because the “Activated Macrophages 1” and “Fibroblasts” cell populations were expanded post injury, we decided to investigate these sub-populations more closely. When we looked at the significantly upregulated genes following injury in the Activated Macrophage populations (Activated Macrophages 1 & 2) and performed a network analysis, we saw that there were many terms related to activation of the immune system that were enriched. Specifically, the activated macrophages were upregulating genes important for cytokine secretion, immune cell differentiation, motility, and chemotaxis (Figure 3.6a). When we looked at the GO terms that were enriched, we confirmed that many processes to do with the immune system and response to stress were the most significantly upregulated following injury (Figure 3.6b). Interestingly, we noticed that some of these significantly upregulated genes were important for the type I IFN response including *Ifnar1, Ifi203, Irf2bp2*, amongst others (Figure 3.6c). An elevated type I IFN signature following TBI and stroke has been shown to be detrimental for long term outcomes [120-122, 124]. These findings suggest that meningeal macrophages upregulate inflammation-related genes one week following brain injury and may contribute to the type I IFN signature that is seen following brain injury.

We wanted to further investigate the fibroblast population, as this population was also expanded following injury. We decided to first look at which meningeal layers the fibroblasts were from, and which layer was likely responsible for the increase in fibroblasts following TBI. To accomplish this, we examined the expression of markers for specific layers in our sample. *Alpl* and *Foxc2* are known dural markers [197-199], *Ptgds* and *Ald1a2* are known arachnoid markers [58, 200], and *Col18a1* is a known pial marker [57, 201]. Not surprisingly, a majority of the fibroblasts in our sample were from the dura, the thickest layer of the meninges [170, 202], with fewer fibroblasts residing in the pia or arachnoid layers (Figure 3.7a). When we looked at the expression level of dural fibroblast genes before and after TBI, we saw that several of the markers (*Foxc2* and *Fxyd5*) were significantly upregulated, indicating that the dural compartment is likely responsible for the

increase in frequency of fibroblast cells one week after brain injury (Figure 3.7b). We determined the differentially expressed genes in the fibroblast group after TBI in comparison to the Sham group, and examined which KEGG terms were enriched. Interestingly, disease pathways that were related to neurodegenerative diseases, including Parkinson's disease (PD), AD, Amyotrophic lateral sclerosis (ALS) and prion disease, were the most highly upregulated following TBI. While this may indicate that the fibroblast response following TBI may be related to an unhealthy and diseased state, it is likely that the fibroblast response is also required for wound healing. Further studies examining the fibroblast population at later timepoints following injury are needed to determine whether they undergo a prolonged change in their transcriptional status, and also to determine the consequences and significance of the fibroblast response to TBI outcomes.

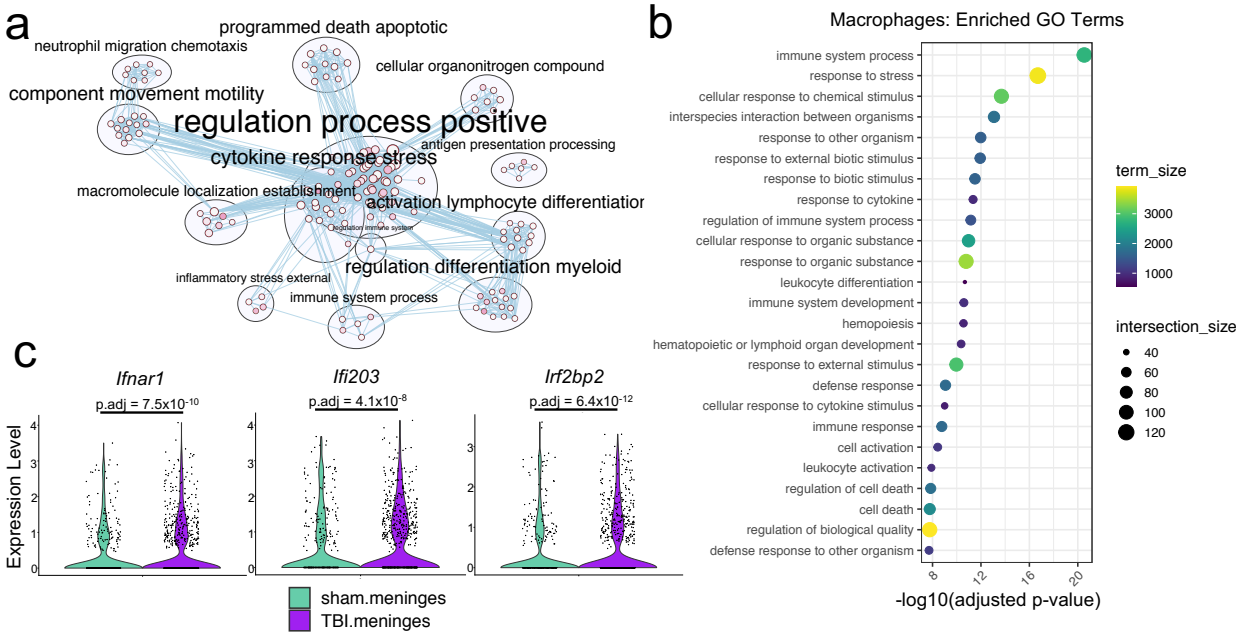

Figure 3.6. Differential gene expression analysis in macrophages following injury shows upregulation of immune-related genes. Male mice at 10 weeks of age received a TBI or sham procedure. One week later, the meninges from 5 mice per group were harvested, pooled, and processed for scRNA-seq. a) Network analysis of differentially upregulated genes in the macrophage group following injury. b) Most enriched GO terms using significantly upregulated genes following TBI in the macrophage population. c) Violin plots depicting several significantly upregulated genes following injury. The width of the violin plot represents the frequency of observations at that given y-value. Therefore, the wider the violin plot, the higher the frequency of observations. Graphs were calculated with Seurat by normalizing the dataset, finding the variable features of the dataset, scaling the data and then reducing the dimensionality. Differential gene expression was calculated using the ZinBWave function for zero-enriched datasets and DESeq2. p.adj; adjusted *p*-value.

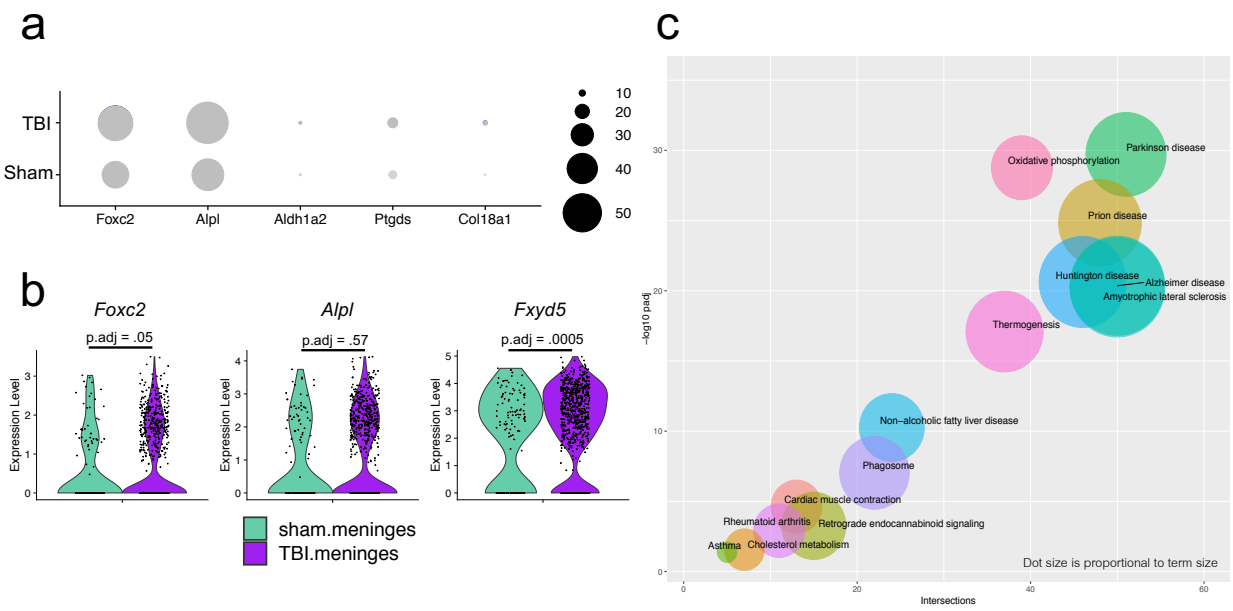

Figure 3.7. Dural fibroblast population expands upon injury and upregulates disease-related gene signatures. Male mice at 10 weeks of age received a TBI or sham procedure. One week later, the meninges from 5 mice per group were harvested, pooled, and processed for scRNA-seq. a) Dotplot depicting dural, arachnoid and pial fibroblasts markers where the size represents the percentage of cells within a class. b) Violin plots of genes characteristic of dural fibroblasts in both sham and TBI conditions. The width of the violin plot represents the frequency of observations at that given y-value. Therefore, the wider the violin plot, the higher the frequency of observations. c) Dot plot representation of the top enriched KEGG terms with significantly upregulated genes in the fibroblast population, where the dot size is proportional to term size. Graphs were calculated with Seurat by normalizing the dataset, finding the variable features of the dataset, scaling the data and then reducing the dimensionality. Differential gene expression was calculated using the ZinBWave function for zero-enriched datasets and DESeq2. p.adj; adjusted p-value.

In addition to determining how cellular populations were altered following injury using scRNA-seq, we were interested in how the meningeal response to injury is altered in aging. To investigate this question, we performed bulk RNA-sequencing (RNA-seq) on the meningeal tissue 1.5 months post injury in both young (10 weeks of age) and aged (20 months of age) mice (Figure 3.8a). While the young mice that had received sham and TBI clustered together, the aged mice clustered separately (Figure 3.8b). Moreover, the aged sham and TBI mice clustered separately, indicating that with age, the effects from TBI have more long-lasting effects on differential gene expression (Figure 3.8b). Indeed, when we looked at the number of differentially expressed genes in all four experimental groups, we saw that there were only a total of 22 differentially expressed genes when comparing Young Sham with Young TBI, while there were a total of 364 differentially expressed genes when comparing Aged Sham with Aged TBI (Figure 3.8c,d). Interestingly, when we compared Young Sham mice with Aged Sham mice, there were 1772 differentially expressed genes, and 2936 differentially regulated genes when comparing Young TBI mice with Aged TBI mice (Figure 3.8c,d). This indicates that the aged meninges are substantially different than the young meninges in their gene expression profile, and that a TBI during old age results in even larger changes in gene expression (Figure 3.8c,d). Overall, while the young mice exhibit very few gene expression changes 1.5 months following TBI, indicating a faster recovery, the aged mice experience many more alterations in gene expression that persist for a longer period of time.

Because aging itself resulted in substantially different gene expression patterns, we decided to look more closely at these differences. When looking at the top 20 up- and down-regulated genes in the Aged Sham mice as compared to the Young Sham mice, we noticed a striking upregulation in genes important for antibody production by B cells (Figure 3.9a). In fact, one half of the top 20 upregulated genes fell into this category (Figure 3.9a). When we examined the top most enriched GO biological processes using the significantly activated genes in the Aged Sham mice as compared to the Young Sham mice, we saw that immune and defense responses were most

highly upregulated, indicating that the cells within the aged meninges have grossly upregulated their immune response, even under homeostatic conditions (Figure 3.9b). This is consistent with previous findings in the brain that indicate an overall upregulation of the immune response with age [113, 114, 118]. Due to the striking nature of the upregulation of antibody production-related genes, and recent findings that report an increase in IgA secreting plasma cells with age [203], we more closely examined some of these genes (Figure 3.9c). There were highly significant upregulations in genes related to the immunoglobulin heavy chain (*Ighm, Ighg2b, Igha*), light chain (*Igkc*), and components of IgA or IgM antibodies (*Jchain*) (Figure 3.9c). The significance of this upregulation in antibody production related genes with age is not fully understood and requires further study. Interestingly, it was recently reported that IgA production in the meningeal tissue provides an "immunological barrier" to help prevent pathogens from gaining access to the CNS [203]. While speculative, perhaps this upregulation in antibody production components in the meninges is in response to weakened barriers that are seen with aging (for example, the changes seen with the BBB [119]). Indeed, "response to external stimulus", "defense response", and "response to other organism" were some of the most highly enriched GO biological processes in aged mice as compared to young mice (Figure 3.9b).

In addition to the antibody-related gene upregulation, we also observed an upregulation of type I interferon (Type I IFN)-related genes (Figure 3.9d). Type I IFNs have been shown to be upregulated in aging and after brain injury in the brain parenchyma, and their elevation has generally been thought to contribute to negative long-term outcomes in these contexts [118, 121-124]. Our data suggests that this type I IFN signature seen with aging is also preserved within the meningeal tissue. Amongst others, we saw highly significant increases in type I IFN-related genes including *Ifit1, Ifit2, Irf7, Ifi213* and *Mx1* (Figure 3.9d). Whether this type I IFN signature in the meninges impacts the brain parenchyma requires further investigation.

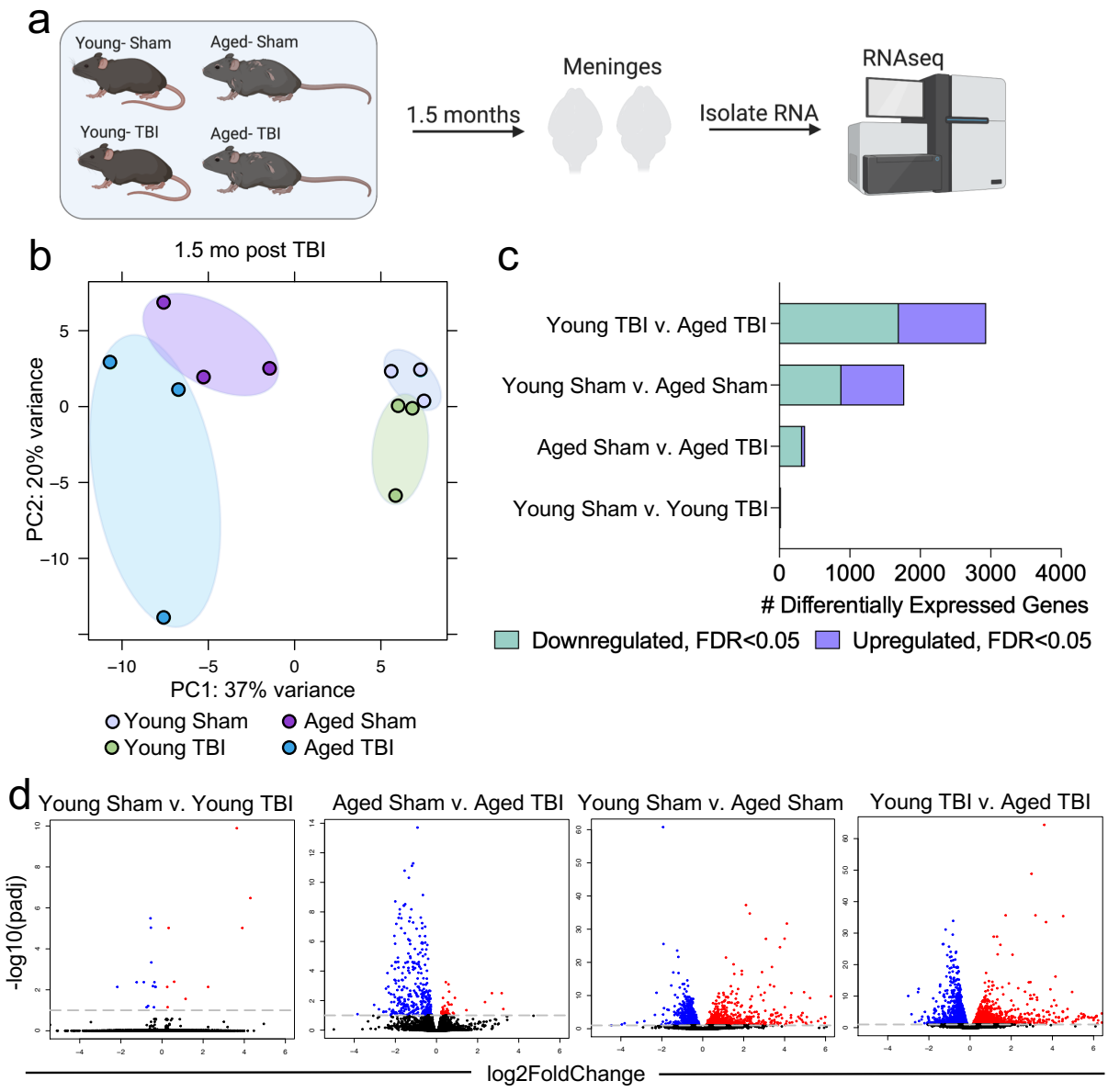

Figure 3.8. The meningeal response to injury in aging is drastically altered both at baseline and in response to injury. a) Schematic depicting experimental layout. Male mice at 10 weeks of age or 20 months of age received a TBI or sham procedure. 1.5 months later, the meninges from 2-3 mice per group were harvested, pooled, and processed for bulk RNA sequencing (RNA-seq). RNA-seq was performed on 4 experimental groups with 3 samples per group. b) Principal component analysis (PCA) showing clustering of samples. c) Graphical representation of the upregulated and downregulated genes in all four experimental groups 1.5 months post TBI. d) Volcano plots illustrate the number of significantly differentially expressed genes (FDR<0.1). Blue data points represent significantly downregulated genes and red data points represent significantly upregulated genes. FDR and *P* values were calculated with DEseq2 using the Wald test for significance following fitting to a negative binomial linear model and the Benjamini-Hochberg procedure to control for false discoveries. FDR; false discovery rate.

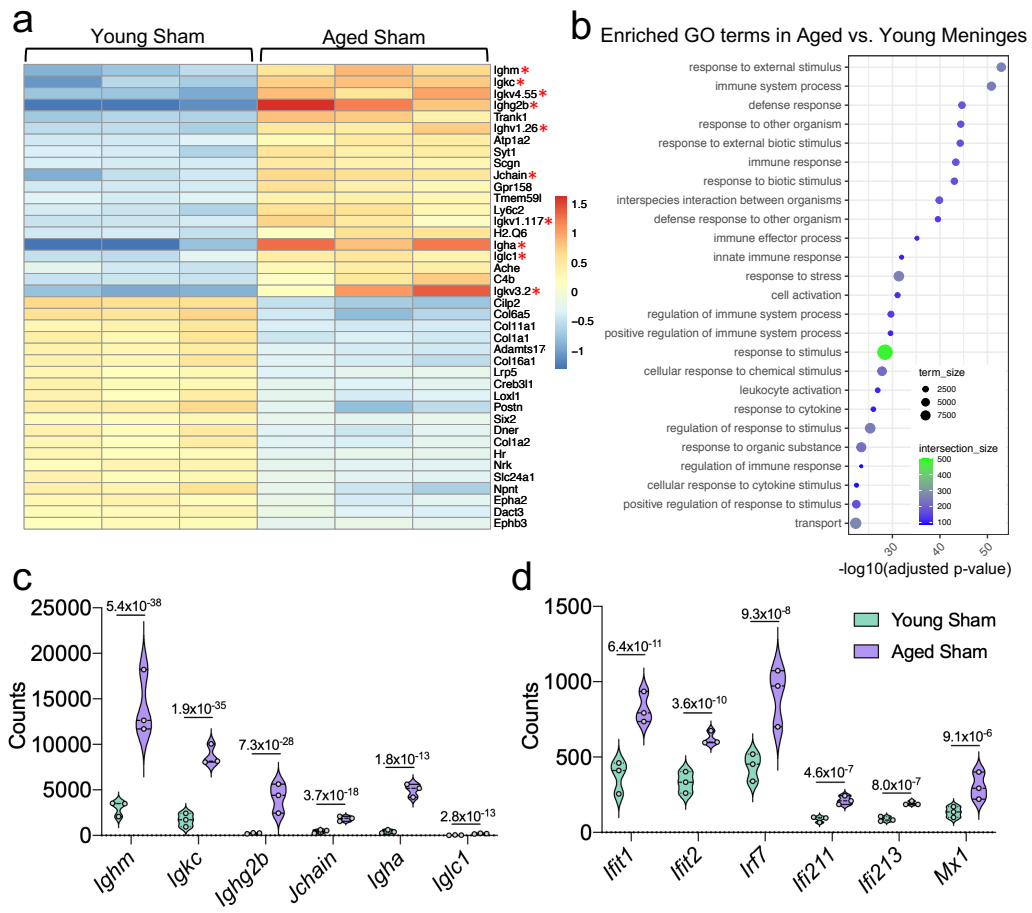

Figure 3.9. Aging results in an upregulation of immune-related genes in the meninges. Male mice at 10 weeks of age or 20 months of age received a TBI or sham procedure. 1.5 months later, the meninges from 2-3 mice per group were harvested, pooled, and processed for bulk RNA-seq. RNA-seq was performed on 4 experimental groups with 3 samples per group. a) Heatmap representation of the top 20 most significantly upregulated and downregulated (FDR<0.1) genes in the Sham Young vs. Sham Aged groups. The red star (*) indicates genes associated with antibody production. b) Dot plot of GO term biological processes shows enrichment of immune-related pathways with differentially expressed genes between young mice as compared to aged mice. c-d) Violin plots depicting counts of significantly activated antibody and B cell related genes (c) and type I interferon-related genes (d) with age (FDR<0.1). The number above each graph represents the adjusted p-value calculated for each gene using DEseq2. The central line within each plot represents the median of the data set. The upper and lower boundaries of the box represent the third (Q3) and first (Q1) quartiles respectively. The violin plot encompasses the three biological repeats. The width of the violin plot represents the frequency of observations at that given y-value. Therefore, the wider the violin plot, the higher the frequency of observations. FDR and *P* values were calculated with DEseq2 using the Wald test for significance following fitting to a negative binomial linear model and the Benjamini-Hochberg procedure to control for false discoveries. FDR; false discovery rate.

In order to assess the transcriptional response to TBI in aged mice as compared to young mice, we analyzed the transcriptional response that was unique to the Young TBI v. Aged TBI comparison and not shared with the Young Sham v. Aged Sham comparison. Of the differentially expressed genes, there were 1186 genes that were shared amongst these two comparisons (including many of the immunoglobulin and type I IFN-related genes), 1750 genes that were unique to the Young TBI v. Aged TBI comparison and 586 genes that were unique to the Young Sham v. Aged Sham comparison (Figure 3.10a). This indicates that while there are some shared responses between aging and TBI, TBI and aging together induces a much larger change in gene expression than aging alone. We examined more closely the differentially expressed genes unique to the Young TBI v. Aged TBI group and not shared with the Young Sham v. Aged Sham comparison. Using the GO molecular function terms, we saw that of the 1101 repressed genes in the Aged TBI group, many of these genes were essential for binding processes including protein binding and cytoskeletal binding (Figure 3.10b). When we looked more closely at the top repressed genes unique to the Aged TBI mice as compared to the Young TBI mice, we saw that many of these genes encode collagenases (*Col4a1, Col4a2* and *Col5a2*) and other proteins important for making cellular junctions (*Jup*) (Figure 3.10c). Many of these proteins likely aid in the wound healing response by the fibroblasts in the meninges, but are downregulated after brain injury in aging.

Additionally, we looked at the genes that were uniquely activated in the Aged TBI mice as compared to the Young TBI mice. Not surprisingly, many of these genes were important for the upregulation of the immune system; the most highly enriched GO biological processes were “defense response” and “immune system process” (Figure 3.10d). However, it is interesting that these genes are still upregulated 1.5 months following injury, whereas the young mice do not experience this prolonged upregulation in immune-related genes (Figure 3.10d). These findings are consistent with other analyses of the brain parenchyma in murine stroke models showing that

while genes important for the immune system are upregulated in aging, they are further upregulated upon injury [113]. Some of the genes that contributed to the upregulation of these immune-related terms include additional genes regulated to immunoglobulin production (*Ighg2c*), genes important for T and B cell signaling (*Cd24a, Zap70, Cxcr6*) and other genes important for innate immunity and cell death (*Casp12, C2*) (Figure 3.10e). These findings highlight some of the distinct changes seen in the aged meningeal tissue following TBI as compared to TBI in young meningeal tissue. Specifically, we have shown a downregulation in genes important for the extracellular matrix and cellular binding and an upregulation in immune-related genes.

Overall, our findings have shed new light on the incredibly heterogeneous and dynamic nature of the meningeal tissue. The meninges respond to injury by proliferation of fibroblasts and macrophages, and upregulation of genes related to the immune system. Moreover, the gene expression patterns of the meninges are drastically altered in aging, with large upregulations in genes essential for immunoglobulin production and the type I IFN pathway. Upon injury, the aged meninges appear to fail to upregulate the production of collagenases and other genes important for cell junction formation, while they continue to upregulate genes involved in immune signaling. These findings are in contrast to the young meninges, that appear to have almost completely returned to baseline 1.5 months following injury.

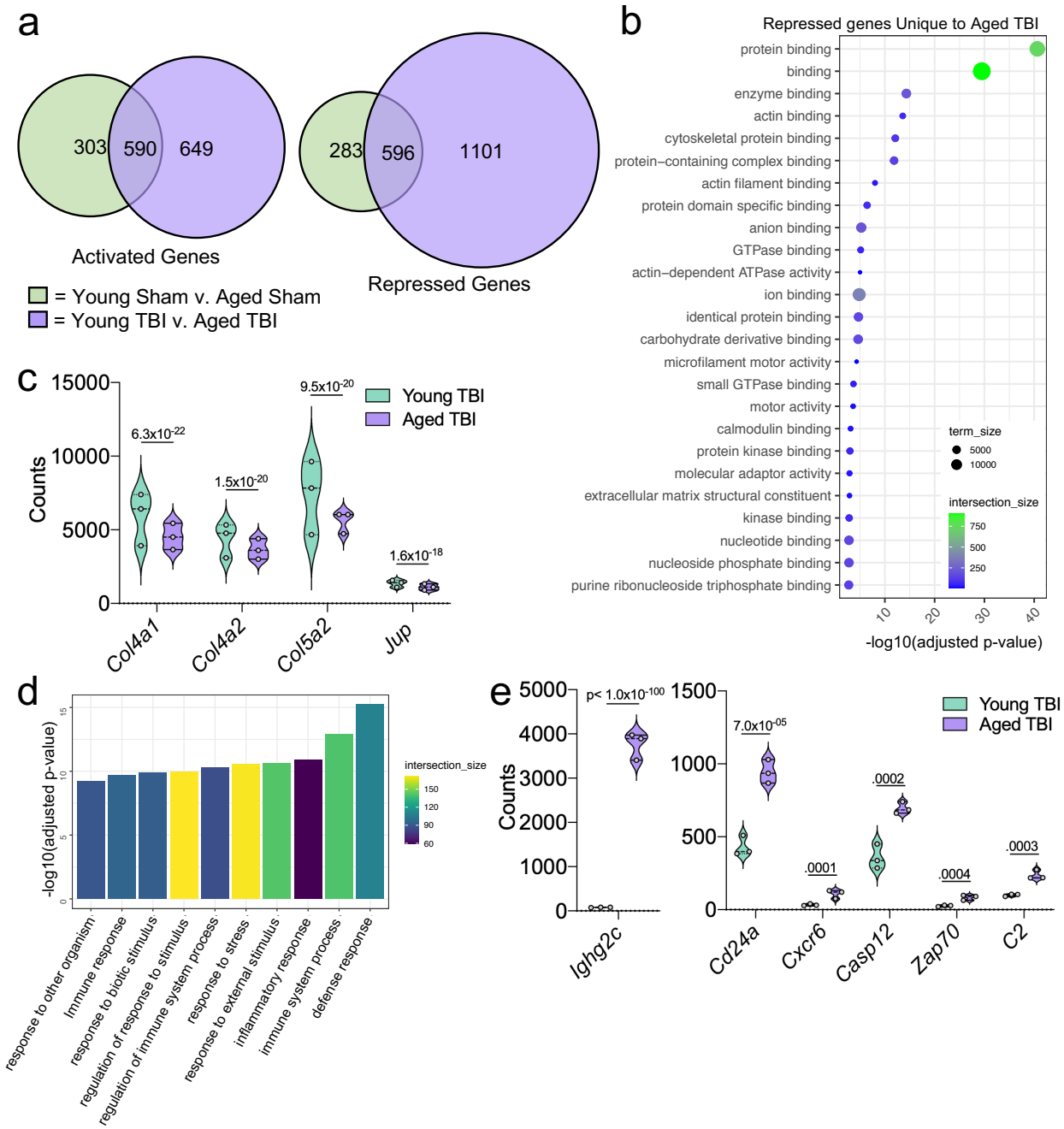
a
303
590
649
Activated Genes
283
596
1101
Repressed Genes
= Young Sham v. Aged Sham
= Young TBI v. Aged TBI
b
Repressed genes Unique to Aged TBI
protein binding
binding
enzyme binding
actin binding
cytoskeletal protein binding
protein−containing complex binding
actin filament binding
protein domain specific binding
anion binding
GTPase binding
actin−dependent ATPase activity
ion binding
identical protein binding
carbohydrate derivative binding
microfilament motor activity
small GTPase binding
motor activity
calmodulin binding
protein kinase binding
molecular adaptor activity
extracellular matrix structural constituent
kinase binding
nucleotide binding
nucleoside phosphate binding
purine ribonucleoside triphosphate binding
term_size
5000
10000
intersection_size
750
500
250
10
20
30
40
-log10(adjusted p-value)
c
15000
10000
5000
0
Counts
6.3x10-22
1.5x10-20
9.5x10-20
1.6x10-18
Young TBI
Aged TBI
Col4a1
Col4a2
Col5a2
Jup
d
-log10(adjusted p-value)
intersection_size
150
120
90
60
response to other organism
immune response
response to biotic stimulus
regulation of response to stimulus
regulation of immune system process
response to stress
response to external stimulus
inflammatory response
immune system process
defense response
e
5000
4000
3000
2000
1000
0
Counts
p< 1.0x10-100
Ighg2c
1500
1000
500
0
7.0x10-05
.0001
.0002
.0004
.0003
Young TBI
Aged TBI
Cd24a
Cxcr6
Casp12
Zap70
C2

Figure 3.10. A unique gene signature following TBI in aged mice shows downregulation of extracellular matrix components and upregulation in immune processes. Male mice at 10 weeks of age or 20 months of age received a TBI or sham procedure. 1.5 months later, the meninges from 2-3 mice per group were harvested, pooled, and processed for bulk RNA-seq. RNA-seq was performed on 4 experimental groups with 3 samples per group. a) Venn Diagram depicting unique and shared differentially regulated genes between the Young Sham v. Aged Sham and Young TBI v. Aged TBI groups (FDR<0.1). b) Dot plot of GO term molecular function shows enrichment in processes important for molecule binding with the genes unique to the Young TBI v. Aged TBI comparison. c) Violin plots depicting counts of significantly repressed extracellular matrix related genes (FDR<0.1). d) Bar plot of GO term biological process shows enrichment in immune-related processes with the genes unique to the Young TBI v. Aged TBI comparison. e) Violin plots depicting counts of significantly activated immune-related genes (FDR<0.1). (c,e) The number above each graph represents the adjusted p-value calculated for each gene using DEseq2. The central line within each plot represents the median of the data set. The upper and lower boundaries of the box represent the third (Q3) and first (Q1) quartiles respectively. The violin plot encompasses the three biological repeats. The width of the violin plot represents the frequency of observations at that given y-value. Therefore, the wider the violin plot, the higher the frequency of observations. FDR and *P* values were calculated with DEseq2 using the Wald test for significance following fitting to a negative binomial linear model and the Benjamini-Hochberg procedure to control for false discoveries. FDR; false discovery rate.

3.2.3 *Investigate how the meningeal lymphatic system shapes brain development and adult behavior.*

The meninges develop alongside the CNS, and are critical for shaping brain development [57, 58]. Important signals released from the meninges in development, including all-trans retinoic acid, have been shown to be critical for corticogenesis [58]. Moreover, meningeal release of Cxcl12 is instrumental for proliferation of cerebellar progenitor cells and proper spatial arrangements of granule cells in the cerebellum and hippocampus [59-62]. While some is known about how the meninges as a whole shape brain development, little is known about how the meningeal lymphatic system can shape brain development. The meningeal lymphatic system serves as a facilitator of neuro-immune interactions, as it drains CSF, cells, and cellular byproducts from the CNS to the peripheral lymph nodes [76, 91]. While its function is important for health in adulthood and its disruption has been linked to disease, it is unclear whether this

system is serving a function in early life. For this future direction, our goals are to investigate the role of the meningeal lymphatic system in brain development.

There are many unanswered questions about the meningeal lymphatic system in development. While one study demonstrated that the lymphatic system appears morphologically similar to the adult lymphatic vasculature by 28 days post birth in mice [78], it is still unknown whether this system is functional in draining at this timepoint. To answer this question, we will perform intra-cisterna magna (ICM) injections of fluorescent beads and harvest the lymph nodes in mice at 21 days old (weanlings) and 28 days old (when the lymphatic system appears morphologically mature) to assess functionality of drainage to the periphery. This will help us determine whether meningeal lymphatic drainage to the periphery is occurring by these timepoints. If both of these timepoints appear to have effective drainage, we will try even earlier timepoints.

Once we have determined when lymphatic drainage is effective, we would like to further investigate the role of the meningeal lymphatic system in CNS development. We will use methods to block or enhance meningeal lymphatic drainage in order to assess its roles in development. If ICM injections are possible at these early ages, we can use the same techniques we utilized in our published work: Visudyne ablation for blocking the meningeal lymphatic system (Figure 2.8), and viral vector delivery of VEGF-C for boosting lymphatic growth (Figure 2.13, Figure 3.3). However, there are many additional possibilities to manipulate the lymphatic system if these methods prove to be unsuccessful. For instance, we could consider utilizing a VEGFR3-antibody fusion protein, $VEGFR3_{1-4}$-Ig, which ablates VEGF-C signaling, and deliver this directly to the lymphatic vasculature through ICM injection [78]. The dorsal meningeal lymphatics require VEGF-C/VEGRR3 signaling for development and maintenance of the vasculature [78, 140], so removing either of these signaling components results in a lack of development or regression of the dorsal meningeal lymphatic vasculature.

Moreover, an mRNA construct that expresses VEGF-C was also developed to avoid the immunogenicity of viral vector delivery of VEGF-C and to promote faster growth of the lymphatics [90]. All of these different techniques for promoting or blocking the lymphatics could be delivered ICM. However, if ICM injections prove to be challenging or unsuccessful in infant or young mice, other methods are available. There are gels that can be applied to thinned skulls in adulthood to promote meningeal lymphatic growth, and the skull is likely sufficiently thinned in young mice to use these gels without further manipulation [15, 76, 139].

Once we have established effective ways to boost and block meningeal lymphatic growth and development in neonatal and young mice, we will study the brain and CSF to determine how normal development of this drainage system affects the developing brain. First, I would like to take more of an unbiased approach using scRNA-seq. I would like to disrupt meningeal lymphatic development and then perform scRNA-seq of the brain parenchyma in adulthood. This will help determine whether there are cell-specific alterations in gene expression that occur as a result of improper meningeal lymphatic system development, and will provide an overview of genes and cell populations that will be interesting to pursue in follow-up studies.

In addition to the scRNA-seq experiment, I would like to harvest and pool CSF from adult mice that have lacked proper meningeal lymphatic vasculature throughout development and mice where the lymphatic system has developed normally. I will then analyze the cellular composition of the CSF, because it is known that the CSF is rich in immune cells, and some of these cells have been implicated in neurodegenerative disease [193]. However, very little is known about how these immune cells within the CSF interact with the brain in homeostasis. By examining the CSF after lymphatic dysfunction in development, I hope to determine whether the meningeal lymphatic system is critical for the makeup of the CSF immune cell population, and hope to further assess the functions of these cells in healthy development.

Finally, I would like to disrupt and prematurely enhance meningeal lymphatic development in developing mice, and then assess behavioral readouts in adulthood in order to determine whether alterations in the timing of meningeal lymphatic system development results in behavioral abnormalities. I will perform tests for memory and learning capabilities (Morris Water Maze, Novel Location Recognition Test), a test for motor performance (Rotarod), tests for anxiety (Open Field and Elevated Plus maze) and a test for sociability (Social Preference). These behavioral tests will allow me to assess a broad spectrum of normal mouse behaviors to determine whether disruptions in the meningeal lymphatic system can have long lasting and broad consequences on brain function.

Overall, the future directions outlined here will deepen the field's understanding of how the brain and the immune system interact to shape normal development. Furthermore, if we find that the meningeal lymphatic system is important for brain development, this system can be interrogated further in other neurodevelopmental disorders such as autism and schizophrenia.

3.2.4 *Determine whether the meningeal lymphatic system affects neuronal health following brain injury.*

In our findings detailed in this dissertation, we highlight that pre-existing lymphatic dysfunction before a TBI results in increased gliosis and poor behavioral outcomes when compared to TBI alone (Figure 2.11). While these findings clearly indicate a role for the meningeal lymphatic system in TBI pathogenesis, it is unclear how this system is influencing specific cell populations in the brain. It is known that TBI can lead to long-lasting changes to neuronal morphology, dendritic spine formation, and synapse formation [26]. However, little is known about how the meningeal lymphatic system may be influencing neuronal health in the context of TBI. For this

future direction, we hope to investigate how the lymphatic system, in the context of TBI, affects the neuronal population (Figure 3.11).

In order to investigate this question, we will use the familiar two-pronged approach of both blocking meningeal lymphatic function before TBI using Visudyne and boosting lymphatic function following TBI using VEGF-C. We hypothesize that, due to the increased inflammation we have seen in our previous studies, that neuronal health will be negatively affected following injury with pre-existing lymphatic dysfunction. Namely, following TBI with prior lymphatic dysfunction, we anticipate that there will be fewer dendritic spines and fewer synapses. Conversely, we anticipate that improving the lymphatic system in aged mice (that already have existing lymphatic dysfunction) may improve neuronal health following injury, including increased synapse and spine density (Figure 3.11). We will use the Thy-1-YFP reporter mouse to analyze neuronal morphology with Imaris and synapses will be stained using antibodies specific for PSD-95 and Synapsin to study pre- and post-synaptic markers, respectively.

Overall, we anticipate that this research will provide a deeper appreciation of how the meningeal lymphatic system can shape the native cells of the brain, which has not been studied to date. Moreover, we believe that further research in this area could lead to a greater understanding of the memory and learning impairments commonly found in TBI patients.[8] Developing a deeper understanding for how pre-existing lymphatic dysfunction affects neuronal health after TBI is critical for understanding why elderly populations and individuals with previous TBIs, two populations that often have impairments in lymphatic drainage, suffer disproportionately from negative long-term outcomes.[9]

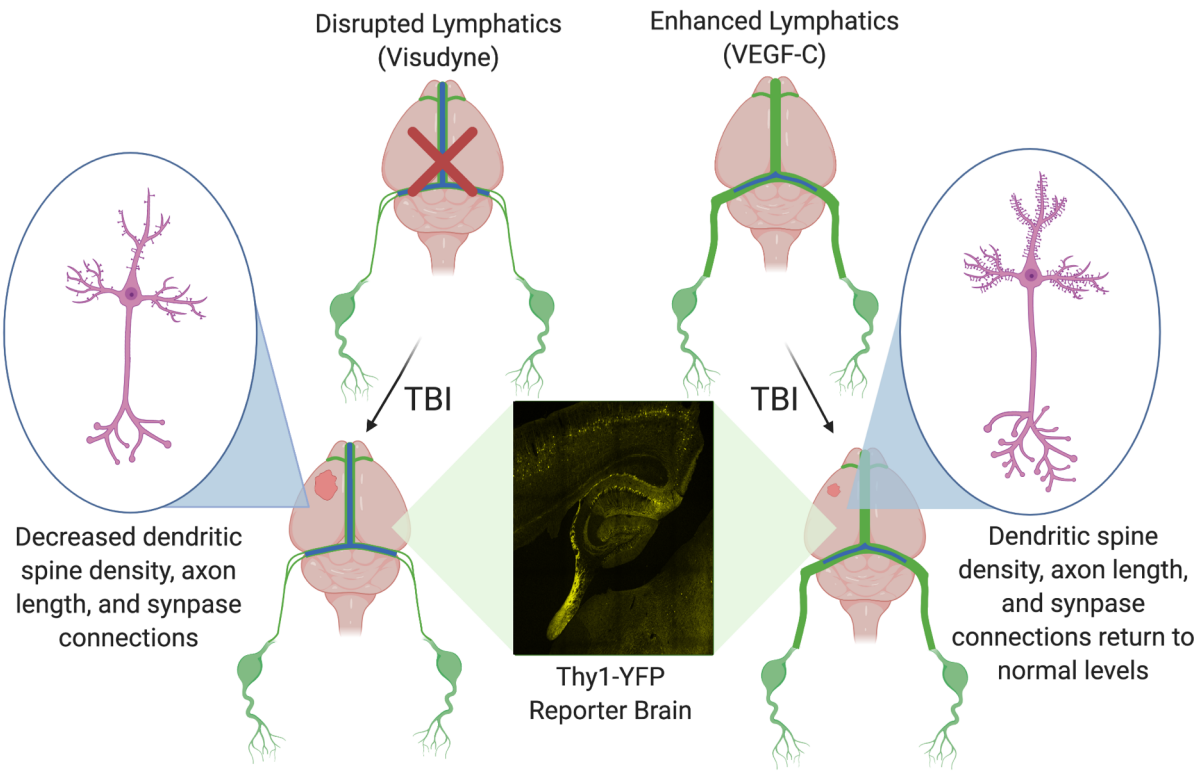

Figure 3.11. Working hypothesis. Schematic depicting the working hypothesis for how the meningeal lymphatic system may affect neuronal health.

3.3 Concluding Remarks

TBI is a common and devastating condition that leads to many debilitating long-term outcomes and a higher risk for neurodegenerative disease. While it is believed that an unchecked immune response may contribute to these negative outcomes, how the brain and the immune system interact with one another following brain injury is very complex and multifaceted. An understanding of how these two systems work together to resolve injury or promote pathogenic features is critical for preventing the devastating long-term outcomes seen following TBI, and also for understanding other neurodegenerative and psychiatric diseases. In this dissertation, we studied the meningeal tissue to understand how the lymphatic network and immune cells within this tissue respond to and affect brain injury. We found that the meningeal lymphatic network is impaired following TBI and that impairment in this system can impact the inflammatory state of the brain post injury. Additionally, using scRNA-seq and bulk RNA-seq in experiments that are still ongoing, we discovered that the cellular composition and transcriptome of meningeal tissue undergoes multiple alterations following TBI and that aging induces striking alterations in the meninges both in the context of injury and in homeostasis. In this dissertation, we provide novel insights into how the meningeal compartment changes following injury, and how the meningeal lymphatic network can then influence the brain. These discoveries presented here shed light on the dynamic immune response following TBI and provide new methods for modulating the immune response following injury.

3.4 Materials and Methods

Mice

All mouse experiments were performed in accordance with the relevant guidelines and regulations of the University of Virginia and approved by the University of Virginia Animal Care and Use

Committee. C57BL/6J mice were obtained from Jackson Laboratories. Mice were housed and behavior was conducted in specific pathogen-free conditions under standard 12-hour light/dark cycle conditions in rooms equipped with control for temperature (21 ± 1.5°C) and humidity (50 ± 10%). Males were used for all studies for consistency within the RNA sequencing data, as sex can influence this readout. All aged mice were between 18 and 24 months of age and were obtained from the National Institute on Aging (NIA) Aged Rodent Colonies.

Traumatic brain injury

This injury paradigm was adapted from the published Hit and Run model [169]. Mice were anesthetized by 4% isoflurane with 0.3 kPa O_2 for 2 minutes and then the right preauricular area was shaved. The mouse was placed prone on an 8 x 4 x 4-inch foam bed (type E bedding, open-cell flexible polyurethane foam with a density of approximately 0.86 pounds per cubic feet and a spring constant of approximately 4.0 Newtons per meter) with its nose in a nosecone delivering 1.5% isoflurane (purchased from Foam to Size, Ashland VA). The head was otherwise unsecured. The device used to deliver TBI was a Controlled Cortical Impact Device (Leica Biosystems, 39463920). A 3 mm impact probe was attached to the impactor device which was secured to a stereotaxic frame and positioned at 45 degrees from vertical. In this study, we used a strike depth of 2 mm, 0.1 s of contact time and an impact velocity of 5.2 meters (m) per second (s). An impact velocity of 6.2 m per s was used for the TBI severity studies in Figure 2.4. The impactor was positioned at the posterior corner of the eye, moved 3 mm towards the ear and adjusted to the specified depth using the stereotaxic frame. A cotton swab was used to apply water to the injury site and the tail in order to establish contact sensing. To induce TBI, the impactor was retracted and dispensed once correctly positioned. The impact was delivered to the piriform region of the brain. Following impact, the mouse was placed supine on a heating pad and allowed to regain consciousness. After anesthesia induction, the delivery of the injuries took less than 1 minute. The time until the mouse returned to the prone position was recorded as the righting time. Upon

resuming the prone position, mice were returned to their home cages to recover on a heating pad for six hours with soft food. For sham procedures, mice were anesthetized by 4% isoflurane with 0.3 kPa O_2 for 2 minutes and then the right preauricular area was shaved. The mouse was placed prone on a foam bed with its nose secured in a nosecone delivering 1.5% isoflurane. The impactor was positioned at the posterior corner of the eye, moved 3 mm towards the ear and adjusted to the specified depth using the stereotaxic frame. A cotton swab was used to apply water to the injury site and the tail in order to establish contact sensing. Then, the impactor was adjusted to a height where no impact would occur, and was retracted and dispensed. Following the sham procedure, the mouse was placed supine on a heating pad and allowed to regain consciousness. Mice were allowed to recover on the heating pad in their home cages for 6 hours with soft food before being returned to the housing facilities.

Tissue collection

Mice were euthanized with CO_2 and then transcardially perfused with 20 ml 1x PBS. For meninges whole mount collection, skin and muscle were stripped from the outer skull and the skullcap was removed with surgical scissors and fixed in 2% PFA for 12 hours at 4 °C. Then the meninges (dura mater and arachnoid mater) were carefully dissected from the skullcaps with Dumont #5 forceps (Fine Science Tools). Meningeal whole-mounts were then moved to PBS and 0.05% azide at 4 °C until further use. For meninges collection for scRNA-seq, the skullcap was removed as previously described, and placed into DMEM medium. Meninges were then scraped from the skullcap and processed further to create a single cell suspension. For meninges collection for bulk RNA-seq, the skullcap was removed as previously described, and placed into DMEM medium. The meninges were scraped from the skullcap and were immediately snap-frozen at −80 °C in TRIzol (15596018, Life Technologies), until further use. Brains were removed and kept in 4% PFA for 24 hours and cryoprotected with 30% sucrose for 3 days. A 4 mm coronal section of brain tissue that surrounded the site of the lesion was removed using a brain sectioning device

and then frozen in Tissue-Plus OCT compound (Thermo Fisher Scientific). Fixed and frozen brains were sliced (50 µm thick sections) with a cryostat (Leica) and kept in PBS + 0.05% azide at 4 °C until further use.

RNA extraction and sequencing

For RNA extraction from the meningeal tissue, the meninges were harvested as described in "Tissue Collection". After defrosting on ice, 10 silica beads were added to each tube and the tissue was homogenized for 30 seconds using a mini bead beater. Following homogenization, the samples were centrifuged for 12,000xg for 10 minutes at 4 °C. The supernatant was transferred to a new tube and incubated at room temperature for 5 minutes. 0.1 mL of chloroform was added to the supernatant, vortexed, incubated for 2 minutes at room temperature and then centrifuged at 12,000xg for 15 minutes at 4 °C. The top aqueous phase was transferred into a new Eppendorf tube and the RNeasy Micro Kit (74004, Qiagen) was used to isolate the RNA. RNA was frozen at −80 °C until sent for sequencing. For sequencing, total RNA samples were sent to GENEWIZ for library preparation and paired end sequencing.

Meningeal preparation for scRNA-seq

The day before meningeal harvest, Eppendorf tubes were coated with FACS buffer (1% BSA, 1mM EDTA in PBS) overnight. Mice were exsanguinated and perfused transcardially with ice-cold PBS with heparin (0.025%). The skull caps were prepared as described in "Tissue Collection". Meninges were peeled from the skull cap and placed in ice-cold DMEM for the entirety of collection. Meninges were then digested for 15 minutes at 37 °C with constant agitation using 1 mL of pre-warmed digestion buffer (DMEM, with 2% FBS, 1 mg/mL collagenase VIII (Sigma Aldrich), and 0.5 mg/mL DNase I (Sigma Aldrich). The enzymes were neutralized with 1 mL of complete medium (DMEM with 10% FBS) and meninges were then filtered through a 70 µm cell strainer. An additional 2 mL of FACS buffer was added, samples were centrifuged at 400xg for

five minutes, and samples were resuspended in FACS buffer. After two washes, cells were resuspended in FACS buffer with DAPI (0.2 µg/mL). Singlet gates were selected using pulse width of the side scatter and forward scatter. Cells negative for DAPI were selected for being live. Cells were sorted into 1.5 ml tubes with ice cold DMEM. Following sorting, cells were centrifuged again at 450xg for 4 mins and the media was aspirated. Cells were resuspended in 200 uL 0.04% BSA in PBS (0.04% non-acetylated BSA) and centrifuged again. Cells were counted in 20 ul of 0.04% BSA in PBS using trypan blue. Approximately 4,000 cells per sample were loaded onto a 10X Genomics Chromium platform to generate cDNAs carrying cell- and transcript-specific barcodes and sequencing libraries constructed using the Chromium Single Cell 3' Library & Gel Bead Kit 2. Libraries were sequenced on the Illumina NextSeq using pair-ended sequencing, resulting in 50,000 reads per cell.

scRNA-seq analysis

The raw sequencing reads (FASTQ files) were aligned to the UCSC mm10 mouse genome build using Cell Ranger (v1.3.1) which performs alignment, filtering, barcode counting and unique molecular identifier (UMI) counting. R studio was used for all downstream analyses and Seurat (v.3.9.9) was used for filtering out low-quality cells, normalization of the data, determination of cluster defining markers and graphing of the data on UMAP [204, 205]. Low-quality cells were excluded in an initial quality-control (QC) step by removing genes expressed in fewer than three cells, cells with fewer than 150 genes expressed, and cells expressing more than 5000 genes. Cells with more than 20% of mitochondrial-associated genes and cells with more than 5% hemoglobin among their expressed genes were also removed. Genes with high variance were selected using the FindVariableGenes function, then the dimensionality of the data was reduced by principle component analysis (PCA) and identified by random sampling of 20 significant principal components (PCs) for each sample with the PCElbowPlot function. Cells were clustered

with Seurat's FindClusters function. Differential gene expression analysis was performed within clusters using the ZinBWave function and DESeq2 [206]. Data was organized and graphs were created using ggplot2, tidyverse and dplyr [207, 208].

RNA-seq analysis

The raw sequencing reads (FASTQ files) were aligned to the UCSC mm10 mouse genome build using the splice-aware read aligner HISAT2 [174]. Samtools was used for quality control filtering [175]. Reads were sorted into feature counts with HTSeq [176]. DESeq2 was used to normalize the raw counts based on read depth and perform principal component analysis and differential expression analysis [177]. The p-values were corrected with the Benjamini-Hochberg procedure to limit false positives arising from multiple testing. The gene set collections from MSigDB were used for differential gene set enrichment analysis [159]. The analysis itself was performed using the Seq2Pathway, fgsea, tidyverse, and dplyr software packages. Heatmaps were generated using the pheatmap R package [https://github.com/raivokolde/pheatmap] while other plots were made with the lattice (http://lattice.r-forge.r-project.org/) or ggplot2 [https://ggplot2.tidyverse.org] packages. All code used for analysis is available upon request.

Immunohistochemistry, imaging and quantification

For immunofluorescence staining, floating brain sections and meningeal whole-mounts in PBS and 0.05% azide were blocked with either 2% donkey serum or 2% goat serum, 1% bovine serum albumin, 0.1% triton, 0.05% tween-20, and 0.05% sodium azide in PBS for 1.5 hours at room temperature. This blocking step was followed by incubation with appropriate dilutions of primary antibodies: anti-Lyve-1–eFluor 660 (eBioscience, clone ALY7, 1:200), anti-Iba1 (Abcam, ab5076, 1:300) and anti-GFAP (Thermo Fisher Scientific, 2.2B10, 1:1000), anti-Aβ (Cell Signaling Technologies, D54D2, 1:200) in the same solution used for blocking overnight at 4°C or for 3 hours at room temperature. Meningeal whole-mounts or brain tissue sections were then washed

3 times for 10 minutes at room temperature in PBS and 0.05% tween-20, followed by incubation with the appropriate donkey Alexa Fluor 488, 594, 647 anti-rat, -goat, -rabbit (Thermo Fisher Scientific, 1:1000) IgG antibodies for 2 hours at room temperature in the same solution used for blocking. The sections or whole-mounts were then washed 3 times for 10 minutes at room temperature before incubation for 10 minutes with 1:1000 DAPI in PBS. The tissue was then transferred to PBS and mounted with ProLong Gold antifade reagent (Invitrogen, P36930) on glass slides with coverslips. Slide preparations were stored at 4°C and imaged using a Lecia TCS SP8 confocal microscope and LAS AF software (Leica Microsystems) within one week of staining. Quantitative analysis of the acquired images was performed using Fiji software. For the assessment of gliosis in the injured and uninjured brains, 3 representative brain sections from the hippocampus were fully imaged. The full brain section was adjusted for brightness/contrast uniformly for each experiment, and the percent area of coverage of each immunohistochemical markers was calculated per hemisphere for each brain section. Each hemisphere was traced, and then the threshold was uniformly set for each experiment to select for stained cells. The mean percent area fraction was calculated using Microsoft Excel.

Statistical analysis and reproducibility

Sample sizes were chosen on the basis of standard power calculations (with $\alpha = 0.05$ and power of 0.8). Experimenters were blinded to the identity of experimental groups from the time of euthanasia until the end of data collection and analysis. One-way ANOVA, with Bonferroni's multiple comparison test, Tukey's multiple comparison test, Dunnett's multiple comparison test, or Holm-Sidak's post hoc test, were used to compare multiple independent groups. Two-group comparisons were made using unpaired Student's t-test. For comparisons of multiple factors (for example, age versus treatment), two-way ANOVA with Bonferroni's post hoc test or Tukey's multiple comparison test was used. Repeated-measures two-way ANOVA with Bonferroni's post hoc test was used for day versus treatment comparisons with repeated observations. Statistical

analysis (data are always presented as mean ± s.e.m.) was performed using Prism 8.0 (GraphPad Software, Inc.).

Literature Cited

1. *The changing landscape of traumatic brain injury research.* Lancet Neurol, 2012. **11**(8): p. 651.
2. Chen, R.L., J.S. Balami, M.M. Esiri, L.K. Chen, and A.M. Buchan, *Ischemic stroke in the elderly: an overview of evidence.* Nat Rev Neurol, 2010. **6**(5): p. 256-65.
3. Sturm, J.W., G.A. Donnan, H.M. Dewey, R.A. Macdonell, A.K. Gilligan, V. Srikanth, and A.G. Thrift, *Quality of life after stroke: the North East Melbourne Stroke Incidence Study (NEMESIS).* Stroke, 2004. **35**(10): p. 2340-5.
4. Mortimer, J.A., C.M. van Duijn, V. Chandra, L. Fratiglioni, A.B. Graves, A. Heyman, A.F. Jorm, E. Kokmen, K. Kondo, W.A. Rocca, and et al., *Head trauma as a risk factor for Alzheimer's disease: a collaborative re-analysis of case-control studies. EURODEM Risk Factors Research Group.* Int J Epidemiol, 1991. **20 Suppl 2**: p. S28-35.
5. Chen, H., M. Richard, D.P. Sandler, D.M. Umbach, and F. Kamel, *Head injury and amyotrophic lateral sclerosis.* Am J Epidemiol, 2007. **166**(7): p. 810-6.
6. Holsinger, T., D.C. Steffens, C. Phillips, M.J. Helms, R.J. Havlik, J.C. Breitner, J.M. Guralnik, and B.L. Plassman, *Head injury in early adulthood and the lifetime risk of depression.* Arch Gen Psychiatry, 2002. **59**(1): p. 17-22.
7. Gardner, R.C., J.F. Burke, J. Nettiksimmons, S. Goldman, C.M. Tanner, and K. Yaffe, *Traumatic brain injury in later life increases risk for Parkinson disease.* Ann Neurol, 2015. **77**(6): p. 987-95.
8. Hoge, C.W., D. McGurk, J.L. Thomas, A.L. Cox, C.C. Engel, and C.A. Castro, *Mild traumatic brain injury in U.S. Soldiers returning from Iraq.* N Engl J Med, 2008. **358**(5): p. 453-63.
9. McKee, A.C., R.C. Cantu, C.J. Nowinski, E.T. Hedley-Whyte, B.E. Gavett, and A.E. Budson, *Chronic traumatic encephalopathy in athletes: progressive taupathy after repetitive head injury.* J Neuropathol Exp Neurol, 2009. **68**.
10. Corps, K.N., T.L. Roth, and D.B. McGavern, *Inflammation and neuroprotection in traumatic brain injury.* JAMA Neurol, 2015. **72**(3): p. 355-62.
11. McKee, C.A. and J.R. Lukens, *Emerging Roles for the Immune System in Traumatic Brain Injury.* Front Immunol, 2016. **7**: p. 556.
12. Woodcock, T. and M.C. Morganti-Kossmann, *The role of markers of inflammation in traumatic brain injury.* Front Neurol, 2013. **4**: p. 18.
13. de Rivero Vaccari, J.P., G. Lotocki, O.F. Alonso, H.M. Bramlett, W.D. Dietrich, and R.W. Keane, *Therapeutic neutralization of the NLRP1 inflammasome reduces the innate immune response and improves histopathology after traumatic brain injury.* J Cereb Blood Flow Metab, 2009. **29**(7): p. 1251-61.
14. Mortezaee, K., N. Khanlarkhani, C. Beyer, and A. Zendedel, *Inflammasome: Its role in traumatic brain and spinal cord injury.* J Cell Physiol, 2018. **233**(7): p. 5160-5169.
15. Roth, T.L., D. Nayak, T. Atanasijevic, A.P. Koretsky, L.L. Latour, and D.B. McGavern, *Transcranial amelioration of inflammation and cell death after brain injury.* Nature, 2014. **505**(7482): p. 223-8.
16. Stevens, B., N.J. Allen, L.E. Vazquez, G.R. Howell, K.S. Christopherson, N. Nouri, K.D. Micheva, A.K. Mehalow, A.D. Huberman, B. Stafford, A. Sher, A.M. Litke, J.D. Lambris, S.J. Smith, S.W. John, and B.A. Barres, *The classical complement cascade mediates CNS synapse elimination.* Cell, 2007. **131**(6): p. 1164-78.
17. Stephan, A.H., B.A. Barres, and B. Stevens, *The complement system: an unexpected role in synaptic pruning during development and disease.* Annu Rev Neurosci, 2012. **35**: p. 369-89.
18. Sierra, A., J.M. Encinas, J.J. Deudero, J.H. Chancey, G. Enikolopov, L.S. Overstreet-Wadiche, S.E. Tsirka, and M. Maletic-Savatic, *Microglia shape adult hippocampal*

neurogenesis through apoptosis-coupled phagocytosis. Cell Stem Cell, 2010. **7**(4): p. 483-95.
19. Marquez-Ropero, M., E. Benito, A. Plaza-Zabala, and A. Sierra, *Microglial Corpse Clearance: Lessons From Macrophages.* Front Immunol, 2020. **11**: p. 506.
20. Schafer, D.P., E.K. Lehrman, A.G. Kautzman, R. Koyama, A.R. Mardinly, R. Yamasaki, R.M. Ransohoff, M.E. Greenberg, B.A. Barres, and B. Stevens, *Microglia sculpt postnatal neural circuits in an activity and complement-dependent manner.* Neuron, 2012. **74**(4): p. 691-705.
21. Davalos, D., J. Grutzendler, G. Yang, J.V. Kim, Y. Zuo, S. Jung, D.R. Littman, M.L. Dustin, and W.B. Gan, *ATP mediates rapid microglial response to local brain injury in vivo.* Nat Neurosci, 2005. **8**(6): p. 752-8.
22. Witcher, K.G., C.E. Bray, J.E. Dziabis, D.B. McKim, B.N. Benner, R.K. Rowe, O.N. Kokiko-Cochran, P.G. Popovich, J. Lifshitz, D.S. Eiferman, and J.P. Godbout, *Traumatic brain injury-induced neuronal damage in the somatosensory cortex causes formation of rod-shaped microglia that promote astrogliosis and persistent neuroinflammation.* Glia, 2018. **66**(12): p. 2719-2736.
23. Kumar, A., D.M. Alvarez-Croda, B.A. Stoica, A.I. Faden, and D.J. Loane, *Microglial/Macrophage Polarization Dynamics following Traumatic Brain Injury.* J Neurotrauma, 2016. **33**(19): p. 1732-1750.
24. Ramlackhansingh, A.F., D.J. Brooks, R.J. Greenwood, S.K. Bose, F.E. Turkheimer, K.M. Kinnunen, S. Gentleman, R.A. Heckemann, K. Gunanayagam, G. Gelosa, and D.J. Sharp, *Inflammation after trauma: microglial activation and traumatic brain injury.* Ann Neurol, 2011. **70**(3): p. 374-83.
25. Johnson, V.E., J.E. Stewart, F.D. Begbie, J.Q. Trojanowski, D.H. Smith, and W. Stewart, *Inflammation and white matter degeneration persist for years after a single traumatic brain injury.* Brain, 2013. **136**(Pt 1): p. 28-42.
26. Erturk, A., S. Mentz, E.E. Stout, M. Hedehus, S.L. Dominguez, L. Neumaier, F. Krammer, G. Llovera, K. Srinivasan, D.V. Hansen, A. Liesz, K.A. Scearce-Levie, and M. Sheng, *Interfering with the Chronic Immune Response Rescues Chronic Degeneration After Traumatic Brain Injury.* J Neurosci, 2016. **36**(38): p. 9962-75.
27. Smith, D.H., V.E. Johnson, and W. Stewart, *Chronic neuropathologies of single and repetitive TBI: substrates of dementia?* Nat Rev Neurol, 2013. **9**(4): p. 211-21.
28. McKee, A.C., R.C. Cantu, C.J. Nowinski, E.T. Hedley-Whyte, B.E. Gavett, A.E. Budson, V.E. Santini, H.S. Lee, C.A. Kubilus, and R.A. Stern, *Chronic traumatic encephalopathy in athletes: progressive tauopathy after repetitive head injury.* J Neuropathol Exp Neurol, 2009. **68**(7): p. 709-35.
29. Webster, S.J., L.J. Van Eldik, D.M. Watterson, and A.D. Bachstetter, *Closed head injury in an age-related Alzheimer mouse model leads to an altered neuroinflammatory response and persistent cognitive impairment.* J Neurosci, 2015. **35**(16): p. 6554-69.
30. Washington, P.M., N. Morffy, M. Parsadanian, D.N. Zapple, and M.P. Burns, *Experimental traumatic brain injury induces rapid aggregation and oligomerization of amyloid-beta in an Alzheimer's disease mouse model.* J Neurotrauma, 2014. **31**(1): p. 125-34.
31. Kokiko-Cochran, O.N. and J.P. Godbout, *The Inflammatory Continuum of Traumatic Brain Injury and Alzheimer's Disease.* Front Immunol, 2018. **9**: p. 672.
32. Williams, W.H., S. Potter, and H. Ryland, *Mild traumatic brain injury and Postconcussion Syndrome: a neuropsychological perspective.* J Neurol Neurosurg Psychiatry, 2010. **81**(10): p. 1116-22.
33. Nolan, A., E. Hennessy, K. Krukowski, C. Guglielmetti, M.M. Chaumeil, V.S. Sohal, and S. Rosi, *Repeated Mild Head Injury Leads to Wide-Ranging Deficits in Higher-Order Cognitive Functions Associated with the Prefrontal Cortex.* J Neurotrauma, 2018. **35**(20): p. 2425-2434.

34. Stern, R.A., C.H. Adler, K. Chen, M. Navitsky, J. Luo, D.W. Dodick, M.L. Alosco, Y. Tripodis, D.D. Goradia, B. Martin, D. Mastroeni, N.G. Fritts, J. Jarnagin, M.D. Devous, Sr., M.A. Mintun, M.J. Pontecorvo, M.E. Shenton, and E.M. Reiman, *Tau Positron-Emission Tomography in Former National Football League Players.* N Engl J Med, 2019. **380**(18): p. 1716-1725.
35. Nemetz, P.N., C. Leibson, J.M. Naessens, M. Beard, E. Kokmen, J.F. Annegers, and L.T. Kurland, *Traumatic brain injury and time to onset of Alzheimer's disease: a population-based study.* Am J Epidemiol, 1999. **149**(1): p. 32-40.
36. Johnson, V.E., W. Stewart, and D.H. Smith, *Widespread tau and amyloid-beta pathology many years after a single traumatic brain injury in humans.* Brain Pathol, 2012. **22**(2): p. 142-9.
37. Block, M.L., L. Zecca, and J.S. Hong, *Microglia-mediated neurotoxicity: uncovering the molecular mechanisms.* Nat Rev Neurosci, 2007. **8**(1): p. 57-69.
38. Keren-Shaul, H., A. Spinrad, A. Weiner, O. Matcovitch-Natan, R. Dvir-Szternfeld, T.K. Ulland, E. David, K. Baruch, D. Lara-Astaiso, B. Toth, S. Itzkovitz, M. Colonna, M. Schwartz, and I. Amit, *A Unique Microglia Type Associated with Restricting Development of Alzheimer's Disease.* Cell, 2017. **169**(7): p. 1276-1290 e17.
39. Holtman, I.R., D.D. Raj, J.A. Miller, W. Schaafsma, Z. Yin, N. Brouwer, P.D. Wes, T. Moller, M. Orre, W. Kamphuis, E.M. Hol, E.W. Boddeke, and B.J. Eggen, *Induction of a common microglia gene expression signature by aging and neurodegenerative conditions: a co-expression meta-analysis.* Acta Neuropathol Commun, 2015. **3**: p. 31.
40. Masuda, T., R. Sankowski, O. Staszewski, C. Bottcher, L. Amann, Sagar, C. Scheiwe, S. Nessler, P. Kunz, G. van Loo, V.A. Coenen, P.C. Reinacher, A. Michel, U. Sure, R. Gold, D. Grun, J. Priller, C. Stadelmann, and M. Prinz, *Spatial and temporal heterogeneity of mouse and human microglia at single-cell resolution.* Nature, 2019. **566**(7744): p. 388-392.
41. Young, A.M.H., N. Kumasaka, F. Calvert, T.R. Hammond, A. Knights, N. Panousis, J. Schwartzentruber, J. Liu, K. Kundu, M. Segel, N. Murphy, C.E. McMurran, H. Bulstrode, J. Correia, K.P. Budohoski, A. Joannides, M.R. Guilfoyle, R. Trivedi, R. Kirollos, R. Morris, et al., *A map of transcriptional heterogeneity and regulatory variation in human microglia.* bioRxiv, 2019.
42. Elmore, M.R., A.R. Najafi, M.A. Koike, N.N. Dagher, E.E. Spangenberg, R.A. Rice, M. Kitazawa, B. Matusow, H. Nguyen, B.L. West, and K.N. Green, *Colony-stimulating factor 1 receptor signaling is necessary for microglia viability, unmasking a microglia progenitor cell in the adult brain.* Neuron, 2014. **82**(2): p. 380-97.
43. Willis, E.F., K.P.A. MacDonald, Q.H. Nguyen, A.L. Garrido, E.R. Gillespie, S.B.R. Harley, P.F. Bartlett, W.A. Schroder, A.G. Yates, D.C. Anthony, S. Rose-John, M.J. Ruitenberg, and J. Vukovic, *Repopulating Microglia Promote Brain Repair in an IL-6-Dependent Manner.* Cell, 2020. **180**(5): p. 833-846 e16.
44. Hilla, A.M., H. Diekmann, and D. Fischer, *Microglia Are Irrelevant for Neuronal Degeneration and Axon Regeneration after Acute Injury.* J Neurosci, 2017. **37**(25): p. 6113-6124.
45. Hanlon, L.A., R. Raghupathi, and J.W. Huh, *Depletion of microglia immediately following traumatic brain injury in the pediatric rat: Implications for cellular and behavioral pathology.* Exp Neurol, 2019. **316**: p. 39-51.
46. Szalay, G., B. Martinecz, N. Lenart, Z. Kornyei, B. Orsolits, L. Judak, E. Csaszar, R. Fekete, B.L. West, G. Katona, B. Rozsa, and A. Denes, *Microglia protect against brain injury and their selective elimination dysregulates neuronal network activity after stroke.* Nat Commun, 2016. **7**: p. 11499.
47. Bellver-Landete, V., F. Bretheau, B. Mailhot, N. Vallières, M. Lessard, M.-E. Janelle, N. Vernoux, M.-È. Tremblay, T. Fuehrmann, M.S. Shoichet, and S. Lacroix, *Microglia are an*

essential component of the neuroprotective scar that forms after spinal cord injury. Nature Communications, 2019. **10**(1).
48. Li, Y., X. He, R. Kawaguchi, Y. Zhang, Q. Wang, A. Monavarfeshani, Z. Yang, B. Chen, Z. Shi, H. Meng, S. Zhou, J. Zhu, A. Jacobi, V. Swarup, P.G. Popovich, D.H. Geschwind, and Z. He, *Microglia-organized scar-free spinal cord repair in neonatal mice.* Nature, 2020. **587**(7835): p. 613-618.
49. Henry, R.J., R.M. Ritzel, J.P. Barrett, S.J. Doran, Y. Jiao, J.B. Leach, G.L. Szeto, J. Wu, B.A. Stoica, A.I. Faden, and D.J. Loane, *Microglial Depletion with CSF1R Inhibitor During Chronic Phase of Experimental Traumatic Brain Injury Reduces Neurodegeneration and Neurological Deficits.* J Neurosci, 2020. **40**(14): p. 2960-2974.
50. Rice, R.A., J. Pham, R.J. Lee, A.R. Najafi, B.L. West, and K.N. Green, *Microglial repopulation resolves inflammation and promotes brain recovery after injury.* Glia, 2017. **65**(6): p. 931-944.
51. Parkhurst, C.N., G. Yang, I. Ninan, J.N. Savas, J.R. Yates, 3rd, J.J. Lafaille, B.L. Hempstead, D.R. Littman, and W.B. Gan, *Microglia promote learning-dependent synapse formation through brain-derived neurotrophic factor.* Cell, 2013. **155**(7): p. 1596-609.
52. Hergenroeder, G.W., A.N. Moore, J.P. McCoy, Jr., L. Samsel, N.H. Ward, 3rd, G.L. Clifton, and P.K. Dash, *Serum IL-6: a candidate biomarker for intracranial pressure elevation following isolated traumatic brain injury.* J Neuroinflammation, 2010. **7**: p. 19.
53. Minambres, E., A. Cemborain, P. Sanchez-Velasco, M. Gandarillas, G. Diaz-Reganon, U. Sanchez-Gonzalez, and F. Leyva-Cobian, *Correlation between transcranial interleukin-6 gradient and outcome in patients with acute brain injury.* Crit Care Med, 2003. **31**(3): p. 933-8.
54. Liddelow, S.A., K.A. Guttenplan, L.E. Clarke, F.C. Bennett, C.J. Bohlen, L. Schirmer, M.L. Bennett, A.E. Munch, W.S. Chung, T.C. Peterson, D.K. Wilton, A. Frouin, B.A. Napier, N. Panicker, M. Kumar, M.S. Buckwalter, D.H. Rowitch, V.L. Dawson, T.M. Dawson, B. Stevens, et al., *Neurotoxic reactive astrocytes are induced by activated microglia.* Nature, 2017. **541**(7638): p. 481-487.
55. Lei, F., N. Cui, C. Zhou, J. Chodosh, D.G. Vavvas, and E.I. Paschalis, *CSF1R inhibition by a small-molecule inhibitor is not microglia specific; affecting hematopoiesis and the function of macrophages.* Proc Natl Acad Sci U S A, 2020. **117**(38): p. 23336-23338.
56. Weller, R.O., M.M. Sharp, M. Christodoulides, R.O. Carare, and K. Mollgard, *The meninges as barriers and facilitators for the movement of fluid, cells and pathogens related to the rodent and human CNS.* Acta Neuropathol, 2018. **135**(3): p. 363-385.
57. DeSisto, J., R. O'Rourke, H.E. Jones, B. Pawlikowski, A.D. Malek, S. Bonney, F. Guimiot, K.L. Jones, and J.A. Siegenthaler, *Single-Cell Transcriptomic Analyses of the Developing Meninges Reveal Meningeal Fibroblast Diversity and Function.* Dev Cell, 2020. **54**(1): p. 43-59 e4.
58. Siegenthaler, J.A., A.M. Ashique, K. Zarbalis, K.P. Patterson, J.H. Hecht, M.A. Kane, A.E. Folias, Y. Choe, S.R. May, T. Kume, J.L. Napoli, A.S. Peterson, and S.J. Pleasure, *Retinoic acid from the meninges regulates cortical neuron generation.* Cell, 2009. **139**(3): p. 597-609.
59. Haldipur, P., G.S. Gillies, O.K. Janson, V.V. Chizhikov, D.S. Mithal, R.J. Miller, and K.J. Millen, *Foxc1 dependent mesenchymal signalling drives embryonic cerebellar growth.* Elife, 2014. **3**.
60. Haldipur, P., G. Gillies, O.K. Janson, V.V. Chizhikov, and K.J. Millen, *ISDN2014_0119: Mesenchymal Foxc1 non-autonomously controls cerebellar development through SDF1α-CXCR4 maintenance of radial glial cells.* International Journal of Developmental Neuroscience, 2015. **47**(Part_A): p. 34-34.

61. Reiss, K., R. Mentlein, J. Sievers, and D. Hartmann, *Stromal cell-derived factor 1 is secreted by meningeal cells and acts as chemotactic factor on neuronal stem cells of the cerebellar external granular layer.* Neuroscience, 2002. **115**(1): p. 295-305.
62. Zhu, Y., T. Yu, X.C. Zhang, T. Nagasawa, J.Y. Wu, and Y. Rao, *Role of the chemokine SDF-1 as the meningeal attractant for embryonic cerebellar neurons.* Nat Neurosci, 2002. **5**(8): p. 719-20.
63. Derecki, N.C., A.N. Cardani, C.H. Yang, K.M. Quinnies, A. Crihfield, K.R. Lynch, and J. Kipnis, *Regulation of learning and memory by meningeal immunity: a key role for IL-4.* J Exp Med, 2010. **207**(5): p. 1067-80.
64. Filiano, A.J., Y. Xu, N.J. Tustison, R.L. Marsh, W. Baker, I. Smirnov, C.C. Overall, S.P. Gadani, S.D. Turner, Z. Weng, S.N. Peerzade, H. Chen, K.S. Lee, M.M. Scott, M.P. Beenhakker, V. Litvak, and J. Kipnis, *Unexpected role of interferon-gamma in regulating neuronal connectivity and social behaviour.* Nature, 2016. **535**(7612): p. 425-9.
65. Alves de Lima, K., J. Rustenhoven, S. Da Mesquita, M. Wall, A.F. Salvador, I. Smirnov, G. Martelossi Cebinelli, T. Mamuladze, W. Baker, Z. Papadopoulos, M.B. Lopes, W.S. Cao, X.S. Xie, J. Herz, and J. Kipnis, *Meningeal γδ T cells regulate anxiety-like behavior via IL-17a signaling in neurons.* Nature Immunology, 2020. **21**(11): p. 1421-1429.
66. Ribeiro, M., H.C. Brigas, M. Temido-Ferreira, P.A. Pousinha, T. Regen, C. Santa, J.E. Coelho, I. Marques-Morgado, C.A. Valente, S. Omenetti, B. Stockinger, A. Waisman, B. Manadas, L.V. Lopes, B. Silva-Santos, and J.C. Ribot, *Meningeal gammadelta T cell-derived IL-17 controls synaptic plasticity and short-term memory.* Sci Immunol, 2019. **4**(40).
67. Baune, B.T., G. Ponath, M. Rothermundt, O. Riess, H. Funke, and K. Berger, *Association between genetic variants of IL-1beta, IL-6 and TNF-alpha cytokines and cognitive performance in the elderly general population of the MEMO-study.* Psychoneuroendocrinology, 2008. **33**(1): p. 68-76.
68. Sparkman, N.L., J.B. Buchanan, J.R. Heyen, J. Chen, J.L. Beverly, and R.W. Johnson, *Interleukin-6 facilitates lipopolysaccharide-induced disruption in working memory and expression of other proinflammatory cytokines in hippocampal neuronal cell layers.* J Neurosci, 2006. **26**(42): p. 10709-16.
69. Turtzo, L.C., N. Jikaria, M.R. Cota, J.P. Williford, V. Uche, T. Davis, J. MacLaren, A.D. Moses, G. Parikh, M.A. Castro, D.L. Pham, J.A. Butman, and L.L. Latour, *Meningeal blood-brain barrier disruption in acute traumatic brain injury.* Brain Communications, 2020.
70. Russo, M.V., L.L. Latour, and D.B. McGavern, *Distinct myeloid cell subsets promote meningeal remodeling and vascular repair after mild traumatic brain injury.* Nat Immunol, 2018. **19**(5): p. 442-452.
71. Koh, B.I., H.J. Lee, P.A. Kwak, M.J. Yang, J.H. Kim, H.S. Kim, G.Y. Koh, and I. Kim, *VEGFR2 signaling drives meningeal vascular regeneration upon head injury.* Nat Commun, 2020. **11**(1): p. 3866.
72. Park, E., J.D. Bell, I.P. Siddiq, and A.J. Baker, *An analysis of regional microvascular loss and recovery following two grades of fluid percussion trauma: a role for hypoxia-inducible factors in traumatic brain injury.* J Cereb Blood Flow Metab, 2009. **29**(3): p. 575-84.
73. Daniel Moreno-Zambrano, D.S., David Avila, Rocío Santibáñez, *Lymphatics of the Central Nervous System: Forgotten first descriptions.* Neurology, 2018.
74. Cserr, H.F., C.J. Harling-Berg, and P.M. Knopf, *Drainage of Brain Extracellular Fluid into Blood and Deep Cervical Lymph and its Immunological Significance.* Brain Pathology, 1992. **2**(4): p. 269-276.
75. Kida, S., A. Pantazis, and R.O. Weller, *CSF drains directly from the subarachnoid space into nasal lymphatics in the rat. Anatomy, histology and immunological significance.* Neuropathology and Applied Neurobiology, 1993. **19**(6): p. 480-488.

76. Louveau, A., I. Smirnov, T.J. Keyes, J.D. Eccles, S.J. Rouhani, J.D. Peske, N.C. Derecki, D. Castle, J.W. Mandell, K.S. Lee, T.H. Harris, and J. Kipnis, *Structural and functional features of central nervous system lymphatic vessels.* Nature, 2015. **523**(7560): p. 337-41.
77. Aspelund, A., S. Antila, S.T. Proulx, T.V. Karlsen, S. Karaman, M. Detmar, H. Wiig, and K. Alitalo, *A dural lymphatic vascular system that drains brain interstitial fluid and macromolecules.* J Exp Med, 2015. **212**(7): p. 991-9.
78. Antila, S., S. Karaman, H. Nurmi, M. Airavaara, M.H. Voutilainen, T. Mathivet, D. Chilov, Z. Li, T. Koppinen, J.H. Park, S. Fang, A. Aspelund, M. Saarma, A. Eichmann, J.L. Thomas, and K. Alitalo, *Development and plasticity of meningeal lymphatic vessels.* J Exp Med, 2017. **214**(12): p. 3645-3667.
79. Esposito, E., B.J. Ahn, J. Shi, Y. Nakamura, J.H. Park, E.T. Mandeville, Z. Yu, S.J. Chan, R. Desai, A. Hayakawa, X. Ji, E.H. Lo, and K. Hayakawa, *Brain-to-cervical lymph node signaling after stroke.* Nat Commun, 2019. **10**(1): p. 5306.
80. Plog, B.A., M.L. Dashnaw, E. Hitomi, W. Peng, Y. Liao, N. Lou, R. Deane, and M. Nedergaard, *Biomarkers of traumatic injury are transported from brain to blood via the glymphatic system.* J Neurosci, 2015. **35**(2): p. 518-26.
81. Iliff, J.J., M. Wang, D.M. Zeppenfeld, A. Venkataraman, B.A. Plog, Y. Liao, R. Deane, and M. Nedergaard, *Cerebral arterial pulsation drives paravascular CSF-interstitial fluid exchange in the murine brain.* J Neurosci, 2013. **33**(46): p. 18190-9.
82. Jessen, N.A., A.S. Munk, I. Lundgaard, and M. Nedergaard, *The Glymphatic System: A Beginner's Guide.* Neurochem Res, 2015. **40**(12): p. 2583-99.
83. Iliff, J.J., M.J. Chen, B.A. Plog, D.M. Zeppenfeld, M. Soltero, L. Yang, I. Singh, R. Deane, and M. Nedergaard, *Impairment of glymphatic pathway function promotes tau pathology after traumatic brain injury.* J Neurosci, 2014. **34**(49): p. 16180-93.
84. Iliff, J.J., M. Wang, Y. Liao, B.A. Plogg, W. Peng, G.A. Gundersen, H. Benveniste, G.E. Vates, R. Deane, S.A. Goldman, E.A. Nagelhus, and M. Nedergaard, *A paravascular pathway facilitates CSF flow through the brain parenchyma and the clearance of interstitial solutes, including amyloid beta.* Sci Transl Med, 2012. **4**(147): p. 147ra111.
85. Louveau, A., B.A. Plog, S. Antila, K. Alitalo, M. Nedergaard, and J. Kipnis, *Understanding the functions and relationships of the glymphatic system and meningeal lymphatics.* J Clin Invest, 2017. **127**(9): p. 3210-3219.
86. Absinta, M., S.K. Ha, G. Nair, P. Sati, N.J. Luciano, M. Palisoc, A. Louveau, K.A. Zaghloul, S. Pittaluga, J. Kipnis, and D.S. Reich, *Human and nonhuman primate meninges harbor lymphatic vessels that can be visualized noninvasively by MRI.* Elife, 2017. **6**.
87. Kuo, P.H., C. Stuehm, S. Squire, and K. Johnson, *Meningeal Lymphatic Vessel Flow Runs Countercurrent to Venous Flow in the Superior Sagittal Sinus of the Human Brain.* Tomography, 2018. **4**(3): p. 99-104.
88. Chen, J., L. Wang, H. Xu, L. Xing, Z. Zhuang, Y. Zheng, X. Li, C. Wang, S. Chen, Z. Guo, Q. Liang, and Y. Wang, *Meningeal lymphatics clear erythrocytes that arise from subarachnoid hemorrhage.* Nat Commun, 2020. **11**(1): p. 3159.
89. Bolte, A.C., A.B. Dutta, M.E. Hurt, I. Smirnov, M.A. Kovacs, C.A. McKee, H.E. Ennerfelt, D. Shapiro, B.H. Nguyen, E.L. Frost, C.R. Lammert, J. Kipnis, and J.R. Lukens, *Meningeal lymphatic dysfunction exacerbates traumatic brain injury pathogenesis.* Nat Commun, 2020. **11**(1): p. 4524.
90. Song, E., T. Mao, H. Dong, L.S.B. Boisserand, S. Antila, M. Bosenberg, K. Alitalo, J.L. Thomas, and A. Iwasaki, *VEGF-C-driven lymphatic drainage enables immunosurveillance of brain tumours.* Nature, 2020. **577**(7792): p. 689-694.
91. Louveau, A., J. Herz, M.N. Alme, A.F. Salvador, M.Q. Dong, K.E. Viar, S.G. Herod, J. Knopp, J.C. Setliff, A.L. Lupi, S. Da Mesquita, E.L. Frost, A. Gaultier, T.H. Harris, R. Cao, S. Hu, J.R. Lukens, I. Smirnov, C.C. Overall, G. Oliver, et al., *CNS lymphatic drainage and*

neuroinflammation are regulated by meningeal lymphatic vasculature. Nature Neuroscience, 2018. **21**(10): p. 1380-1391.
92. Hsu, M., A. Rayasam, J.A. Kijak, Y.H. Choi, J.S. Harding, S.A. Marcus, W.J. Karpus, M. Sandor, and Z. Fabry, *Neuroinflammation-induced lymphangiogenesis near the cribriform plate contributes to drainage of CNS-derived antigens and immune cells.* Nat Commun, 2019. **10**(1): p. 229.
93. Planas, A.M., M. Gomez-Choco, X. Urra, R. Gorina, M. Caballero, and A. Chamorro, *Brain-derived antigens in lymphoid tissue of patients with acute stroke.* J Immunol, 2012. **188**(5): p. 2156-63.
94. van Zwam, M., R. Huizinga, M.J. Melief, A.F. Wierenga-Wolf, M. van Meurs, J.S. Voerman, K.P. Biber, H.W. Boddeke, U.E. Hopken, C. Meisel, A. Meisel, I. Bechmann, R.Q. Hintzen, B.A. t Hart, S. Amor, J.D. Laman, and L.A. Boven, *Brain antigens in functionally distinct antigen-presenting cell populations in cervical lymph nodes in MS and EAE.* J Mol Med (Berl), 2009. **87**(3): p. 273-86.
95. Urra, X., F. Miro, A. Chamorro, and A.M. Planas, *Antigen-specific immune reactions to ischemic stroke.* Front Cell Neurosci, 2014. **8**: p. 278.
96. de Vos, A.F., M. van Meurs, H.P. Brok, L.A. Boven, R.Q. Hintzen, P. van der Valk, R. Ravid, S. Rensing, L. Boon, B.A. t Hart, and J.D. Laman, *Transfer of central nervous system autoantigens and presentation in secondary lymphoid organs.* J Immunol, 2002. **169**(10): p. 5415-23.
97. Cai, R., C. Pan, A. Ghasemigharagoz, M.I. Todorov, B. Forstera, S. Zhao, H.S. Bhatia, A. Parra-Damas, L. Mrowka, D. Theodorou, M. Rempfler, A.L.R. Xavier, B.T. Kress, C. Benakis, H. Steinke, S. Liebscher, I. Bechmann, A. Liesz, B. Menze, M. Kerschensteiner, et al., *Panoptic imaging of transparent mice reveals whole-body neuronal projections and skull-meninges connections.* Nat Neurosci, 2019. **22**(2): p. 317-327.
98. Kang, J.H. and H.C. Lin, *Increased risk of multiple sclerosis after traumatic brain injury: a nationwide population-based study.* J Neurotrauma, 2012. **29**(1): p. 90-5.
99. Montgomery, S., A. Hiyoshi, S. Burkill, L. Alfredsson, S. Bahmanyar, and T. Olsson, *Concussion in adolescence and risk of multiple sclerosis.* Ann Neurol, 2017. **82**(4): p. 554-561.
100. Sara, W., V. Maria, G. Barbara, V. Anaïs, M.H. Keuters, A. Salli, A. Kari, K. Jari, and F.M. Noe, *The CNS lymphatic system modulates the adaptive neuro-immune response in the perilesional cortex in a mouse model of traumatic brain injury.* bioRxiv, 2020.
101. Daglas, M., D.F. Draxler, H. Ho, F. McCutcheon, A. Galle, A.E. Au, P. Larsson, J. Gregory, F. Alderuccio, M. Sashindranath, and R.L. Medcalf, *Activated CD8(+) T Cells Cause Long-Term Neurological Impairment after Traumatic Brain Injury in Mice.* Cell Rep, 2019. **29**(5): p. 1178-1191 e6.
102. Zhang, H., X. Xiong, L. Gu, W. Xie, and H. Zhao, *CD4 T cell deficiency attenuates ischemic stroke, inhibits oxidative stress, and enhances Akt/mTOR survival signaling pathways in mice.* Chin Neurosurg J, 2018. **4**.
103. Yilmaz, G., T.V. Arumugam, K.Y. Stokes, and D.N. Granger, *Role of T lymphocytes and interferon-gamma in ischemic stroke.* Circulation, 2006. **113**(17): p. 2105-12.
104. Susman, M., S. DiRusso, T. Sullivan, D. Risucci, P. Nealon, S. Cuff, A. Haider, and D. Benzil, *Traumatic Brain Injury in the Elderly: Increased Mortality and Worse Functional Outcomes at Discharge Despite Lower Injury Severity.* J Trauma, 2002. **53**(2): p. 219-223.
105. Thompson, H.J., W.C. McCormick, and S.H. Kagan, *Traumatic brain injury in older adults: epidemiology, outcomes, and future implications.* J Am Geriatr Soc, 2006. **54**(10): p. 1590-5.
106. Flanagan, S.R., M.R. Hibbard, B. Riordan, and W.A. Gordon, *Traumatic brain injury in the elderly: diagnostic and treatment challenges.* Clin Geriatr Med, 2006. **22**(2): p. 449-68; x.

107. DiNapoli, V.A., J.D. Huber, K. Houser, X. Li, and C.L. Rosen, *Early disruptions of the blood-brain barrier may contribute to exacerbated neuronal damage and prolonged functional recovery following stroke in aged rats.* Neurobiol Aging, 2008. **29**(5): p. 753-64.
108. Marin, J.R., M.D. Weaver, and R.C. Mannix, *Burden of USA hospital charges for traumatic brain injury.* Brain Inj, 2017. **31**(1): p. 24-31.
109. Ritzel, R.M., S.J. Doran, E.P. Glaser, V.E. Meadows, A.I. Faden, B.A. Stoica, and D.J. Loane, *Old age increases microglial senescence, exacerbates secondary neuroinflammation, and worsens neurological outcomes after acute traumatic brain injury in mice.* Neurobiol Aging, 2019. **77**: p. 194-206.
110. Itoh, T., M. Imano, S. Nishida, M. Tsubaki, N. Mizuguchi, S. Hashimoto, A. Ito, and T. Satou, *Increased apoptotic neuronal cell death and cognitive impairment at early phase after traumatic brain injury in aged rats.* Brain Struct Funct, 2013. **218**(1): p. 209-20.
111. Kumar, A., B.A. Stoica, B. Sabirzhanov, M.P. Burns, A.I. Faden, and D.J. Loane, *Traumatic brain injury in aged animals increases lesion size and chronically alters microglial/macrophage classical and alternative activation states.* Neurobiol Aging, 2013. **34**(5): p. 1397-411.
112. Wang, M., N.J. Gamo, Y. Yang, L.E. Jin, X.J. Wang, M. Laubach, J.A. Mazer, D. Lee, and A.F. Arnsten, *Neuronal basis of age-related working memory decline.* Nature, 2011. **476**(7359): p. 210-3.
113. Androvic, P., D. Kirdajova, J. Tureckova, D. Zucha, E. Rohlova, P. Abaffy, J. Kriska, M. Valny, M. Anderova, M. Kubista, and L. Valihrach, *Decoding the Transcriptional Response to Ischemic Stroke in Young and Aged Mouse Brain.* Cell Rep, 2020. **31**(11): p. 107777.
114. Boisvert, M.M., G.A. Erikson, M.N. Shokhirev, and N.J. Allen, *The Aging Astrocyte Transcriptome from Multiple Regions of the Mouse Brain.* Cell Rep, 2018. **22**(1): p. 269-285.
115. Grabert, K., T. Michoel, M.H. Karavolos, S. Clohisey, J.K. Baillie, M.P. Stevens, T.C. Freeman, K.M. Summers, and B.W. McColl, *Microglial brain region-dependent diversity and selective regional sensitivities to aging.* Nat Neurosci, 2016. **19**(3): p. 504-16.
116. Spitzer, S.O., S. Sitnikov, Y. Kamen, K.A. Evans, D. Kronenberg-Versteeg, S. Dietmann, O. de Faria, Jr., S. Agathou, and R.T. Karadottir, *Oligodendrocyte Progenitor Cells Become Regionally Diverse and Heterogeneous with Age.* Neuron, 2019. **101**(3): p. 459-471 e5.
117. Marschallinger, J., T. Iram, M. Zardeneta, S.E. Lee, B. Lehallier, M.S. Haney, J.V. Pluvinage, V. Mathur, O. Hahn, D.W. Morgens, J. Kim, J. Tevini, T.K. Felder, H. Wolinski, C.R. Bertozzi, M.C. Bassik, L. Aigner, and T. Wyss-Coray, *Lipid-droplet-accumulating microglia represent a dysfunctional and proinflammatory state in the aging brain.* Nat Neurosci, 2020. **23**(2): p. 194-208.
118. Baruch, K., A. Deczkowska, E. David, J.M. Castellano, O. Miller, A. Kertser, T. Berkutzki, Z. Barnett-Itzhaki, D. Bezalel, T. Wyss-Coray, I. Amit, and M. Schwartz, *Aging. Aging-induced type I interferon response at the choroid plexus negatively affects brain function.* Science, 2014. **346**(6205): p. 89-93.
119. Yang, A.C., M.Y. Stevens, M.B. Chen, D.P. Lee, D. Stahli, D. Gate, K. Contrepois, W. Chen, T. Iram, L. Zhang, R.T. Vest, A. Chaney, B. Lehallier, N. Olsson, H. du Bois, R. Hsieh, H.C. Cropper, D. Berdnik, L. Li, E.Y. Wang, et al., *Physiological blood-brain transport is impaired with age by a shift in transcytosis.* Nature, 2020. **583**(7816): p. 425-430.
120. Chen, H.Z., S. Guo, Z.Z. Li, Y. Lu, D.S. Jiang, R. Zhang, H. Lei, L. Gao, X. Zhang, Y. Zhang, L. Wang, L.H. Zhu, M. Xiang, Y. Zhou, Q. Wan, H. Dong, D.P. Liu, and H. Li, *A critical role for interferon regulatory factor 9 in cerebral ischemic stroke.* J Neurosci, 2014. **34**(36): p. 11897-912.

121. Barrett, J.P., R.J. Henry, K.A. Shirey, S.J. Doran, O.D. Makarevich, R.M. Ritzel, V.A. Meadows, S.N. Vogel, A.I. Faden, B.A. Stoica, and D.J. Loane, *Interferon-beta Plays a Detrimental Role in Experimental Traumatic Brain Injury by Enhancing Neuroinflammation That Drives Chronic Neurodegeneration.* J Neurosci, 2020. **40**(11): p. 2357-2370.
122. Zhang, M., C.E. Downes, C.H.Y. Wong, K.M. Brody, P.L. Guio-Agulair, J. Gould, R. Ates, P.J. Hertzog, J.M. Taylor, and P.J. Crack, *Type-I interferon signalling through IFNAR1 plays a deleterious role in the outcome after stroke.* Neurochem Int, 2017. **108**: p. 472-480.
123. Abdullah, A., M. Zhang, T. Frugier, S. Bedoui, J.M. Taylor, and P.J. Crack, *STING-mediated type-I interferons contribute to the neuroinflammatory process and detrimental effects following traumatic brain injury.* J Neuroinflammation, 2018. **15**(1): p. 323.
124. Karve, I.P., M. Zhang, M. Habgood, T. Frugier, K.M. Brody, M. Sashindranath, C.J. Ek, S. Chappaz, B.T. Kile, D. Wright, H. Wang, L. Johnston, M. Daglas, R.C. Ates, R.L. Medcalf, J.M. Taylor, and P.J. Crack, *Ablation of Type-1 IFN Signaling in Hematopoietic Cells Confers Protection Following Traumatic Brain Injury.* eNeuro, 2016. **3**(1).
125. Makinde, H.M., T.B. Just, G.T. Gadhvi, D.R. Winter, and S.J. Schwulst, *Microglia Adopt Longitudinal Transcriptional Changes After Traumatic Brain Injury.* J Surg Res, 2020. **246**: p. 113-122.
126. Xu, K., X. Sun, M.A. Puchowicz, and J.C. LaManna, *Increased sensitivity to transient global ischemia in aging rat brain.* Adv Exp Med Biol, 2007. **599**: p. 199-206.
127. Foster, K.A., R.R. Margraf, and D.A. Turner, *NADH hyperoxidation correlates with enhanced susceptibility of aged rats to hypoxia.* Neurobiol Aging, 2008. **29**(4): p. 598-613.
128. Wang, X. and E.K. Michaelis, *Selective neuronal vulnerability to oxidative stress in the brain.* Front Aging Neurosci, 2010. **2**: p. 12.
129. He, S. and N.E. Sharpless, *Senescence in Health and Disease.* Cell, 2017. **169**(6): p. 1000-1011.
130. Plassman, B.L., R.J. Havlik, D.C. Steffens, M.J. Helms, T.N. Newman, D. Drosdick, C. Phillips, B.A. Gau, K.A. Welsh-Bohmer, J.R. Burke, J.M. Guralnik, and J.C. Breitner, *Documented head injury in early adulthood and risk of Alzheimer's disease and other dementias.* Neurology, 2000. **55**(8): p. 1158-66.
131. Ritzel, R.M., Y.J. Lai, J.D. Crapser, A.R. Patel, A. Schrecengost, J.M. Grenier, N.S. Mancini, A. Patrizz, E.R. Jellison, D. Morales-Scheihing, V.R. Venna, J.K. Kofler, F. Liu, R. Verma, and L.D. McCullough, *Aging alters the immunological response to ischemic stroke.* Acta Neuropathol, 2018. **136**(1): p. 89-110.
132. Morganti, J.M., L.K. Riparip, A. Chou, S. Liu, N. Gupta, and S. Rosi, *Age exacerbates the CCR2/5-mediated neuroinflammatory response to traumatic brain injury.* J Neuroinflammation, 2016. **13**(1): p. 80.
133. Joy, M.T., E. Ben Assayag, D. Shabashov-Stone, S. Liraz-Zaltsman, J. Mazzitelli, M. Arenas, N. Abduljawad, E. Kliper, A.D. Korczyn, N.S. Thareja, E.L. Kesner, M. Zhou, S. Huang, T.K. Silva, N. Katz, N.M. Bornstein, A.J. Silva, E. Shohami, and S.T. Carmichael, *CCR5 Is a Therapeutic Target for Recovery after Stroke and Traumatic Brain Injury.* Cell, 2019. **176**(5): p. 1143-1157.e13.
134. Lee, S., A. Mattingly, A. Lin, J. Sacramento, L. Mannent, M.N. Castel, B. Canolle, S. Delbary-Gossart, B. Ferzaz, J.M. Morganti, S. Rosi, A.R. Ferguson, G.T. Manley, J.C. Bresnahan, and M.S. Beattie, *A novel antagonist of p75NTR reduces peripheral expansion and CNS trafficking of pro-inflammatory monocytes and spares function after traumatic brain injury.* J Neuroinflammation, 2016. **13**(1): p. 88.
135. Hammond, M.D., R.A. Taylor, M.T. Mullen, Y. Ai, H.L. Aguila, M. Mack, S.E. Kasner, L.D. McCullough, and L.H. Sansing, *CCR2+ Ly6C(hi) inflammatory monocyte recruitment exacerbates acute disability following intracerebral hemorrhage.* J Neurosci, 2014. **34**(11): p. 3901-9.

136. Zhou, M., S. Greenhill, S. Huang, T.K. Silva, Y. Sano, S. Wu, Y. Cai, Y. Nagaoka, M. Sehgal, D.J. Cai, Y.S. Lee, K. Fox, and A.J. Silva, *CCR5 is a suppressor for cortical plasticity and hippocampal learning and memory.* Elife, 2016. **5**.
137. Li, S., J.J. Overman, D. Katsman, S.V. Kozlov, C.J. Donnelly, J.L. Twiss, R.J. Giger, G. Coppola, D.H. Geschwind, and S.T. Carmichael, *An age-related sprouting transcriptome provides molecular control of axonal sprouting after stroke.* Nat Neurosci, 2010. **13**(12): p. 1496-504.
138. Overman, J.J., A.N. Clarkson, I.B. Wanner, W.T. Overman, I. Eckstein, J.L. Maguire, I.D. Dinov, A.W. Toga, and S.T. Carmichael, *A role for ephrin-A5 in axonal sprouting, recovery, and activity-dependent plasticity after stroke.* Proceedings of the National Academy of Sciences, 2012. **109**(33): p. E2230-E2239.
139. Da Mesquita, S., A. Louveau, A. Vaccari, I. Smirnov, R.C. Cornelison, K.M. Kingsmore, C. Contarino, S. Onengut-Gumuscu, E. Farber, D. Raper, K.E. Viar, R.D. Powell, W. Baker, N. Dabhi, R. Bai, R. Cao, S. Hu, S.S. Rich, J.M. Munson, M.B. Lopes, et al., *Functional aspects of meningeal lymphatics in ageing and Alzheimer's disease.* Nature, 2018. **560**(7717): p. 185-191.
140. Ahn, J.H., H. Cho, J.H. Kim, S.H. Kim, J.S. Ham, I. Park, S.H. Suh, S.P. Hong, J.H. Song, Y.K. Hong, Y. Jeong, S.H. Park, and G.Y. Koh, *Meningeal lymphatic vessels at the skull base drain cerebrospinal fluid.* Nature, 2019.
141. Ma, Q., B.V. Ineichen, M. Detmar, and S.T. Proulx, *Outflow of cerebrospinal fluid is predominantly through lymphatic vessels and is reduced in aged mice.* Nat Commun, 2017. **8**(1): p. 1434.
142. Gadani, S.P., J.T. Walsh, J.R. Lukens, and J. Kipnis, *Dealing with Danger in the CNS: The Response of the Immune System to Injury.* Neuron, 2015. **87**(1): p. 47-62.
143. Labzin, L.I., M.T. Heneka, and E. Latz, *Innate Immunity and Neurodegeneration.* Annu Rev Med, 2018. **69**: p. 437-449.
144. Patel, T.K., L. Habimana-Griffin, X. Gao, B. Xu, S. Achilefu, K. Alitalo, C.A. McKee, P.W. Sheehan, E.S. Musiek, C. Xiong, D. Coble, and D.M. Holtzman, *Dural lymphatics regulate clearance of extracellular tau from the CNS.* Mol Neurodegener, 2019. **14**(1): p. 11.
145. Zou, W., T. Pu, W. Feng, M. Lu, Y. Zheng, R. Du, M. Xiao, and G. Hu, *Blocking meningeal lymphatic drainage aggravates Parkinson's disease-like pathology in mice overexpressing mutated alpha-synuclein.* Transl Neurodegener, 2019. **8**: p. 7.
146. Tammela, T. and K. Alitalo, *Lymphangiogenesis: Molecular mechanisms and future promise.* Cell, 2010. **140**(4): p. 460-76.
147. Salehi, A., J.H. Zhang, and A. Obenaus, *Response of the cerebral vasculature following traumatic brain injury.* J Cereb Blood Flow Metab, 2017. **37**(7): p. 2320-2339.
148. Balestreri, M., M. Czosnyka, P. Hutchinson, L.A. Steiner, M. Hiler, P. Smielewski, and J.D. Pickard, *Impact of Intracranial Pressure and Cerebral Perfusion Pressure on Severe Disability and Mortality After Head Injury.* Neurocritical Care, 2006. **4**(1): p. 008-013.
149. Serdar Ensari, E.K., Kagan Tun, Taylan Gun, Etem Beskonakli, Serdar Celikkanat, Huseyin Dere, Saruhan Cekirge, *Venous Outflow of the Brain after Bilateral Complete Jugular Ligation* Turkish Neurosurgery, 2008. **18**(1): p. 56-60.
150. Kevin L Weiss, M.K.W., Richard C. Haydon, Howard H. Kaufman, Michael K Hurst, *Intracranial Pressure changes during bilateral radial neck dissections.* Head and Neck, 1993.
151. LeBlanc, J., E. de Guise, N. Gosselin, and M. Feyz, *Comparison of functional outcome following acute care in young, middle-aged and elderly patients with traumatic brain injury.* Brain Inj, 2006. **20**(8): p. 779-90.
152. Chou, A., K. Krukowski, J.M. Morganti, L.K. Riparip, and S. Rosi, *Persistent Infiltration and Impaired Response of Peripherally-Derived Monocytes after Traumatic Brain Injury in the Aged Brain.* Int J Mol Sci, 2018. **19**(6).

153. Krukowski, K., A. Chou, X. Feng, B. Tiret, M.S. Paladini, L.K. Riparip, M.M. Chaumeil, C. Lemere, and S. Rosi, *Traumatic Brain Injury in Aged Mice Induces Chronic Microglia Activation, Synapse Loss, and Complement-Dependent Memory Deficits.* Int J Mol Sci, 2018. **19**(12).
154. Winston, C.N., A. Noel, A. Neustadtl, M. Parsadanian, D.J. Barton, D. Chellappa, T.E. Wilkins, A.D. Alikhani, D.N. Zapple, S. Villapol, E. Planel, and M.P. Burns, *Dendritic Spine Loss and Chronic White Matter Inflammation in a Mouse Model of Highly Repetitive Head Trauma.* Am J Pathol, 2016. **186**(3): p. 552-67.
155. Coronado, V.G., K.E. Thomas, R.W. Sattin, and R.L. Johnson, *The CDC traumatic brain injury surveillance system: characteristics of persons aged 65 years and older hospitalized with a TBI.* J Head Trauma Rehabil, 2005. **20**(3): p. 215-28.
156. Didehbani, N., C. Munro Cullum, S. Mansinghani, H. Conover, and J. Hart, Jr., *Depressive symptoms and concussions in aging retired NFL players.* Arch Clin Neuropsychol, 2013. **28**(5): p. 418-24.
157. Tammela, T., A. Saaristo, T. Holopainen, S. Yla-Herttuala, L.C. Andersson, S. Virolainen, I. Immonen, and K. Alitalo, *Photodynamic ablation of lymphatic vessels and intralymphatic cancer cells prevents metastasis.* Sci Transl Med, 2011. **3**(69): p. 69ra11.
158. Stephan, A.H., D.V. Madison, J.M. Mateos, D.A. Fraser, E.A. Lovelett, L. Coutellier, L. Kim, H.H. Tsai, E.J. Huang, D.H. Rowitch, D.S. Berns, A.J. Tenner, M. Shamloo, and B.A. Barres, *A dramatic increase of C1q protein in the CNS during normal aging.* J Neurosci, 2013. **33**(33): p. 13460-74.
159. Liberzon, A., C. Birger, H. Thorvaldsdottir, M. Ghandi, J.P. Mesirov, and P. Tamayo, *The Molecular Signatures Database (MSigDB) hallmark gene set collection.* Cell Syst, 2015. **1**(6): p. 417-425.
160. Shepherd, J.D. and M.F. Bear, *New views of Arc, a master regulator of synaptic plasticity.* Nat Neurosci, 2011. **14**(3): p. 279-84.
161. Plath, N., O. Ohana, B. Dammermann, M.L. Errington, D. Schmitz, C. Gross, X. Mao, A. Engelsberg, C. Mahlke, H. Welzl, U. Kobalz, A. Stawrakakis, E. Fernandez, R. Waltereit, A. Bick-Sander, E. Therstappen, S.F. Cooke, V. Blanquet, W. Wurst, B. Salmen, et al., *Arc/Arg3.1 is essential for the consolidation of synaptic plasticity and memories.* Neuron, 2006. **52**(3): p. 437-44.
162. Gabory, A., H. Jammes, and L. Dandolo, *The H19 locus: role of an imprinted non-coding RNA in growth and development.* Bioessays, 2010. **32**(6): p. 473-80.
163. Jassal, B., L. Matthews, G. Viteri, C. Gong, P. Lorente, A. Fabregat, K. Sidiropoulos, J. Cook, M. Gillespie, R. Haw, F. Loney, B. May, M. Milacic, K. Rothfels, C. Sevilla, V. Shamovsky, S. Shorser, T. Varusai, J. Weiser, G. Wu, et al., *The reactome pathway knowledgebase.* Nucleic Acids Res, 2020. **48**(D1): p. D498-D503.
164. Nishimura, D., *BioCarta.* Biotech Software & Internet Report, 2001. **2**(3): p. 117-120.
165. Buniello, A., J.A.L. MacArthur, M. Cerezo, L.W. Harris, J. Hayhurst, C. Malangone, A. McMahon, J. Morales, E. Mountjoy, E. Sollis, D. Suveges, O. Vrousgou, P.L. Whetzel, R. Amode, J.A. Guillen, H.S. Riat, S.J. Trevanion, P. Hall, H. Junkins, P. Flicek, et al., *The NHGRI-EBI GWAS Catalog of published genome-wide association studies, targeted arrays and summary statistics 2019.* Nucleic Acids Res, 2019. **47**(D1): p. D1005-D1012.
166. Karve, I.P., J.M. Taylor, and P.J. Crack, *The contribution of astrocytes and microglia to traumatic brain injury.* Br J Pharmacol, 2016. **173**(4): p. 692-702.
167. Loane, D.J., A. Kumar, B.A. Stoica, R. Cabatbat, and A.I. Faden, *Progressive neurodegeneration after experimental brain trauma: association with chronic microglial activation.* J Neuropathol Exp Neurol, 2014. **73**(1): p. 14-29.
168. Loane, D.J. and A. Kumar, *Microglia in the TBI brain: The good, the bad, and the dysregulated.* Exp Neurol, 2016. **275 Pt 3**: p. 316-327.

169. Ren, Z., J.J. Iliff, L. Yang, J. Yang, X. Chen, M.J. Chen, R.N. Giese, B. Wang, X. Shi, and M. Nedergaard, *'Hit & Run' model of closed-skull traumatic brain injury (TBI) reveals complex patterns of post-traumatic AQP4 dysregulation.* J Cereb Blood Flow Metab, 2013. **33**(6): p. 834-45.
170. Alves de Lima, K., J. Rustenhoven, and J. Kipnis, *Meningeal Immunity and Its Function in Maintenance of the Central Nervous System in Health and Disease.* Annu Rev Immunol, 2020. **38**: p. 597-620.
171. Goodman, J.R. and J.J. Iliff, *Vasomotor influences on glymphatic-lymphatic coupling and solute trafficking in the central nervous system.* J Cereb Blood Flow Metab, 2019: p. 271678X19874134.
172. Schatz, P., R.S. Moser, T. Covassin, and R. Karpf, *Early indicators of enduring symptoms in high school athletes with multiple previous concussions.* Neurosurgery, 2011. **68**(6): p. 1562-7; discussion 1567.
173. Centers for Disease, C. and Prevention, *Incidence rates of hospitalization related to traumatic brain injury--12 states, 2002.* MMWR Morb Mortal Wkly Rep, 2006. **55**(8): p. 201-4.
174. Kim, D., J.M. Paggi, C. Park, C. Bennett, and S.L. Salzberg, *Graph-based genome alignment and genotyping with HISAT2 and HISAT-genotype.* Nat Biotechnol, 2019. **37**(8): p. 907-915.
175. Li, H., B. Handsaker, A. Wysoker, T. Fennell, J. Ruan, N. Homer, G. Marth, G. Abecasis, R. Durbin, and S. Genome Project Data Processing, *The Sequence Alignment/Map format and SAMtools.* Bioinformatics, 2009. **25**(16): p. 2078-9.
176. Anders, S., P.T. Pyl, and W. Huber, *HTSeq--a Python framework to work with high-throughput sequencing data.* Bioinformatics, 2015. **31**(2): p. 166-9.
177. Love, M.I., W. Huber, and S. Anders, *Moderated estimation of fold change and dispersion for RNA-seq data with DESeq2.* Genome Biol, 2014. **15**(12): p. 550.
178. Gu, Z., L. Gu, R. Eils, M. Schlesner, and B. Brors, *circlize Implements and enhances circular visualization in R.* Bioinformatics, 2014. **30**(19): p. 2811-2.
179. Flierl, M.A., P.F. Stahel, K.M. Beauchamp, S.J. Morgan, W.R. Smith, and E. Shohami, *Mouse closed head injury model induced by a weight-drop device.* Nat Protoc, 2009. **4**(9): p. 1328-37.
180. Susaki, E.A., K. Tainaka, D. Perrin, H. Yukinaga, A. Kuno, and H.R. Ueda, *Advanced CUBIC protocols for whole-brain and whole-body clearing and imaging.* Nat Protoc, 2015. **10**(11): p. 1709-27.
181. Denes, A. and J.A. Miyan, *Brain-immune interactions in health and disease.* Front Neurosci, 2014. **8**: p. 382.
182. Dinet, V., K.G. Petry, and J. Badaut, *Brain-Immune Interactions and Neuroinflammation After Traumatic Brain Injury.* Front Neurosci, 2019. **13**: p. 1178.
183. Marques-Deak, A., G. Cizza, and E. Sternberg, *Brain-immune interactions and disease susceptibility.* Mol Psychiatry, 2005. **10**(3): p. 239-50.
184. Ransohoff, R.M. and B. Engelhardt, *The anatomical and cellular basis of immune surveillance in the central nervous system.* Nat Rev Immunol, 2012. **12**(9): p. 623-35.
185. Juul, N., G.F. Morris, S.B. Marshall, and L.F. Marshall, *Intracranial hypertension and cerebral perfusion pressure: influence on neurological deterioration and outcome in severe head injury. The Executive Committee of the International Selfotel Trial.* J Neurosurg, 2000. **92**(1): p. 1-6.
186. Rangel-Castilla, L., S. Gopinath, and C.S. Robertson, *Management of intracranial hypertension.* Neurol Clin, 2008. **26**(2): p. 521-41, x.
187. El Ahmadieh, T.Y., J.G. Adel, N.E. El Tecle, M.R. Daou, S.G. Aoun, A.D. Nanney, 3rd, and B.R. Bendok, *Surgical treatment of elevated intracranial pressure: decompressive*

craniectomy and intracranial pressure monitoring. Neurosurg Clin N Am, 2013. **24**(3): p. 375-91.
188. Pu, T., W. Zou, W. Feng, Y. Zhang, L. Wang, H. Wang, and M. Xiao, *Persistent Malfunction of Glymphatic and Meningeal Lymphatic Drainage in a Mouse Model of Subarachnoid Hemorrhage.* Exp Neurobiol, 2019. **28**(1): p. 104-118.
189. Schofield, P.W., M. Tang, K. Marder, K. Bell, G. Dooneief, M. Chun, M. Sano, Y. Stern, and R. Mayeux, *Alzheimer's disease after remote head injury: an incidence study.* J Neurol Neurosurg Psychiatry, 1997. **62**(2): p. 119-24.
190. Hall, A.M. and E.D. Roberson, *Mouse models of Alzheimer's disease.* Brain Res Bull, 2012. **88**(1): p. 3-12.
191. Ashe, K.H., *Learning and memory in transgenic mice modeling Alzheimer's disease.* Learn Mem, 2001. **8**(6): p. 301-8.
192. Morimoto, K. and K. Nakajima, *Role of the Immune System in the Development of the Central Nervous System.* Front Neurosci, 2019. **13**: p. 916.
193. Gate, D., N. Saligrama, O. Leventhal, A.C. Yang, M.S. Unger, J. Middeldorp, K. Chen, B. Lehallier, D. Channappa, M.B. De Los Santos, A. McBride, J. Pluvinage, F. Elahi, G.K. Tam, Y. Kim, M. Greicius, A.D. Wagner, L. Aigner, D.R. Galasko, M.M. Davis, et al., *Clonally expanded CD8 T cells patrol the cerebrospinal fluid in Alzheimer's disease.* Nature, 2020. **577**(7790): p. 399-404.
194. Lepennetier, G., Z. Hracsko, M. Unger, M. Van Griensven, V. Grummel, M. Krumbholz, A. Berthele, B. Hemmer, and M.C. Kowarik, *Cytokine and immune cell profiling in the cerebrospinal fluid of patients with neuro-inflammatory diseases.* J Neuroinflammation, 2019. **16**(1): p. 219.
195. Ringstad, G. and P.K. Eide, *Cerebrospinal fluid tracer efflux to parasagittal dura in humans.* Nat Commun, 2020. **11**(1): p. 354.
196. Peng, W., T.M. Achariyar, B. Li, Y. Liao, H. Mestre, E. Hitomi, S. Regan, T. Kasper, S. Peng, F. Ding, H. Benveniste, M. Nedergaard, and R. Deane, *Suppression of glymphatic fluid transport in a mouse model of Alzheimer's disease.* Neurobiol Dis, 2016. **93**: p. 215-25.
197. Doro, D., A. Liu, A.E. Grigoriadis, and K.J. Liu, *The Osteogenic Potential of the Neural Crest Lineage May Contribute to Craniosynostosis.* Mol Syndromol, 2019. **10**(1-2): p. 48-57.
198. Cooper, G.M., E.L. Durham, J.J. Cray, Jr., M.I. Siegel, J.E. Losee, and M.P. Mooney, *Tissue interactions between craniosynostotic dura mater and bone.* J Craniofac Surg, 2012. **23**(3): p. 919-24.
199. Zarbalis, K., J.A. Siegenthaler, Y. Choe, S.R. May, A.S. Peterson, and S.J. Pleasure, *Cortical dysplasia and skull defects in mice with a Foxc1 allele reveal the role of meningeal differentiation in regulating cortical development.* Proc Natl Acad Sci U S A, 2007. **104**(35): p. 14002-7.
200. Kalamarides, M., A.O. Stemmer-Rachamimov, M. Niwa-Kawakita, F. Chareyre, E. Taranchon, Z.Y. Han, C. Martinelli, E.A. Lusis, B. Hegedus, D.H. Gutmann, and M. Giovannini, *Identification of a progenitor cell of origin capable of generating diverse meningioma histological subtypes.* Oncogene, 2011. **30**(20): p. 2333-44.
201. Caglayan, A.O., J.F. Baranoski, F. Aktar, W. Han, B. Tuysuz, A. Guzel, B. Guclu, H. Kaymakcalan, B. Aktekin, G.T. Akgumus, P.B. Murray, E.Z. Erson-Omay, C. Caglar, M. Bakircioglu, Y.B. Sakalar, E. Guzel, N. Demir, O. Tuncer, S. Senturk, B. Ekici, et al., *Brain malformations associated with Knobloch syndrome--review of literature, expanding clinical spectrum, and identification of novel mutations.* Pediatr Neurol, 2014. **51**(6): p. 806-813 e8.
202. Rua, R. and D.B. McGavern, *Advances in Meningeal Immunity.* Trends Mol Med, 2018. **24**(6): p. 542-559.

203. Fitzpatrick, Z., G. Frazer, A. Ferro, S. Clare, N. Bouladoux, J. Ferdinand, Z.K. Tuong, M.L. Negro-Demontel, N. Kumar, O. Suchanek, T. Tajsic, K. Harcourt, K. Scott, R. Bashford-Rogers, A. Helmy, D.S. Reich, Y. Belkaid, T.D. Lawley, D.B. McGavern, and M.R. Clatworthy, *Gut-educated IgA plasma cells defend the meningeal venous sinuses.* Nature, 2020. **587**(7834): p. 472-476.
204. Stuart, T., A. Butler, P. Hoffman, C. Hafemeister, E. Papalexi, W.M. Mauck, 3rd, Y. Hao, M. Stoeckius, P. Smibert, and R. Satija, *Comprehensive Integration of Single-Cell Data.* Cell, 2019. **177**(7): p. 1888-1902 e21.
205. Butler, A., P. Hoffman, P. Smibert, E. Papalexi, and R. Satija, *Integrating single-cell transcriptomic data across different conditions, technologies, and species.* Nat Biotechnol, 2018. **36**(5): p. 411-420.
206. Risso, D., F. Perraudeau, S. Gribkova, S. Dudoit, and J.P. Vert, *A general and flexible method for signal extraction from single-cell RNA-seq data.* Nat Commun, 2018. **9**(1): p. 284.
207. Wickham, H., *ggplot2: Elegant Graphics for Data Analysis*. 2016: Springer-Verlag New York.
208. Wickham, H., M. Averick, J. Bryan, W. Chang, L. McGowan, R. François, G. Grolemund, A. Hayes, L. Henry, J. Hester, M. Kuhn, T. Pedersen, E. Miller, S. Bache, K. Müller, J. Ooms, D. Robinson, D. Seidel, V. Spinu, K. Takahashi, et al., *Welcome to the Tidyverse.* Journal of Open Source Software, 2019. **4**(43).